Intrinsic optical absorption in Dirac metals

Adamya P. Goyal, Prachi Sharma,* and Dmitrii L. Maslov

Department of Physics, University of Florida, P. O. Box 118440, Gainesville, FL 32611-8440, USA

(Dated: August 21, 2023)

A Dirac metal is a doped (gated) Dirac material with the Fermi energy (E_F) lying either in the conduction or valence bands. In the non-interacting picture, optical absorption in gapless Dirac metals occurs only if the frequency of incident photons (Ω) exceeds the direct (Pauli) frequency threshold, equal to $2E_F$. In this work, we study, both analytically and numerically, the role of electron-electron (ee) and electron-hole (eh) interactions in optical absorption of two-dimensional (2D) and three-dimensional (3D) Dirac metals in the entire interval of frequencies below $2E_F$. We show that, for $\Omega \ll E_F$, the optical conductivity, $\Re\sigma(\Omega)$, arising from the combination of ee and certain eh scattering processes, scales as $\Omega^2 \ln \Omega$ in 2D and as Ω^2 in 3D, respectively, both for short-range (Hubbard) and long-range (screened Coulomb) interactions. Another type of eh processes, similar to Auger-Meitner (AM) processes in atomic physics, starts to contribute for Ω above the direct threshold, equal to E_F. Similar to the case of doped semiconductors with parabolic bands studied in prior literature, the AM contribution to $\Re\sigma(\Omega)$ in Dirac metals is manifested by a threshold singularity, $\Re\sigma(\Omega) \propto (\Omega - E_F)^{d+2}$, where d is the spatial dimensionality and $0 < \Omega - E_F \ll E_F$. In contrast to doped semiconductors, however, the AM contribution in Dirac metals is completely overshadowed by the ee and other eh contributions. Numerically, $\Re\sigma(\Omega)$ happens to be small in almost the entire range of $\Omega < 2E_F$. This finding may have important consequences for collective modes in Dirac metals lying below $2E_F$.

I. INTRODUCTION

The characteristic feature of Dirac materials is the presence of symmetry-protected band-touching points which, in certain cases, is accompanied by the eponymous Dirac dispersion near these points. Realizations of these systems include monolayer graphene [1] and the surface state of a three-dimensional topological insulator [2] in two dimensions (2D), and Weyl/Dirac semi-metals [3–5] in three dimensions (3D).[6] Owing to zero band gap, these materials exhibit semi-metallic behavior at charge neutrality.

At the level of non-interacting (NI) electrons, a pristine 2D Dirac material is characterized by a frequency-independent and universal optical conductivity [1]

$$\Re\sigma_{\mathrm{NI2}}(\Omega) = \frac{Ne^2}{16\hbar}, \tag{1}$$

whereas the conductivity of a pristine 3D Dirac material scales linear with frequency [7, 8]

$$\Re\sigma_{\mathrm{NI3}}(\Omega) = \frac{Ne^2\Omega}{24\pi\hbar v_D}, \tag{2}$$

where N is the total (spin times valley) degeneracy, v_D is the Dirac velocity.[9] These predictions were corroborated by multiple experiments, see for e.g., reviews Ref. [3–5, 10–13].

The effect of electron-electron (ee) interactions on the optical conductivity of Dirac materials was studied extensively in 2D, see, e.g., reviews [10–12] and references

———————

* Current address: School of Physics and Astronomy, University of Minnesota, Minneapolis, MN 55455, USA
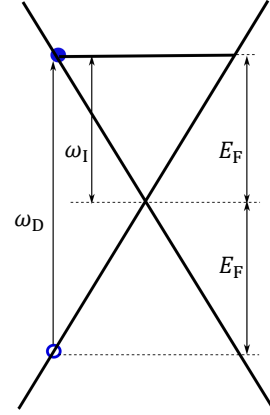
Figure 1. Band diagram of Dirac metal symmetric conduction and valence bands showing the direct (Pauli) threshold $\omega_D = 2E_F$ for single-particle inter-band transitions. Also shown is the indirect threshold for many-body Auger-Meitner transitions, $\omega_I = E_F$.

therein, and also in 3D [14, 15]. As Coulomb interaction is marginally irrelevant both in 2D and 3D, it leads to a logarithmic renormalization of the Dirac velocity and thus of the coupling constant, e^2/v_D [12, 16]. Consequently, $\Re\sigma_{\mathrm{NI2}}(\Omega)$ acquires a multiplicative renormalization factor, which varies with Ω logarithmically and, at $\Omega \to 0$, approaches a constant equal to 1 [12] or $1 + 1/(N+1)$ [15] in 2D and 3D, respectively. Note that this renormalization starts already at first order in the bare Coulomb potential, which implies that it does not involve collisions between particles in the intermediate states (the latter start at second order). On the other hand, a short-range (Hubbard) interaction is irrelevant in both 2D and 3D.

In a typical experiment, Dirac materials are doped (gated) away from charge neutrality, either intentionally or unintentionally. From now on, we will be referring to such systems as "Dirac metals". In this case, the Pauli principle dictates that the optical conductivity of an ideal Dirac metal is strictly zero below the "direct" (or Pauli) threshold,

$$\omega_{\mathrm{D}} = 2E_{\mathrm{F}}, \tag{3}$$

where E_{F} is the Fermi energy, measured from the Dirac point. Experimentally, however, one observes significant absorption for frequencies above the Drude tail but below ω_{D} [17–21] and significant Raman response in the same frequency range [22], both of which indicate a deviation from the single-particle picture. Absorption below the Pauli threshold in doped graphene due to a combined effect of disorder, electron-phonon and electron-electron interaction has also been addressed theoretically in Refs. [23–26]. In this paper, we focus on intrinsic absorption due to ee and electron-hole (eh) interactions for $\Omega < \omega_{\mathrm{D}}$.[27]

Absorption due to ee interaction in a Dirac metal was studied in Refs. [28, 29]. For $\Omega \ll E_{\mathrm{F}}$, the conductivity was found to scale as $\Omega^2 \ln \Omega$ and Ω^2 in 2D and 3D, respectively [29].[30] A quadratic scaling of the conductivity can be understood as the consequence of partially broken Galilean invariance in a Dirac-Fermi liquid (DFL). (By "partially broken Galilean invariance" we mean the case of an isotropic but non-parabolic spectrum, such that current relaxation due to ee interaction is allowed but suppressed compared to the case when Galilean invariance is broken completely, e.g., by umklapp processes.) Indeed, the optical conductivity can be cast into a Drude-like form

$$\Re\sigma_{\mathrm{ee}}(\Omega) \propto \frac{1}{\Omega^2 \tau_j(\Omega)}, \tag{4}$$

where $\tau_j(\Omega)$ is the current relaxation time. If Galilean invariance is broken completely, $\tau_j(\Omega)$ is of the same order as the quasiparticle lifetime in a Fermi liquid (FL): $\tau_j(\Omega) \sim \tau_{\mathrm{qp}}(\Omega) \propto \Omega^{-2}$. In this case, Eq. (4) produces a familiar "FL foot": $\Re\sigma(\Omega) = \mathrm{const}$. On the other hand, if Galilean invariance is intact, current cannot be relaxed in ee collisions: although $\tau_{\mathrm{qp}}(\Omega)$ is finite, $\tau_j(\Omega) = \infty$ and thus $\Re\sigma(\Omega) = 0$. A DFL occupies an intermediate niche between the two limits described above. On one hand, its non-parabolic spectrum allows for current relaxation; on the other hand, the spectrum is still isotropic (at low doping) and current relaxation is impossible for electrons right on the Fermi surface (FS) [29]. For states away from the FS, the current relaxation time is finite but long, $\tau_j(\Omega) \propto \Omega^{-4}$ (modulo a $\ln \Omega$ factor in 2D), while $\tau_{\mathrm{qp}}(\Omega)$ still scales in a FL way, i.e., as Ω^{-2}. According to Eq. (4), the quartic scaling of $1/\tau_j(\Omega)$ translates into the quadratic scaling of the conductivity.

In this paper, we extend the results of Ref. [29] to the entire interval of frequencies below ω_{D}. Such an extension necessarily requires to account for both ee and eh interaction processes. We consider 2D and 3D Dirac metals with two types of interaction: Hubbard and Coulomb. Our analytic results follow from the analysis of the Kubo formula and are applicable in two regions: i) for $\Omega \ll \omega_{\mathrm{I}}$, where

$$\omega_{\mathrm{I}} = E_{\mathrm{F}}, \tag{5}$$

is the "indirect" threshold and ii) just above the indirect threshold, i.e, for $\Omega \gtrsim \omega_{\mathrm{I}}$. In the rest of the interval $0 < \Omega < \omega_{\mathrm{D}}$, the conductivity is calculated numerically, but only for a Dirac metal with Hubbard interaction. For $\Omega \ll \omega_{\mathrm{I}}$, we show that the eh contribution to the conductivity scales as Ω^2, i.e., it is comparable to the ee one found in Ref. [29] in 3D and is subleading to the ee one in 2D, but only in the leading logarithm sense.

This Ω^2-scaling of the eh contribution to the conductivity can also be understood in terms of the Drude formula (4). Current relaxation due to eh scattering is not limited by (partially broken) Galilean invariance, so that $\tau_j(\Omega) \sim \tau_{\mathrm{qp}}(\Omega) \propto \Omega^{-2}$. [Unlike $\tau_{\mathrm{qp}}(\Omega)$, $\tau_j(\Omega)$ does not have an extra logarithmic factor in 2D.] However, the energies of electrons and holes differ now by E_{F} rather than Ω; therefore, the factor of Ω^2 in Eq. (4) is replaced by E_{F}^2, and the conductivity scales as Ω^2.

Another channel of absorption due to eh interaction opens up when Ω exceeds the indirect threshold ω_{I} [Eq. (5)]. Since the seminal 1969 paper by Gavoret et al. [31], absorption of light by degenerate semiconductors due to a particular type of eh interaction processes, similar to Auger-Meitner (AM) processes in atomic physics [32–34], have been studied by a large number of researchers, see, e.g., Refs. [35–38]. Although we consider only gapless systems, our result for the AM contribution just above ω_{I} exhibits a threshold singularity of the same type as found for a gapped spectrum [31, 35–38], i.e.,

$$\Re\sigma_{\mathrm{AM}}(\Omega) \propto \theta(\delta\Omega)\delta\Omega^{\beta_{\mathrm{A}}}, \tag{6}$$

where $\delta\Omega \equiv \Omega - \omega_{\mathrm{I}} \ll \omega_{\mathrm{I}}$ and $\beta_{\mathrm{A}} = d + 2$ with d being the spatial dimensionality and $\theta(x)$ is the Heaviside step function. Equation (6) can be obtained by estimating the conductivity as $\Re\sigma_{\mathrm{AM}}(\Omega) \propto \delta\Omega\mathcal{N}(\delta\Omega)/\tau_{\mathrm{qp}}(\delta\Omega)$, where $\mathcal{N}(\epsilon) \propto \epsilon^{d-1}$ is the density of states of a gapless Dirac metal and $1/\tau_{\mathrm{qp}}(\epsilon) \propto \epsilon^2$.

More important, however, is the fact that for a non-parabolic spectrum the AM contribution occurs at the background of ee and other eh contributions, which start at the lowest frequencies (as Ω^2 and $\Omega^2 \ln \Omega$ in 3D and 2D, respectively) and are still present both near and above ω_{I}. Therefore, the AM threshold singularity is masked by these other contributions. These competing contributions were not taken into account in the previous work on AM processes [31, 35–38], which considered two strictly parabolic bands separated by a gap (2Δ). To clarify the difference in absorption by materials with parabolic and Dirac bands, we invoke temporarily a gapped Dirac spectrum, $\epsilon_{\mathbf{k}} = \pm\sqrt{v_{\mathrm{D}}^2 k^2 + \Delta^2}$. A gapped semiconductor with parabolic conduction and valence band can be viewed as the $\Delta \to \infty$ limit of this spectrum. In this case,

intra-band *ee* interaction does not affect the conductivity due to Galilean invariance, as we already discussed above. Moreover, inter-band absorption accompanied by electron-hole conversion processes, i.e., processes that do not conserve the numbers of electrons and holes separately, is also forbidden in the parabolic limit, because the corresponding eigenstates are either purely electron-like or purely hole-like, with zero overlap between the two. Therefore, the interaction part of the corresponding Hamiltonian conserves the numbers of electrons and holes separately, and absorption is absent for $\Omega < \omega_\mathrm{I}$. For a strongly non-parabolic, e.g., gapless Dirac spectrum, the *ee* contribution is not suppressed by Galilean invariance, while electron-hole conversion processes are generically as important as other processes.

As far as the interval of $\Omega > \omega_\mathrm{D}$ is concerned, Abedinpour et al. [39] showed that the conductivity of doped graphene (a 2D Dirac metal, in our terminology) with Coulomb interaction exhibits a logarithmic renormalization which, for $\Omega \gg \omega_\mathrm{D}$, is reduced to the well-studied case of undoped graphene, and is logarithmically enhanced for $\Omega \gtrsim \omega_\mathrm{D}$ both for Coulomb and Hubbard interactions Both of these effects arise already at first order in the corresponding interaction and reflect renormalization of the Dirac velocity and, consequently, of the coupling constant. To the best of our knowledge, the interval of $\Omega \gg \omega_\mathrm{D}$ has not been studied for a 3D Dirac metal but, in analogy with the results for the undoped 3D case [14, 15], we would also expect a logarithmic renormalization starting at first order. On the other hand, absorption processes studied in our paper correspond to real collisions between electrons, and between electrons and holes, which occur starting from the second order in the interaction. Therefore, these processes are subleading to the first-order effects described above studied in Ref. [39], and we will not extend our results above ω_D.

Our numerical results agree with analytic ones, where applicable, and allow one to trace the behavior of the conductivity for almost entire frequency range of interest, $0 < \Omega < \omega_\mathrm{D}$, except for a narrow interval of width $\mathcal{O}(\alpha_\mathrm{H,C}^2 E_\mathrm{F})$ around ω_D, where $\alpha_\mathrm{H,C} \ll 1$ is the dimensionless coupling constant of Hubbard and Coulomb interactions, respectively. In this interval, our perturbative expansion breaks down and one needs to re-sum the diagrammatic series.

The rest the paper is organized as follows. In Sec. II, we set up the model Hamiltonians for 2D and 3D Dirac metals. In Sec. III, we outline the formalism for calculating the optical conductivity via the Kubo formula. In Sec. IV, we identify the *ee* and *eh* scattering processes that contribute to the conductivity in a given frequency range. In section IV B, we analyze the general structure of the contributions to the conductivity from the self-energy and vertex diagrams, which serve as archetypes for other contributions. In sections V and VI, we present our analytical and numerical results for the optical conductivity of 3D and 2D Dirac metals, respectively. Our conclusions are given in Sec. VII.

II. MODEL HAMILTONIANS OF DIRAC METALS

In this section we define our model Hamiltonians for 2D and 3D Dirac metals.

A. 3D Hamiltonian

A single Dirac point in 3D can be modeled by a 4×4 low-energy Hamiltonian with two orbital degrees of freedom per spin: which describes

$$\hat{\mathcal{H}}_\mathrm{3D} = \hat{\mathcal{H}}_0 + \hat{\mathcal{H}}_\mathrm{int}, \tag{7a}$$

$$\hat{\mathcal{H}}_0 = \sum_\mathbf{k} \Psi_\mathbf{k}^\dagger \left[v_\mathrm{D} \hat{\sigma}_x \otimes (\hat{\boldsymbol{\varsigma}} \cdot \mathbf{k}) - E_\mathrm{F} \hat{\sigma}_0 \otimes \hat{\varsigma}_0 \right] \Psi_\mathbf{k}, \tag{7b}$$

$$\hat{\mathcal{H}}_\mathrm{int} = \frac{1}{2\mathcal{V}} \sum_\mathbf{q} V_\mathrm{3D}(\mathbf{q}) \hat{n}_\mathbf{q} \hat{n}_{-\mathbf{q}}, \tag{7c}$$

where v_D is the Dirac velocity, $\Psi_\mathbf{k}$ is the 4×1 Dirac spinor, Pauli matrices $\hat{\boldsymbol{\varsigma}} = (\hat{\varsigma}_x, \hat{\varsigma}_y, \hat{\varsigma}_z)$ and $\hat{\boldsymbol{\sigma}} = (\hat{\sigma}_x, \hat{\sigma}_y, \hat{\sigma}_z)$ represent (real) spin and pseudospin, respectively, $\hat{\varsigma}_0$ and $\hat{\sigma}_0$ are the identity matrices in the corresponding subspaces, $\hat{n}_\mathbf{q} = \sum_\mathbf{k} \Psi_\mathbf{k}^\dagger \Psi_{\mathbf{k}+\mathbf{q}}$ is the density operator, $V_\mathrm{3D}(\mathbf{q})$ is the interaction potential, and $\mathcal{V}$ is the system volume. In general, we assume that there are N identical Dirac points. Fermions near a given Dirac point interact with other fermions at all other points but swapping of fermions between different Dirac points is not allowed (see more details on the model of interaction near the end of this section).

The eigenvalues and orthonormal eigenfunctions of $\hat{\mathcal{H}}_0$ in Eq. (7b) are given by

$$\xi_\mathbf{k}^s = s\epsilon_\mathbf{k} - E_\mathrm{F}, \ \epsilon_\mathbf{k} = v_\mathrm{D} k \tag{8}$$

and

$$|\mathbf{k}, +\rangle = \frac{1}{\sqrt{2}} \left[\begin{array}{c} \psi_1 \\ \left(\hat{\boldsymbol{\varsigma}} \cdot \hat{k}\right)\psi_1 \end{array} \right], |\mathbf{k}, -\rangle = \frac{1}{\sqrt{2}} \left[\begin{array}{c} -\left(\hat{\boldsymbol{\varsigma}} \cdot \hat{k}\right)\psi_2 \\ \psi_2 \end{array} \right], \tag{9}$$

respectively. Here $\hat{k} = \mathbf{k}/k$, $s = \pm 1$ is the helicity index, and $\psi_{1,2}$ are the 2×1 spinor states such that $\psi_{1,2}^\dagger \psi_{1,2} = 1$. Without loss of generality, we choose $\psi_1 = \psi_2 = (0, 1)^T$. The Green's function of $\hat{\mathcal{H}}_0$ is given by

$$\hat{G}(\mathbf{k}, i\omega) = \frac{1}{2} \sum_{s=\pm} \hat{M}_\mathbf{k}^s g_s(\mathbf{k}, i\omega), \tag{10a}$$

$$\hat{M}_\mathbf{k}^s = \hat{\sigma}_0 \otimes \hat{\varsigma}_0 + s\left(\hat{\sigma}_x \otimes (\hat{\boldsymbol{\varsigma}} \cdot \hat{k})\right), \tag{10b}$$

$$g_s(\mathbf{k}, i\omega) = \frac{1}{i\omega - \xi_\mathbf{k}^s}. \tag{10c}$$

For the sake of brevity, we will be omitting index n in Matsubara frequencies, which will be distinguished from real ones by a factor of the imaginary unit, i. For example, ω in Eq. (10c) stands for a Matsubara frequency. As

mentioned in Sec. I (footnote VII), we will be referring to the bands with helicity $s = \pm 1$ as the "conduction" and "valence" bands, respectively, while the fermions occupying the conduction and valence bands will be referred to as "electrons" and "holes". The density of states in the conduction band per spin per valley is equal to $\mathcal{N}_{F,3} = E_F^2/2\pi^2 v_D^3$.

The velocity operator corresponding to $\hat{\mathcal{H}}_0$ in (7b) is

$$\hat{\mathbf{v}} = v_D \hat{\sigma}_x \otimes \hat{\boldsymbol{\varsigma}} \tag{11}$$

with matrix elements

$$\mathbf{v}_{\mathbf{k}}^{s,s'} = \langle \mathbf{k}, s | \hat{\mathbf{v}} | \mathbf{k}, s' \rangle . \tag{12}$$

In what follows, we will need explicit expressions for the intra- and inter-band matrix elements of the velocity operator, which are given by

$$\mathbf{v}_{\mathbf{k}}^{s,s} = \langle \mathbf{k}, s | \hat{\mathbf{v}} | \mathbf{k}, s \rangle = s v_D \hat{k} \tag{13}$$

and

$$\begin{aligned} \mathbf{v}_{\mathbf{k}}^{+,-} = \left(\mathbf{v}_{\mathbf{k}}^{-,+} \right)^* &= \langle \mathbf{k}, + | \hat{\mathbf{v}} | \mathbf{k}, - \rangle \\ &= v_D \psi_1^\dagger \left[\hat{\boldsymbol{\varsigma}} - \left(\hat{\boldsymbol{\varsigma}} \cdot \hat{k} \right) \hat{\boldsymbol{\varsigma}} \left(\hat{\boldsymbol{\varsigma}} \cdot \hat{k} \right) \right] \psi_2, \end{aligned} \tag{14}$$

respectively.

We now turn to the interaction part of the Hamiltonian. In what follows, we will consider two models for the interaction $V_{3D}(\mathbf{q})$:

$$V_{3D}(\mathbf{q}) = \begin{cases} \lambda_3, & \text{(3D, Hubbard)} \tag{15a} \\ \dfrac{4\pi e^2}{q^2}, & \text{(3D, Coulomb)} \tag{15b} \end{cases}$$

where $\lambda_3 > 0$ is a constant and e is the magnitude of electron charge. We focus on the case of low doping, when k_F is much smaller than the distance between the nearby Dirac points, b. By "Hubbard interaction" we then mean an interaction that is constant for q less or comparable to k_F and falls off rapidly in the interval $k_F \ll q \ll b$. In that case, one can neglect scattering processes that swap electrons between the Dirac points. The Hubbard model, though not completely realistic, captures the essential physics and allows one to obtain both analytic results for the optical conductivity in certain frequency regimes and numerical results for all frequencies. Thus, we focus most of our discussion on the Hubbard model. The Coulomb model allows one to obtain analytic results in certain frequency regimes but is very expensive computationally for arbitrary frequencies, and we will restrict our analysis of this model to analytic results only. We discuss both Hubbard and Coulomb interactions in more detail in Section III B.

Note that in the basis of electron and hole creation/annihilation operators, which diagonalizes $\hat{\mathcal{H}}_0$, the Hamiltonian (7c) accounts for *all* possible interaction processes, including those that do not conserve the number of electrons and holes. As mentioned in Sec. I, our

approach is more general in this regard than the one in prior studies of optical absorption in doped semiconductors [31, 35–38]. These studies considered a model Hamiltonian, which allows only for the density-density interaction between electrons and holes

$$\hat{\mathcal{H}}'_{\text{int}} = \frac{1}{2\mathcal{V}} \sum_{\substack{\mathbf{k}, \mathbf{p}, \mathbf{q}, \\ \varsigma = \pm, s = \pm}} V_{\text{int}}(\mathbf{q}) \hat{d}^\dagger_{\mathbf{k}+\mathbf{q}, \varsigma, s} \hat{d}^\dagger_{\mathbf{p}-\mathbf{q}, \varsigma', -s} \hat{d}_{\mathbf{p}, \varsigma'-s} \hat{d}_{\mathbf{k}, \varsigma, s}, \tag{16}$$

where $\hat{d}^\dagger_{\mathbf{k}, \varsigma, \pm}$ is the operator creating an electron/hole with momentum $\mathbf{k}$ and spin ς. Such a Hamiltonian is correct for a parabolic spectrum, in which case intra-band absorption is forbidden by Galilean invariance while processes of electron-hole conversion are absent due to the vanishing overlap of the electron and hole states. However, it is not applicable to the gapless Dirac spectrum studied in this paper.

B. 2D Hamiltonian

As an example of a 2D Dirac metal, we consider monolayer graphene described by the standard Hamiltonian [1]:

$$\hat{\mathcal{H}}_{2D} = \hat{\mathcal{H}}_0 + \hat{\mathcal{H}}_{\text{int}}, \tag{17a}$$

$$\hat{\mathcal{H}}_0 = \sum_{\mathbf{k}} \Psi_{\mathbf{k}}^\dagger \left[v_D \left(\tau_z \hat{\sigma}_x k_x + \hat{\sigma}_y k_y \right) - \hat{\sigma}_0 E_F \right] \Psi_{\mathbf{k}}, \tag{17b}$$

$$\hat{\mathcal{H}}_{\text{int}} = \frac{1}{2\mathcal{V}} \sum_{\mathbf{q}} V_{2D}(\mathbf{q}) \hat{n}_{\mathbf{q}} \hat{n}_{-\mathbf{q}}, \tag{17c}$$

where $\tau_z = \pm 1$, $\Psi_{\mathbf{k}}$ is a 2×1 Dirac spinor, the set of Pauli matrices $\hat{\boldsymbol{\sigma}} = (\hat{\sigma}_x, \hat{\sigma}_y, \hat{\sigma}_z)$ describes pseudospin, $\hat{\sigma}_0$ is the identity matrix in the same subspace, $\hat{n}_{\mathbf{q}} = \sum_{\mathbf{k}} \Psi_{\mathbf{k}}^\dagger \Psi_{\mathbf{k}+\mathbf{q}}$ is the density operator, and $\mathcal{V}$ is the system area. In cases when the large-N approximation is needed, we will be assuming that fermions carry large (half-integer) spin ς, such that the total degeneracy $N = 2(2\varsigma + 1) \gg 1$.

The eigenvalues of $\hat{\mathcal{H}}_0$ in Eq. (17b) are the same as in Eq. (8), while its orthonormal eigenfunctions are given by

$$|\mathbf{k}, +\rangle = \frac{1}{\sqrt{2}} \begin{bmatrix} 1 \\ \tau_z e^{i\tau_z \phi_{\mathbf{k}}} \end{bmatrix}, |\mathbf{k}, -\rangle = \frac{1}{\sqrt{2}} \begin{bmatrix} -\tau_z e^{-i\tau_z \phi_{\mathbf{k}}} \\ 1 \end{bmatrix}, \tag{18}$$

where $\phi_{\mathbf{k}}$ is the azimuthal angle of $\mathbf{k}$. The Green's function of $\hat{\mathcal{H}}_0$ is given by

$$\hat{G}(\mathbf{k}, i\omega) = \frac{1}{2} \sum_{s=\pm} \hat{M}_{\mathbf{k}}^s g_s(\mathbf{k}, i\omega), \tag{19a}$$

$$\hat{M}_{\mathbf{k}}^s = \hat{\sigma}_0 + s \left(v_D \frac{\hat{\sigma}_x \tau_z k_x + \hat{\sigma}_y k_y}{\epsilon_{\mathbf{k}}} \right), \tag{19b}$$

where $g_s(\mathbf{k}, i\omega)$ is the same as in Eq. (10c). The density of states at the Fermi level per spin per valley is equal to $\mathcal{N}_{F,2} = E_F/2\pi v_D^2$.

The velocity operator corresponding to $\hat{\mathcal{H}}_0$ is

$$\hat{\mathbf{v}} = v_{\mathrm{D}} \left(\tau_z \hat{\sigma}_x, \hat{\sigma}_y \right), \qquad (20)$$

with its intra-band matrix element being the same as in Eq. (13), while the inter-band matrix element is given by

$$\mathbf{v}_{\mathbf{k}}^{+,-} = \left(\mathbf{v}_{\mathbf{k}}^{-,+} \right)^* = \langle \mathbf{k}, +| \, \hat{\mathbf{v}} \, |\mathbf{k}, -\rangle$$
$$= i v_{\mathrm{D}} e^{-i\tau_z \phi_{\mathbf{k}}} \left(\hat{k} \times \hat{z} \right), \qquad (21)$$

where $(\hat{x}, \hat{y}, \hat{z})$ are the Cartesian unit vectors. As in 3D, the intra- and inter-band velocities are orthogonal to each other.

Lastly, similar to the 3D case, we consider two models of the interaction

$$V_{2\mathrm{D}}(\mathbf{q}) = \begin{cases} \lambda_2, & \text{(2D, Hubbard)} \quad (22\mathrm{a}) \\ \dfrac{2\pi e^2}{q}, & \text{(2D, Coulomb)} \quad (22\mathrm{b}) \end{cases}$$

where $\lambda_2 > 0$ is a constant. As in 3D, by "Hubbard" interaction we mean the interaction with radius shorter than the Fermi wavelength but longer that the lattice constant, which cannot transfer electrons between the valleys. As in 3D, we will present both the analytical and numerical results for the Hubbard case, and only the analytical results for the Coulomb case.

III. OPTICAL CONDUCTIVITY: GENERAL FORMALISM

A. Kubo formula

In linear response, the real part of the optical conductivity is given by the Kubo formula

$$\Re\sigma_{\alpha\beta}(\Omega) = -\frac{1}{\Omega} \Im\Pi_{\alpha\beta,\mathrm{R}}(\mathbf{Q} = \mathbf{0}, \Omega), \qquad (23)$$

where $\alpha, \beta = x, y(z)$ in 2D and 3D, respectively, and $\Pi_{\alpha\beta,\mathrm{R}}(\mathbf{Q} = \mathbf{0}, \Omega)$ is the retarded current-current correlation function (denoted by subscript "R"), which is obtained by analytic continuation of its Matsubara counterpart:

$$\Pi_{\alpha\beta,\mathrm{R}}(\mathbf{Q}, \Omega) = \Pi_{\alpha\beta}(\mathbf{Q}, i\Omega \to \Omega + i0^+),$$
$$\Pi_{\alpha\beta}(\mathbf{Q}, i\Omega) = -\frac{1}{\mathcal{V}} \int\limits_0^{1/k_{\mathrm{B}}T} d\tau e^{i\Omega\tau} \left\langle T_\tau \hat{j}_\alpha^\dagger(\mathbf{Q}, \tau) \hat{j}_\beta(\mathbf{Q}, 0) \right\rangle.$$
$$(24)$$

In the basis of conduction/valence bands, the current operator is written as

$$\hat{\boldsymbol{j}}(\mathbf{Q}, \tau) = -e \sum_{\mathbf{k}, s, s'} \mathbf{v}_{\mathbf{k}}^{s,s'} \quad \hat{d}_{\mathbf{k}-\frac{\mathbf{Q}}{2}, s}^\dagger(\tau) \hat{d}_{\mathbf{k}+\frac{\mathbf{Q}}{2}, s'}(\tau), \quad (25)$$

where $\mathbf{v}_{\mathbf{k}}^{s,s'}$ is given by Eq. (12).

For isotropic systems, considered in this paper, the conductivity tensor is diagonal and symmetric. In this case, we define

$$\Pi(\mathbf{Q}, i\Omega) \equiv \frac{1}{d} \sum_\alpha \Pi_{\alpha\alpha}(\mathbf{Q}, i\Omega),$$
$$\Pi_{\mathrm{R}}(\mathbf{Q}, \Omega) \equiv \frac{1}{d} \sum_\alpha \Pi_{\alpha\alpha,\mathrm{R}}(\mathbf{Q}, \Omega),$$
$$\Re\sigma(\Omega) = -\frac{1}{\Omega} \Im\Pi_{\mathrm{R}}(\mathbf{Q} = \mathbf{0}, \Omega). \qquad (26)$$

We also assume that temperature is much smaller than any other energy scale of the problem and consider only the $T = 0$ limit.

B. Relevant diagrams

In Dirac metals, optical absorption occurs already for non-interacting particles, if the frequency of incident light exceeds the direct threshold, $\omega_{\mathrm{D}} = 2E_{\mathrm{F}}$. The main focus of this paper is the range of $0 < \Omega < 2E_{\mathrm{F}}$, where absorption occurs only if electrons interact with other degrees in freedom, in particular, both among themselves and with holes. Dissipation occurs only if the interaction is dynamic, i.e., if the bare interaction, either Hubbard or Coulomb, is dressed by particle-hole pairs. Diagrammatically, this corresponds to renormalizing the interaction lines either by particle-hole polarization bubbles or "Aslamazov-Larkin triangles" (cf. Fig. 2).

1. Hubbard interaction

To make the analysis tractable, we assume that the number of identical Dirac points is large ($N \gg 1$) and also adopt the weak-coupling approximation, i.e, we assume that $\alpha_{\mathrm{H}} N \ll 1$, where

$$\alpha_{\mathrm{H}} = \lambda_d \mathcal{N}_{\mathrm{F},d} \qquad (27)$$

is the dimensionless coupling constant. The first assumption allows us to retain only diagrams with the highest number of fermion loops, while the second one allows us to keep the lowest order in the interaction at which dissipation occurs, to wit: the second. The relevant diagrams for the current-current correlation function are shown in Fig. 2. For the Hubbard case, the solid and broken interaction lines are identical and denote the Hubbard coupling λ_d.

2. Coulomb interaction

Within the random-phase approximation (RPA), the dynamically screened Coulomb interaction is given by

$$V(\mathbf{q}, i\nu) = \frac{1}{V_0^{-1}(\mathbf{q}) + \pi_0(\mathbf{q}, i\nu)} \qquad (28)$$
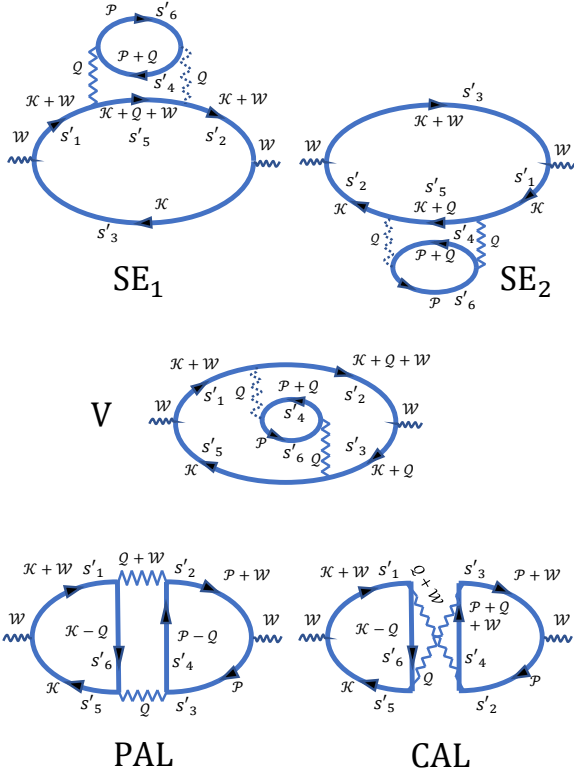
Figure 2. Leading-order diagrams for the current-current correlation function. Thick solid lines depict the matrix Green's functions, given by Eqs. (10a) and (19a) in 3D and 2D, respectively. For Hubbard interaction, the solid and broken wavy lines are identical and depict the Hubbard interaction $\lambda_d = $ const in d dimensions, and the displayed diagrams are the leading ones in the large N-approximation. For Coulomb interaction, the solid and broken wavy lines depict the dynamically and statically screened Coulomb potentials, respectively [Eqs. (28), (35a), (35b)], and the displayed diagrams are the leading ones within the random-phase approximation. The external momentum has only the frequency component: $\mathcal{W} = (\mathbf{0}, i\Omega)$. From top to bottom: self-energy (SE_1 and SE_2), vertex (V), parallel (PAL) and crossed Aslamazov-Larkin (CAL) diagrams. Indices $s'_1 \dots s'_6 = \pm 1$ indicate helicities that are being summed over.

where

$$\pi_0(\mathbf{q}, i\nu) = -\int_{\mathcal{K}} \text{Tr}\left[\hat{G}(\mathbf{k} + \mathbf{q}, i\omega + i\nu)\hat{G}(\mathbf{k}, i\omega)\right], (29)$$

is the polarization bubble, $\int_{\mathcal{K}}$ is a short-hand for $(2\pi)^{-(d+1)} \int \mathrm{d}^d k \int \mathrm{d}\omega$, and $\hat{G}$ is the free-electron Green's function given by Eqs. (10a) and (19a) in 3D and 2D, respectively. Since only the dynamic interaction contributes to dissipation, it is convenient to subtract off the static part of the interaction and treat the remaining dynamic part as the effective interaction. The dynamic

part is given by

$$V_{\text{dyn}}(\mathbf{q}, i\nu) \equiv V(\mathbf{q}, i\nu) - V(\mathbf{q}, 0)$$
$$= -V(\mathbf{q}, i\nu)V(\mathbf{q}, 0)\pi_{0,\text{dyn}}(\mathbf{q}, i\nu), \quad (30)$$

where

$$\pi_{0,\text{dyn}}(\mathbf{q}, i\nu) = \pi_0(\mathbf{q}, i\nu) - \pi_0(\mathbf{q}, 0) \qquad (31)$$

is the dynamic part of the polarization bubble. The lowest two-loop order diagrams in $V_{\text{dyn}}(\mathbf{q}, i\nu)$ are shown in Fig. 2, where now the solid and broken wavy lines depict the dynamic and static parts of the interaction, respectively.

As opposed to the Hubbard case, the Coulomb one has an additional energy scale,

$$\omega_{\text{p}d} = v_{\text{D}}\kappa_d, \qquad (32)$$

where

$$\kappa_3 = \left(4\pi e^2 N\mathcal{N}_{\text{F},3}\right)^{1/2} \qquad (33a)$$

and

$$\kappa_2 = 2\pi e^2 N\mathcal{N}_{\text{F},2} \qquad (33b)$$

are the inverse screening radii in 3D and 2D, respectively. For $d = 3$, $\omega_{\text{p}3}$ is on the order of the plasmon frequency at $q = 0$. For $d = 2$, $\omega_{\text{p}2}$ is on the order of the plasmon dispersion evaluated at $q \sim \kappa_2$. The condition for the Coulomb interaction to be treated via within RPA is $\kappa_d \ll k_{\text{F}}$, which implies that $\omega_{\text{p}d} \ll E_{\text{F}}$. Correspondingly, the frequency region $0 < \Omega \ll E_{\text{F}}$ is divided into two subregions: $0 < \Omega \ll \omega_{\text{p}d}$ and $\omega_{\text{p}d} \ll \Omega \ll E_{\text{F}}$. In the first subregion, a typical energy transfer, ν, is on the order of Ω, while a typical momentum transfer, q, is on the order of κ_d. Therefore, $\nu \ll v_{\text{D}}q \sim \omega_{\text{p}d}$. In this case, one can set $\nu = 0$ in the first factor on the RHS of Eq. (30) with the result

$$V_{\text{dyn}}(\mathbf{q}, i\nu) \approx -V^2(\mathbf{q}, 0)\pi_{0,\text{dyn}}(\mathbf{q}, i\nu). \qquad (34)$$

Diagrammatically, this amounts to replacing all the solid wavy lines by broken wavy ones in Fig. 2. Because $q \ll k_{\text{F}}$, the static screened potential is described by the usual Thomas-Fermi form:

$$V(\mathbf{q}, 0) = \begin{cases} \dfrac{4\pi e^2}{q^2 + \kappa_3^2}, & \text{for 3D} \quad (35a) \\ \dfrac{2\pi e^2}{q + \kappa_2}, & \text{for 2D.} \quad (35b) \end{cases}$$

In the second subregion ($\omega_{\text{p}d} \ll \Omega \ll E_{\text{F}}$), typical energy and momentum transfers are $\nu \sim v_{\text{D}}q \sim \Omega \gg \omega_{\text{p}d}$. In this case, screening is irrelevant and the effective dynamic interaction is given by

$$V_{\text{dyn}}(\mathbf{q}, i\nu) = -V_0^2(\mathbf{q})\pi_{0,\text{dyn}}(\mathbf{q}, i\nu), \qquad (36)$$

where $V_0(\mathbf{q})$ is the bare Coulomb potential.

Note that we do not need to use the large-N approximation for the Coulomb case, it is enough to require that the dimensional coupling constant of the Coulomb interaction

$$\alpha_{\mathrm{C}} = \frac{v_{\mathrm{D}}\kappa_d}{E_{\mathrm{F}}} \qquad (37)$$

is small, which is the condition for the validity of RPA. For the Coulomb case, therefore, we will restrict our analysis to the actual value of N for a specific system.

C. Current-current correlation function on the Matsubara axis

In this section, we describe the general structure of the diagrams for the current-current correlation function. The set of diagrams in Fig. 2 includes two self-energy (SE) diagrams, SE_1 and SE_2, a vertex correction diagram (V), and two Aslamazov-Larkin (AL) diagrams in the particle-particle and particle-hole channels, labelled as PAL ("parallel AL") and CAL ("crossed AL"), respectively. The contributions of individual diagrams to the current-current correlation function at the external $d+1$ momentum $\mathcal{W} \equiv (\mathbf{0}, i\Omega)$ are given by

$$\Pi^{\mathrm{SE}_1}(\mathcal{W}) = \frac{1}{d}\int_{\mathcal{K}} \mathrm{Tr}\left[\hat{\mathbf{v}}\hat{S}(\mathcal{K}+\mathcal{W})\cdot\hat{\mathbf{v}}\hat{G}(\mathcal{K})\right], \qquad (38\mathrm{a})$$

$$\Pi^{\mathrm{SE}_2}(\mathcal{W}) = \frac{1}{d}\int_{\mathcal{K}} \mathrm{Tr}\left[\hat{\mathbf{v}}\hat{G}(\mathcal{K}+\mathcal{W})\cdot\hat{\mathbf{v}}\hat{S}(\mathcal{K})\right], \qquad (38\mathrm{b})$$

$$\Pi^{\mathrm{V}}(\mathcal{W}) = \frac{1}{d}\int_{\mathcal{K}'} \mathrm{Tr}\left[\hat{\mathbf{\Gamma}}(\mathcal{K}';\mathcal{W})\,\hat{G}(\mathcal{K}'+\mathcal{W})\cdot\hat{\mathbf{v}}\hat{G}(\mathcal{K}')\right], \qquad (38\mathrm{c})$$

$$\Pi^{\mathrm{PAL}}(\mathcal{W}) = -\frac{1}{d}\int_{\mathcal{Q}} V_{\mathrm{st}}^2(\mathbf{q})\mathbf{A}(\mathcal{Q},\mathcal{W})\cdot\mathbf{B}(\mathcal{Q},\mathcal{W}), \qquad (38\mathrm{d})$$

$$\Pi^{\mathrm{CAL}}(\mathcal{W}) = -\frac{1}{d}\int_{\mathcal{Q}} V_{\mathrm{st}}^2(\mathbf{q})\mathbf{A}(\mathcal{Q},\mathcal{W})\cdot\mathbf{C}(\mathcal{Q},\mathcal{W}), \qquad (38\mathrm{e})$$

where

$$\hat{S}(\mathcal{L}) = \hat{G}(\mathcal{L})\hat{\Sigma}(\mathcal{L})\hat{G}(\mathcal{L}), \qquad (39\mathrm{a})$$

$$\hat{\Sigma}(\mathcal{L}) = -\int_{\mathcal{Q}} \tilde{V}(\mathcal{Q})\hat{G}(\mathcal{L}+\mathcal{Q}), \qquad (39\mathrm{b})$$

$$\tilde{V}(\mathcal{Q}) = -V_{\mathrm{st}}^2(\mathbf{q})\pi_0(\mathcal{Q}), \qquad (39\mathrm{c})$$

$$\hat{\mathbf{\Gamma}}(\mathcal{K}';\mathcal{W}) = -\int_{\mathcal{K}} \tilde{V}(\mathcal{K}'-\mathcal{K})\hat{G}(\mathcal{K})\hat{\mathbf{v}}\hat{G}(\mathcal{K}+\mathcal{W}), \qquad (39\mathrm{d})$$

$$\mathbf{A}(\mathcal{Q},\mathcal{W}) = -\int_{\mathcal{K}} \mathrm{Tr}\left[\hat{G}(\mathcal{K})\hat{\mathbf{v}}\hat{G}(\mathcal{K}+\mathcal{W})\hat{G}(\mathcal{K}-\mathcal{Q})\right], (39\mathrm{e})$$

$$\mathbf{B}(\mathcal{Q},\mathcal{W}) = -\int_{\mathcal{P}} \mathrm{Tr}\left[\hat{G}(\mathcal{P}+\mathcal{W})\hat{\mathbf{v}}\hat{G}(\mathcal{P})\hat{G}(\mathcal{P}-\mathcal{Q})\right], (39\mathrm{f})$$

$$\mathbf{C}(\mathcal{Q},\mathcal{W}) = -\int_{\mathcal{P}} \mathrm{Tr}\left[\hat{G}(\mathcal{P})\hat{G}(\mathcal{P}+\mathcal{W}+\mathcal{Q})\hat{G}(\mathcal{P}+\mathcal{W})\hat{\mathbf{v}}\right], \qquad (39\mathrm{g})$$

$\mathcal{K} \equiv (\mathbf{k},i\omega)$, $\mathcal{K}' \equiv (\mathbf{k}',i\omega)$, $\mathcal{P} \equiv (\mathbf{p},i\omega)$, $\mathcal{Q} \equiv (\mathbf{q},i\nu)$, $\pi_0(\mathcal{Q})$ is defined by Eq. (29), and $V_{\mathrm{st}}(\mathbf{q})$ is the static part of the interaction, equal to $V(\mathbf{q},0)$ [Eqs. (35a) and

(35b)] and to λ_d for the Coulomb and Hubbard cases, respectively. The expressions above are valid for Coulomb interaction at the lowest frequencies ($\Omega \ll E_{\mathrm{F}}$) and for any frequency for Hubbard interaction. Using the free rather than dressed Green's functions is justified for any frequency except for a narrow region near the direct threshold (a precise condition will be formulated later, cf. Sec. V B). The total current-current correlation function is the sum of all the contributions displayed above:

$$\Pi(\mathcal{W}) = \sum_J \Pi^J(\mathcal{W}), \qquad (40)$$

where $J \in \{\mathrm{SE}, \mathrm{V}, \mathrm{PAL}, \mathrm{CAL}\}$, and "SE" refers to both the self-energy diagrams collectively.

Equations (38a)-(38e) become more transparent if written in the electron-hole basis, in which $\hat{\mathcal{H}}_0$ is diagonal. Indeed, any diagram contains six Green's functions, each being the sum of an electron and hole parts with helicities $s' = \pm 1$, respectively. This gives rise to a set of six helicities $\mathcal{S}' = \{s_1' \ldots s_6'\}$ that are to be summed over. Thus, each diagram is the sum of $2^6 = 64$ terms

$$\Pi^J(\mathcal{W}) = \sum_{\mathcal{S}'} \Pi^J_{\mathcal{S}'}(\mathcal{W}), \qquad (41)$$

where summation goes over all 64 configurations of $\mathcal{S}'$. Each $\Pi^J_{\mathcal{S}'}(\mathcal{W})$ term in the sum contains a product of two integrals over the frequency

$$\int d\omega \prod_{l=1}^L g_{s_l}(\mathbf{k}_l, i\omega + i\nu_l)\int d\omega' \prod_{l'=1}^{L'} g_{s_{l'}}(\mathbf{k}_{l'}, i\omega' + i\nu_{l'}), \qquad (42)$$

where $L = 4$ for all diagrams, $L' = 2$ for $\mathrm{SE}_{1,2}$ and V diagrams, and $L = L' = 3$ for PAL and CAL diagrams, $s_l, s_{l'} \in \mathcal{S}'$, and $g_s(\mathbf{k}, i\omega)$ is the Green's function in the diagonal basis, defined by Eq. (10c). The integrals in Eq. (42) vanish if the poles of the integrands are located in the same halves of the complex plane. Because $\xi_{\mathbf{k}_l}^{s_l} < 0$ for $s_l = -1$, at least one of the helicities in each of the integrals in Eq. (42) must be positive for a non-zero result. Thus, instead of $2^6 = 64$ terms we would, in general, have only $2^4 = 16$ terms in the sum of helicities in Eq. (41).

D. Retarded current-current correlation function

Upon analytic continuation, the imaginary part of the retarded current-current correlation function can be written as a sum over the new terms, $\mathcal{R}^J_{\mathcal{S}}(\Omega)$:

$$\Im\Pi^J_{\mathrm{R}}(\Omega) = \sum_{\mathcal{S}'} \Im\Pi^J_{\mathcal{S}',\mathrm{R}}(\Omega) = \sum_{\mathcal{S}} \mathcal{R}^J_{\mathcal{S}}(\Omega), \qquad (43)$$

where $\mathcal{S} \in \{s_1 \ldots s_6\}$ is another set of helicities, which is different from $\mathcal{S}'$, and the subscript "R" stands for "retarded". Note that while the equality between the sums

in Eq. (43) is always valid, there is, in general, no one-to-one correspondence between the individual terms of the two sums.[40] Looking ahead, it will be convenient to represent not only the self-energy but also all other diagrams as sums of two terms, which we will distinguish by assigning a label $u = 1, 2$ to the diagram index J, i.e.,

$$\mathcal{R}_{\mathcal{S}}^{J}(\Omega) = \sum_{u=1,2} \mathcal{R}_{\mathcal{S}}^{J_u}(\Omega), \tag{44}$$

where $J_{1,2} \in \{SE_{1,2}, V_{1,2}, PAL_{1,2}, CAL_{1,2}\}$. Note that whereas the subscript u refers to two topologically dis-tinct diagrams for the SE case, its meaning for the V, PAL and CAL contributions is purely algebraic. For example, the contribution of the vertex diagram is represented by a sum of two terms in Eq. (A46), and similarly for the AL diagrams.

We remind the reader that we chose $\Omega > 0$. With this choice, as shown in Appendix A, any of the $\mathcal{R}_{\mathcal{S}}^{J_u}(\Omega)$ terms has the following structure

$$\mathcal{R}_{\mathcal{S}}^{J_u}(\Omega) = K^{J_u} \int_{\mathbf{k},\mathbf{p},\mathbf{q}} \int_{\nu} V_{\mathrm{st}}^2(\mathbf{q}) \mathcal{T}_{\mathcal{S}}^{J_u}(\mathbf{k},\mathbf{p},\mathbf{q}) \, \mathcal{G}_{\mathcal{S}}^{J_u}(\mathbf{k},\mathbf{p},\mathbf{q},\Omega)$$
$$\times \theta(\Omega + \xi_{\mathbf{k}}^{s_3})\theta(-\xi_{\mathbf{k}}^{s_3})\theta(\xi_{\mathbf{k+q}}^{s_5})\theta(-\xi_{\mathbf{p}}^{s_4})\theta(\xi_{\mathbf{p+q}}^{s_6})\delta(\Omega + \nu + \xi_{\mathbf{k}}^{s_3} - \xi_{\mathbf{k+q}}^{s_5})\delta(\nu + \xi_{\mathbf{p+q}}^{s_6} - \xi_{\mathbf{p}}^{s_4}). \tag{45}$$

[A rather complicated form of Eq. (45) will be clarified later by an example of the SE_1 diagram; see Eq. (55) and Sec. IV B.] Here, $\int_{\mathbf{n}}$ is a shorthand for $\int d^d n/(2\pi)^d$, $\int_{\nu}$ stands for $\int_{-\infty}^{\infty} d\nu/2\pi$, and

$$K^{J_u} = \begin{cases} -\pi^2/32, & \text{for } J_u = SE_{1,2}, CAL_{1,2}, \\ \pi^2/32, & \text{for } J_u = V_{1,2}, PAL_{1,2}. \end{cases} \tag{46}$$

Further, $\mathcal{T}_{\mathcal{S}}^{J_u}$ denote the trace of matrix products coming from the spinor wavefunctions and $\mathcal{G}_{\mathcal{S}}^{J_u}$ are the products of the real parts of the Green's functions, given by

$$\mathcal{T}_{\mathcal{S}}^{SE_1} = \frac{1}{d} \mathrm{Tr}\left(\hat{\mathbf{v}}\hat{M}_{\mathbf{k}}^{s_1}\hat{M}_{\mathbf{k+q}}^{s_5}\hat{M}_{\mathbf{k}}^{s_2} \cdot \hat{\mathbf{v}}\hat{M}_{\mathbf{k}}^{s_3}\right)$$
$$\times \mathrm{Tr}\left(\hat{M}_{-\mathbf{p-q}}^{s_6}\hat{M}_{-\mathbf{p}}^{s_4}\right),$$
$$\mathcal{T}_{\mathcal{S}}^{SE_2} = \frac{1}{d} \mathrm{Tr}\left(\hat{\mathbf{v}}\hat{M}_{-\mathbf{k-q}}^{s_1}\hat{M}_{-\mathbf{k}}^{s_3}\hat{M}_{-\mathbf{k-q}}^{s_2} \cdot \hat{\mathbf{v}}\hat{M}_{-\mathbf{k-q}}^{s_5}\right)$$
$$\times \mathrm{Tr}\left(\hat{M}_{\mathbf{p}}^{s_4}\hat{M}_{\mathbf{p+q}}^{s_6}\right),$$
$$\mathcal{G}_{\mathcal{S}}^{SE_1} = \frac{1}{\Omega - \xi_{\mathbf{k}}^{s_1} + \xi_{\mathbf{k}}^{s_3}} \frac{1}{\Omega - \xi_{\mathbf{k}}^{s_2} + \xi_{\mathbf{k}}^{s_3}},$$
$$\mathcal{G}_{\mathcal{S}}^{SE_2} = \frac{1}{\Omega - \xi_{\mathbf{k+q}}^{s_5} + \xi_{\mathbf{k+q}}^{s_1}} \frac{1}{\Omega - \xi_{\mathbf{k+q}}^{s_5} + \xi_{\mathbf{k+q}}^{s_2}}, \tag{47}$$

$$\mathcal{T}_{\mathcal{S}}^{V_1} = \frac{1}{d} \mathrm{Tr}\left(\hat{\mathbf{v}}\hat{M}_{\mathbf{k}}^{s_1}\hat{M}_{\mathbf{k+q}}^{s_5} \cdot \hat{\mathbf{v}}\hat{M}_{\mathbf{k+q}}^{s_2}\hat{M}_{\mathbf{k}}^{s_3}\right)$$
$$\times \mathrm{Tr}\left(\hat{M}_{-\mathbf{p-q}}^{s_6}\hat{M}_{-\mathbf{p}}^{s_4}\right),$$
$$\mathcal{T}_{\mathcal{S}}^{V_2} = \frac{1}{d} \mathrm{Tr}\left(\hat{\mathbf{v}}\hat{M}_{-\mathbf{k-q}}^{s_5}\hat{M}_{-\mathbf{k}}^{s_1} \cdot \hat{\mathbf{v}}\hat{M}_{-\mathbf{k}}^{s_3}\hat{M}_{-\mathbf{k-q}}^{s_2}\right)$$
$$\times \mathrm{Tr}\left(\hat{M}_{\mathbf{p}}^{s_4}\hat{M}_{\mathbf{p+q}}^{s_6}\right),$$
$$\mathcal{G}_{\mathcal{S}}^{V_1} = \mathcal{G}_{\mathcal{S}}^{V_2} = \frac{1}{\Omega - \xi_{\mathbf{k}}^{s_1} + \xi_{\mathbf{k}}^{s_3}} \frac{1}{\Omega - \xi_{\mathbf{k+q}}^{s_5} + \xi_{\mathbf{k+q}}^{s_2}}, \tag{48}$$

$$\mathcal{T}_{\mathcal{S}}^{PAL_1} = \frac{1}{d} \mathrm{Tr}\left(\hat{\mathbf{v}}\hat{M}_{-\mathbf{k}}^{s_1}\hat{M}_{-\mathbf{k-q}}^{s_5}\hat{M}_{-\mathbf{k}}^{s_3}\right)$$
$$\times \cdot \mathrm{Tr}\left(\hat{\mathbf{v}}\hat{M}_{\mathbf{p+q}}^{s_2}\hat{M}_{\mathbf{p}}^{s_4}\hat{M}_{\mathbf{p+q}}^{s_6}\right),$$
$$\mathcal{T}_{\mathcal{S}}^{PAL_2} = \frac{1}{d} \mathrm{Tr}\left(\hat{\mathbf{v}}\hat{M}_{-\mathbf{k}}^{s_3}\hat{M}_{-\mathbf{k-q}}^{s_5}\hat{M}_{-\mathbf{k}}^{s_1}\right)$$
$$\times \cdot \mathrm{Tr}\left(\hat{\mathbf{v}}\hat{M}_{\mathbf{p+q}}^{s_6}\hat{M}_{\mathbf{p}}^{s_4}\hat{M}_{\mathbf{p+q}}^{s_2}\right),$$
$$\mathcal{G}_{\mathcal{S}}^{PAL_1} = \mathcal{G}_{\mathcal{S}}^{PAL_2} = \frac{1}{\Omega - \xi_{\mathbf{k}}^{s_1} + \xi_{\mathbf{k}}^{s_3}} \frac{1}{\Omega - \xi_{\mathbf{p+q}}^{s_6} + \xi_{\mathbf{p+q}}^{s_2}}, \tag{49}$$

$$\mathcal{T}_{\mathcal{S}}^{CAL_1} = \frac{1}{d} \mathrm{Tr}\left(\hat{\mathbf{v}}\hat{M}_{-\mathbf{k}}^{s_1}\hat{M}_{-\mathbf{k-q}}^{s_5}\hat{M}_{-\mathbf{k}}^{s_3}\right)$$
$$\times \cdot \mathrm{Tr}\left(\hat{\mathbf{v}}\hat{M}_{\mathbf{p}}^{s_4}\hat{M}_{\mathbf{p+q}}^{s_6}\hat{M}_{\mathbf{p}}^{s_2}\right),$$
$$\mathcal{T}_{\mathcal{S}}^{CAL_2} = \frac{1}{d} \mathrm{Tr}\left(\hat{\mathbf{v}}\hat{M}_{\mathbf{k+q}}^{s_5}\hat{M}_{\mathbf{k}}^{s_3}\hat{M}_{\mathbf{k+q}}^{s_1}\right)$$
$$\times \cdot \mathrm{Tr}\left(\hat{\mathbf{v}}\hat{M}_{-\mathbf{p-q}}^{s_2}\hat{M}_{-\mathbf{p}}^{s_4}\hat{M}_{-\mathbf{p-q}}^{s_6}\right),$$
$$\mathcal{G}_{\mathcal{S}}^{CAL_1} = \frac{1}{\Omega - \xi_{\mathbf{p}}^{s_2} + \xi_{\mathbf{p}}^{s_4}} \frac{1}{\Omega - \xi_{\mathbf{k}}^{s_1} + \xi_{\mathbf{k}}^{s_3}},$$
$$\mathcal{G}_{\mathcal{S}}^{CAL_2} = \frac{1}{\Omega - \xi_{\mathbf{p+q}}^{s_6} + \xi_{\mathbf{p+q}}^{s_2}} \frac{1}{\Omega - \xi_{\mathbf{k+q}}^{s_5} + \xi_{\mathbf{k+q}}^{s_1}}. \tag{50}$$

Here, $\hat{M}_{\mathbf{l}}^{t}$ is the matrix part of the Green's function given by Eqs. (10b) and (19b) in 3D and 2D, respectively. Note that for all diagrams $\mathcal{T}_{\mathcal{S}}^{J_u}$ are separable functions of the momenta $\mathbf{k}$ and $\mathbf{p}$, i.e.,

$$\mathcal{T}_{\mathcal{S}}^{J_u}(\mathbf{k},\mathbf{p},\mathbf{q}) = \mathcal{T}_{1}^{J_u}(\mathbf{k},\mathbf{q})\mathcal{T}_{2}^{J_u}(\mathbf{p},\mathbf{q}). \tag{51}$$

From the θ-functions in Eq. (45), we see that the result is non-zero only if $\xi_{\mathbf{k+q}}^{s_5} > 0$ and $\xi_{\mathbf{p+q}}^{s_6} > 0$, which implies that

$$s_5 = s_6 = +1, \tag{52}$$

i.e., the corresponding solid lines in diagrams describe electrons in the conduction band. This is a particular instance of the general constraint discussed after Eq. (42),

thanks to which the sum over helicities contains now only $2^4 = 16$ instead of $2^6 = 64$ terms. The remaining helicities belong to the subset

$$\mathcal{S}_A \in \{s_1, s_2, s_3, s_4\}. \tag{53}$$

Therefore, the contribution of diagram J to the sum in Eq. (43) is given by the sum of 16 terms of the type $\mathcal{R}_{\mathcal{S}_A}^J(\Omega)$:

$$\Im\Pi_{\mathrm{R}}^J(\Omega) = \sum_{\mathcal{S}_A} \mathcal{R}_{\mathcal{S}_A}^J(\Omega) = \sum_{\mathcal{S}_A, u} \mathcal{R}_{\mathcal{S}_A}^{J_u}(\Omega). \tag{54}$$

Thus, the total retarded current-current correlation function $\Im\Pi_{\mathrm{R}}(\Omega)$, is given by [cf. Eqs. (40) and (43)]:

$$\Im\Pi_{\mathrm{R}}(\Omega) = \sum_J \Im\Pi_{\mathrm{R}}^J(\Omega) = \sum_{\mathcal{S}_A, J} \mathcal{R}_{\mathcal{S}_A}^J(\Omega) = \sum_{\mathcal{S}_A, J_u} \mathcal{R}_{\mathcal{S}_A}^{J_u}(\Omega)$$
$$= \sum_{s_3, s_4} \int_{\mathbf{k}, \mathbf{p}, \mathbf{q}, \nu} \mathcal{D}(\mathbf{k}, \mathbf{p}, \mathbf{q}, \nu, \Omega)$$
$$\times \sum_{J_u, s_1, s_2} K^{J_u} \mathcal{T}_{\mathcal{S}_A}^{J_u}(\mathbf{k}, \mathbf{p}, \mathbf{q}) \mathcal{G}_{\mathcal{S}_A}^{J_u}(\mathbf{k}, \mathbf{p}, \mathbf{q}, \Omega), \tag{55}$$

where

$$\mathcal{D}(\mathbf{k}, \mathbf{p}, \mathbf{q}, \nu, \Omega) = \theta(\Omega + \xi_{\mathbf{k}}^{s_3}) \theta(-\xi_{\mathbf{k}}^{s_3}) \theta(\xi_{\mathbf{k}+\mathbf{q}}^+) \theta(-\xi_{\mathbf{p}}^{s_4}) \theta(\xi_{\mathbf{p}+\mathbf{q}}^+)$$
$$\times \delta(\Omega + \nu + \xi_{\mathbf{k}}^{s_3} - \xi_{\mathbf{k}+\mathbf{q}}^+) \delta(\nu + \xi_{\mathbf{p}+\mathbf{q}}^+ - \xi_{\mathbf{p}}^{s_4}) \tag{56}$$

is the block of kinematic constraints represented by the theta- and delta-functions with Eq. (52) implemented. The θ-functions reflect the Pauli principle, while the δ-functions manifest the energy conservation. Note that $\mathcal{D}(\mathbf{k}, \mathbf{p}, \mathbf{q}, \nu)$ depends only on helicities s_3, s_4 and is the same for all diagrams; therefore, it can be pulled out of the sum over J_u, s_1, and s_2. From now onward, we assume that the constraint Eq. (52) has already been implemented.

IV. SCATTERING PROCESSES

A. Frequency thresholds

Different terms in Eq. (54) start to contribute at frequencies above certain thresholds. These thresholds can be deduced from the kinematic constraints in Eq. (56), which depend only on the helicities s_3, s_4 and are the same for all diagram types. (For the reader's convenience, helicity sets corresponding to different scattering processes are summarized in Table I.)

Equation (56) gives rise to the following kinematic constraints:

$$\xi_{\mathbf{k}+\mathbf{q}}^+ = \epsilon_{\mathbf{k}+\mathbf{q}} - E_{\mathrm{F}} > 0, \ \xi_{\mathbf{p}+\mathbf{q}}^+ = \epsilon_{\mathbf{p}+\mathbf{q}} - E_{\mathrm{F}} > 0, \tag{57a}$$

$$\xi_{\mathbf{k}}^{s_3} = s_3 \epsilon_{\mathbf{k}} - E_{\mathrm{F}} < 0, \ \xi_{\mathbf{p}}^{s_4} = s_4 \epsilon_{\mathbf{p}} - E_{\mathrm{F}} < 0, \tag{57b}$$

$$\Omega + \nu + \xi_{\mathbf{k}}^{s_3} = \xi_{\mathbf{k}+\mathbf{q}}^+; \ \xi_{\mathbf{p}}^{s_4} - \nu = \xi_{\mathbf{p}+\mathbf{q}}^+. \tag{57c}$$

The inequalities (57a) and (57c) imply that

$$E_{\mathrm{F}} - \Omega - s_3 \epsilon_{\mathbf{k}} < \nu < s_4 \epsilon_{\mathbf{p}} - E_{\mathrm{F}}, \tag{58}$$

which, in its turn, leads to

$$s_4 \epsilon_{\mathbf{p}} + s_3 \epsilon_{\mathbf{k}} > 2E_{\mathrm{F}} - \Omega. \tag{59}$$

Making all possible choices of $s_4 = \pm 1$ and $s_3 = \pm 1$, we obtain the frequency thresholds which delineate three frequency regimes, as described in the following sections.

1. All frequencies: $0 < \Omega < \omega_D$

The choice of $s_3 = s_4 = +1$ corresponds to processes whose contributions start right at $\Omega > 0$ and continue up to $\omega_D = 2E_{\mathrm{F}}$ (and beyond). Combining Eqs. (57b) and (59), we see that dispersions $\epsilon_{\mathbf{k}}$ and $\epsilon_{\mathbf{p}}$ are constrained by the following inequalities:

$$0 < \epsilon_{\mathbf{k}} < E_{\mathrm{F}}, \ 0 < \epsilon_{\mathbf{p}} < E_{\mathrm{F}}, \ \epsilon_{\mathbf{k}} + \epsilon_{\mathbf{p}} > 2E_{\mathrm{F}} - \Omega. \tag{61}$$

Geometrically, these constraints are shown in Fig. 3a. At $\Omega = 0$, the slanted line $\epsilon_{\mathbf{k}} + \epsilon_{\mathbf{p}} = 2E_{\mathrm{F}} - \Omega$ touches the corner of the square, which formed by the horizontal line $\epsilon_{\mathbf{k}} = E_{\mathrm{F}}$ and vertical line $\epsilon_{\mathbf{p}} = E_{\mathrm{F}}$. For $0 < \Omega < 2E_{\mathrm{F}}$, the slanted line $\epsilon_{\mathbf{k}} + \epsilon_{\mathbf{p}} = 2E_{\mathrm{F}}$ cuts through the square, such that the allowed values of $\epsilon_{\mathbf{k}}$ and $\epsilon_{\mathbf{p}}$ lie in the diagonally hatched region.

This regime includes processes of pure intra-band absorption ($s_1 = s_2 = +1$), when all the six states are in the conduction band, and dissipation occurs in the same way as in a DFL [29]. In addition, this regime includes scattering processes between electrons and holes. With four out of six helicities chosen positive ($s_3 = s_4 = s_5 = s_6 = +1$), either one of helicities s_1 and s_2 or both of them can be negative. Therefore, such scattering processes involve up to two states in the valence band, while the numbers of electrons and holes are not conserved separately.

As we discussed in Sec. I, absorption due to all processes described above is absent within the model of a gapped semiconductor with parabolic bands and the interaction Hamiltonian given in Eq. (16), which was considered in Refs. [31, 35–38].

2. Intermediate frequencies: $\omega_I \leq \Omega < \omega_D$

In addition to still active ee and eh processes, described in the previous section, another type of eh processes contributes to the conductivity in the intermediate-frequency regime, defined as $\omega_{\mathrm{I}} \leq \Omega < \omega_{\mathrm{D}}$. This regime corresponds to the following helicity choices: 1) $s_3 = -1$, $s_4 = +1$ and 2) $s_3 = +1$, $s_4 = -1$. For the first choice, Eqs. (57b) and (59) imply that

$$0 < \epsilon_{\mathbf{k}} < \infty, \ 0 < \epsilon_{\mathbf{p}} < E_{\mathrm{F}},$$
$$\epsilon_{\mathbf{p}} - \epsilon_{\mathbf{k}} > 2E_{\mathrm{F}} - \Omega = E_{\mathrm{F}} - \delta\Omega, \tag{62}$$

Table I. Summary of the helicity sets for different scattering processes. Here $\omega_{\mathrm{D}} = 2E_{\mathrm{F}}$, $\omega_{\mathrm{I}} = E_{\mathrm{F}}$, while *ee*, *eh1*, *eh2* stand for absorption processes involving electrons only, one hole, and two holes, respectively. Note that for Auger-Meitner (AM) processes, the choices of $s_1 = \pm 1$ and $s_2 = \pm 1$ are not correlated either to each other or to the choices of s_3 and s_4, while the choices of s_3 and s_4 are correlated to each other. Examples of diagrams involving *eh1* and *eh2* processes are shown in Fig. 5; examples of diagrams involving AM processes are shown in Fig. 6.

Frequency range	Type	s_1	s_2	s_3	s_4	s_5	s_6
$0 < \Omega < \omega_{\mathrm{D}}$	*ee*	$+1$	$+1$	$+1$	$+1$	$+1$	$+1$
$0 < \Omega < \omega_{\mathrm{D}}$	*eh1*	± 1	∓ 1	$+1$	$+1$	$+1$	$+1$
$0 < \Omega < \omega_{\mathrm{D}}$	*eh2*	-1	-1	$+1$	$+1$	$+1$	$+1$
$\omega_{\mathrm{I}} < \Omega < \omega_{\mathrm{D}}$	AM	± 1	± 1	± 1	∓ 1	$+1$	$+1$

where $\delta\Omega \equiv \Omega - E_{\mathrm{F}}$. Geometrically, these constraints are depicted in Fig. 3b. The constraints are satisfied if the line $\epsilon_{\mathbf{p}} - \epsilon_{\mathbf{k}} = E_{\mathrm{F}} - \delta\Omega$ cuts across the semi-infinite band, defined by the inequalities $0 < \epsilon_{\mathbf{k}} < \infty$ and $0 < \epsilon_{\mathbf{p}} < E_{\mathrm{F}}$, which is only possible if $\Omega > E_{\mathrm{F}} = \omega_{\mathrm{I}}$. The contribution from the second choice, $s_4 = -1, s_3 = +1$, can be re-written in terms of the first one via an appropriate re-labelling of helicities, and thus this case does not need to be analyzed separately.

The threshold $\Omega = \omega_{\mathrm{I}}$ demarcates the onset of AM-like processes, first introduced in the context of doped semi-conductors in Ref. [31] and further studied in Refs. [35–38]. Feynman diagrams for absorption due to AM processes can be understood pictorially by looking at Fig. 4, which shows two kinds of AM processes: for $s_3 = -s_4 = -1$ (panel *a*) and $s_3 = -s_4 = +1$ (panel *b*). In Fig. 4a, an incoming photon of energy $\Omega > \omega_{\mathrm{I}}$ creates a hole state and a virtual state at the same momentum. The virtual state decays into an electron and a particle-hole pair, formed by two electron states with energy ν. The particle-hole pair and the electron then decay into another virtual state, which annihilates the hole, and the photon is emitted back. In Fig. 4b, an incoming photon creates an electron and a virtual state. The virtual state decays into a real electron and a particle-hole pair, formed by the electron in the conduction band and hole in the valence band. Finally the virtual state annihilates

the electron, and the photon is emitted back.

3. High frequencies: $\Omega > \omega_{\mathrm{D}}$

As we said before, absorption for $\Omega > \omega_{\mathrm{D}}$ occurs even in the absence of electron-electron interaction. The corresponding optical conductivity is plateaued at the universal value in 2D and increases linearly with frequency in 3D. Electron-electron interaction gives rise to logarithmic renormalizations of the velocity and coupling constant [1, 12, 13], which occur already to first order in the static interaction. Dissipative processes, considered in this paper, contribute only to second order in the interaction (cf. Fig. 2) and thus can be neglected in this frequency range.

As the final remark for this section, we note that, in addition to being independent of the diagram type, the frequency thresholds are also independent of a particular form of the dispersion and dimensionality.

B. Archetypal contributions to the optical conductivity

We now analyze the structure of $\mathcal{R}_{\mathcal{S}_A}^{J_u}$ [Eq. (55)], using one of the self-energy diagram, namely, SE_1 in Fig. 2, as an example. As follows from Eq. (55), the contribution of this diagram can be written as

$$\sum_{\mathcal{S}_A} \mathcal{R}_{\mathcal{S}_A}^{\mathrm{SE}_1}(\Omega) = -\frac{\pi^2}{32} \int_{\mathbf{k},\mathbf{p},\mathbf{q}} \theta(-\xi_{\mathbf{k}}^{s_3})\theta(\Omega + \xi_{\mathbf{k}}^{s_3}) \sum_{\mathcal{S}_A} \frac{\mathcal{T}_{\mathcal{S}_A}^{\mathrm{SE}_1}(\mathbf{k},\mathbf{p},\mathbf{q})}{(\Omega - \xi_{\mathbf{k}}^{s_1} + \xi_{\mathbf{k}}^{s_3})(\Omega - \xi_{\mathbf{k}}^{s_2} + \xi_{\mathbf{k}}^{s_3})}\mathcal{U}(\mathbf{k},\mathbf{p},\mathbf{q},\Omega + \xi_{\mathbf{k}}^{s_3}), \quad (64)$$

where we used the third line of Eq. (47) for $\mathcal{G}_{\mathcal{S}_A}^{\mathrm{SE}_1}$, $\mathcal{T}_{\mathcal{S}_A}^{\mathrm{SE}_1}$ is given by first line of the same equation, and

$$\mathcal{U}(\mathbf{k},\mathbf{p},\mathbf{q},\omega) = \int_{\nu} V_{\mathrm{st}}^2(\mathbf{q})\theta(\xi_{\mathbf{k}+\mathbf{q}}^+)\theta(-\xi_{\mathbf{p}}^{s_4})\theta(\xi_{\mathbf{p}+\mathbf{q}}^+)\delta(\omega + \nu - \xi_{\mathbf{k}+\mathbf{q}}^+)\delta(\nu + \xi_{\mathbf{p}+\mathbf{q}}^+ - \xi_{\mathbf{p}}^{s_4}). \quad (65)$$

The structure of the expressions above can be understood by comparing them to their counterparts for the scalar case, when the trace part in Eq. (64) is equal to

unity. For our choice of $\Omega > 0$, the theta-functions in Eq. (64) come from the difference of the Fermi functions in the current-current bubble of the SE_1 diagram, where

Table II. Summary of the analytic results for the optical conductivity of 2D and 3D Dirac metals, $\Re\sigma(\Omega)$, with Hubbard interaction. Here, $\eta_d = \Re\sigma(\Omega)/\sigma_{0d}\alpha_{\rm H}^2 N^2$, $\sigma_{0d} = e^2 k_{\rm F}^{d-2}/\hbar$, $k_{\rm F}$ is the Fermi momentum, $d = 2, 3$ is the spatial dimensionality, $\alpha_{\rm H}$ is the dimensionless coupling constant of Hubbard interaction [Eq. (27)], and N is number of flavors. The results are valid in two regions: at the lowest frequencies (first row), $\Omega \ll E_{\rm F}$, and just above $\omega_{\rm I} = E_{\rm F}$ (second row), where Auger-Meitner (AM) processes start to contribute, i.e., for $0 \le \delta\Omega \equiv \Omega - \omega_{\rm I} \ll E_{\rm F}$, where $\omega_{\rm I} = E_{\rm F}$ is the indirect threshold. Equation numbers after the formulas refer to their locations in the text.

Frequency range	η_3	η_2
$\Omega \ll E_{\rm F}$	$\frac{4}{175\pi}\left(\frac{\Omega}{E_{\rm F}}\right)^2$; (90)	$\left(\frac{1}{80\pi^2}\ln\frac{E_{\rm F}}{\Omega} + \frac{5\ln 2 + 4}{200\pi^2}\right)\left(\frac{\Omega}{E_{\rm F}}\right)^2$; (107)
$0 < \delta\Omega \ll E_{\rm F}$	$\frac{71}{3240\pi}\left(\frac{\delta\Omega}{E_{\rm F}}\right)^5$; (94)	$\frac{5}{108\sqrt{3}\pi}\left(\frac{\delta\Omega}{E_{\rm F}}\right)^4$; (108)

Table III. Summary of the analytic results for the optical conductivity of 2D and 3D Dirac metals, $\Re\sigma^{\rm C}(\Omega)$, with Coulomb interaction. Here, $\eta_d^{\rm C} = \Re\sigma^{\rm C}(\Omega)/\sigma_{0d}$, $\alpha_{\rm C}$ is the dimensionless coupling constant of the Coulomb interaction [Eq. (37)], and $\omega_{{\rm p}d}$ is the effective plasma frequency in d dimensions, defined in Eq. (32). The rest of notations are the same as Table II. Equation numbers after the formulas refer to their location in the text.

Frequency range	$\eta_3^{\rm C}$	$\eta_2^{\rm C}$
$\Omega \ll \omega_{{\rm p}d} \ll E_{\rm F}$	$\frac{1}{480}\alpha_{\rm C}\left(\frac{\Omega}{E_{\rm F}}\right)^2$; (80)	$\left(\frac{1}{80\pi^2}\ln\frac{v_{\rm D}\kappa_2}{\Omega} + \frac{5\ln 2 - 2}{16\pi^2}\right)\left(\frac{\Omega}{E_{\rm F}}\right)^2$; (101)
$\omega_{{\rm p}d} \ll \Omega \ll E_{\rm F}$	$\frac{(3-4\ln 2)}{24\pi}\alpha_{\rm C}^4\left(\frac{E_{\rm F}}{\Omega}\right)$; (83)	$\frac{5}{576\pi^2}\frac{e^2}{v_{\rm D}}$; (103)
$0 < \delta\Omega \ll E_{\rm F}$	$\frac{71}{3240\pi}\alpha_{\rm C}^4\left(\frac{\delta\Omega}{E_{\rm F}}\right)^5$; (95)	$\frac{5}{108\sqrt{3}\pi}\alpha_{\rm C}^2\left(\frac{\delta\Omega}{E_{\rm F}}\right)^4$; (109)

the imaginary part of the Green's function at the bottom of SE$_1$ diagram was replaced by the δ-function, and the ensuing constraint on the frequency ($\omega = \xi_{\bf k}^{s_3}$) was resolved. Next, with the trace part replaced by unity, the integral of $\mathcal{U}({\bf k}, {\bf p}, {\bf q}, \Omega + \xi_{\bf k}^{s_3})$ in Eq. (65) over ${\bf p}$ and ${\bf q}$ gives the imaginary part of the self-energy at momentum ${\bf k}$ and frequency $\omega = \Omega + \xi_{\bf k}^{s_3}$. The denominator of the integrand in Eq. (64) comes from the product of the real parts of two Green's functions adjacent to the self-energy block.

As noted earlier, the theta- and delta-function constraints are the same for all diagrams with the only difference being the scalar factors K^{J_u}, the trace factors $\mathcal{T}_{\mathcal{S}}^{J_u}$ and the products $\mathcal{G}_{\mathcal{S}}^{J_u}$. Thus, similarly, the contribution from V$_1$ diagram is given by

$$\sum_{\mathcal{S}_A} \mathcal{R}_{\mathcal{S}_A}^{{\rm V}_1}(\Omega) = \frac{\pi^2}{32}\int_{{\bf k},{\bf p},{\bf q}}\theta(-\xi_{\bf k}^{s_3})\theta(\Omega + \xi_{\bf k}^{s_3})\sum_{\mathcal{S}_A}\frac{\mathcal{T}_{\mathcal{S}_A}^{{\rm V}_1}({\bf k},{\bf p},{\bf q})}{(\Omega - \xi_{\bf k}^{s_1} + \xi_{\bf k}^{s_3})(\Omega - \xi_{{\bf k}+{\bf q}}^{+} + \xi_{{\bf k}+{\bf q}}^{s_2})}\mathcal{U}({\bf k},{\bf p},{\bf q},\Omega + \xi_{\bf k}^{s_3}), \qquad (66)$$

and so on for other values of J_u.

For the reader's convenience, the analytic results for the optical conductivity are summarized in Tables II and III for Hubbard and Coulomb interactions, respectively.

V. OPTICAL CONDUCTIVITY OF A 3D DIRAC METAL

In this section, we derive the analytic results for the optical conductivity of a 3D Dirac metal.

A. Lowest frequencies: $\Omega \ll E_{\rm F}$

This is the case with $s_3 = s_4 = +1$ (cf. Sec. IV A 1). With s_3 and s_4 being fixed, the only free helicities remaining are s_1 and s_2. The case $s_1 = s_2 = +1$ corresponds to a purely intra-band absorption, with all states being in the conduction band. The cases of $s_1 = -s_2 = \pm 1$ and $s_1 = s_2 = -1$ correspond to absorption due to scattering processes which involve up to two holes.

1. Intra-band absorption due to electron-electron interaction

We start with purely intra-band absorption due to electron-electron (ee) interaction, when all the helicities are positive: $s_i = +1$, $i = 1 \ldots 6$. Because the hole states
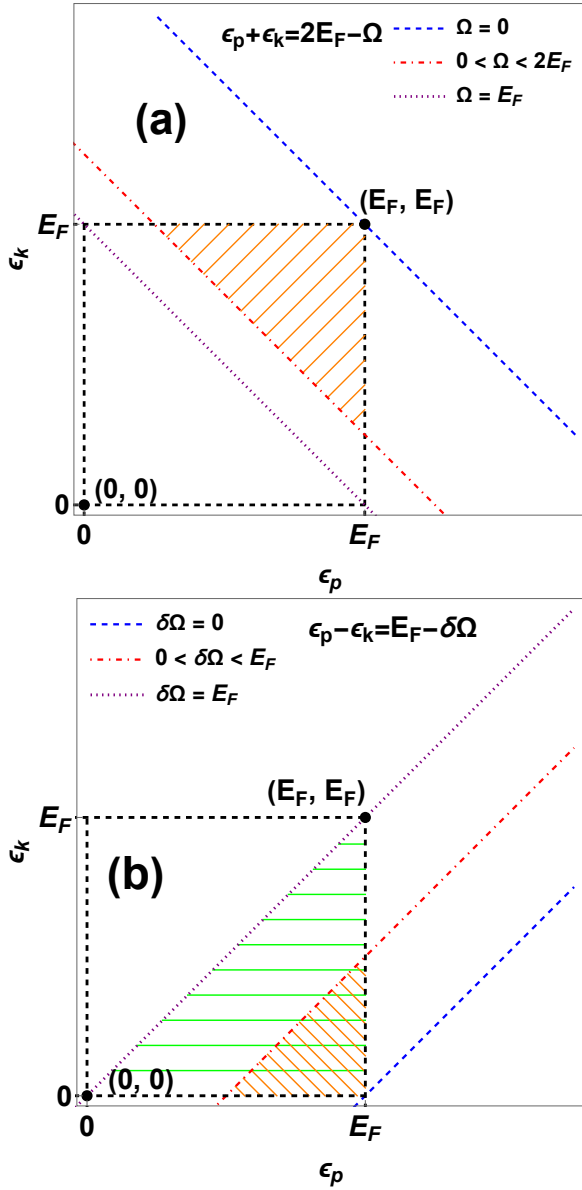
Figure 4. Examples of Auger-Meitner–like processes corresponding to two different helicity sets: $s_3 = -1, s_4 = +1$ (panel a) and $s_3 = +1, s_4 = -1$ (panel b). The state on the horizontal dashed line is a virtual (off-shell) one.

balance", $(\Delta \mathbf{v})^2$, to the integrand of the expression of the conductivity. Here, $\Delta \mathbf{v}$ is the difference between the velocities of the initial and final states of an *ee* scattering process. The same factor appears in our case as well. To see this, we first note that in the *ee* case the denominators of the fractions in Eqs. (64) and (66) are reduced to a factor of Ω^2 (and the same is true for other contributions). Next, as shown in Appendix C, the sum of the trace parts of all diagrams in Fig. 2 is given by

$$
\begin{aligned}
\mathcal{T}_{\mathcal{S}_+} &= \sum_{J_u} K^{J_u} \mathcal{T}_{\mathcal{S}_+}^{J_u}(\mathbf{k}, \mathbf{p}, \mathbf{q}) \\
&= -\frac{\pi^2}{64} (\Delta \mathbf{v})^2 \left| \Phi_{\mathbf{p}, \mathbf{p}+\mathbf{q}}^{+,+} \right|^2 \left| \Phi_{\mathbf{k}, \mathbf{k}+\mathbf{q}}^{+,+} \right|^2,
\end{aligned}
\tag{67}
$$

where K^{J_u} is defined in Eq. (46), $\mathcal{S}_+$ denotes the set $\{s_1 = +1, s_2 = +1 \ldots s_6 = +1\}$, $J_{1,2} \in \{\mathrm{SE}_{1,2}, \mathrm{V}_{1,2}, \mathrm{PAL}_{1,2}, \mathrm{CAL}_{1,2}\}$,

$$
\Delta \mathbf{v} = \mathbf{v}_{\mathbf{k}}^{+,+} + \mathbf{v}_{\mathbf{p}+\mathbf{q}}^{+,+} - \mathbf{v}_{\mathbf{k}+\mathbf{q}}^{+,+} - \mathbf{v}_{\mathbf{p}}^{+,+}, \tag{68}
$$

$\mathbf{v}_{\mathbf{k}}^{+,+}$ is the matrix element of the velocity operator between electron-like states, given by Eq. (13), and $\Phi_{\mathbf{k}, \mathbf{k}'}^{+,+} = \langle \mathbf{k}, +|\mathbf{k}', +\rangle$ is the matrix element of two electron-like states.[44] $\Delta \mathbf{v}$ in Eq. (68) is the change in the total velocity (proportional to the current) due a to collision between two electrons with initial momenta $\mathbf{k}$ and

Figure 3. a) Region in the $(\epsilon_{\mathbf{k}}, \epsilon_{\mathbf{p}})$ plane contributing to absorption due to electron-electron and electron-hole scattering processes, described in Sec. IV A 1, for frequencies in the range $0 < \Omega < \omega_{\mathrm{D}} = 2E_{\mathrm{F}}$. Straight lines are the equations $\epsilon_{\mathbf{p}} + \epsilon_{\mathbf{k}} = 2E_{\mathrm{F}} - \Omega$, for different choices of Ω, as specified in the legend. b) Region in the $(\epsilon_{\mathbf{k}}, \epsilon_{\mathbf{p}})$ plane contributing to absorption due to AM-like processes, described in Sec. IV A 2, which occur in the range $\omega_{\mathrm{I}} = E_{\mathrm{F}} < \Omega < 2E_{\mathrm{F}}$. Straight lines are the equations $\epsilon_{\mathbf{p}} - \epsilon_{\mathbf{k}} = E_{\mathrm{F}} - \delta\Omega$, for different choices of Ω, as specified in the legend.

in this case are totally passive, one can view the system as a FL, which is isotropic yet not Galilean-invariant due to a non-parabolicity of the electron spectrum, i.e., as a DFL. The absorption probability in this case is severely restricted by momentum conservation. In Refs. [29, 41–43] it was shown that, for the single-band case, momentum conservation brings in a factor of the "velocity im-
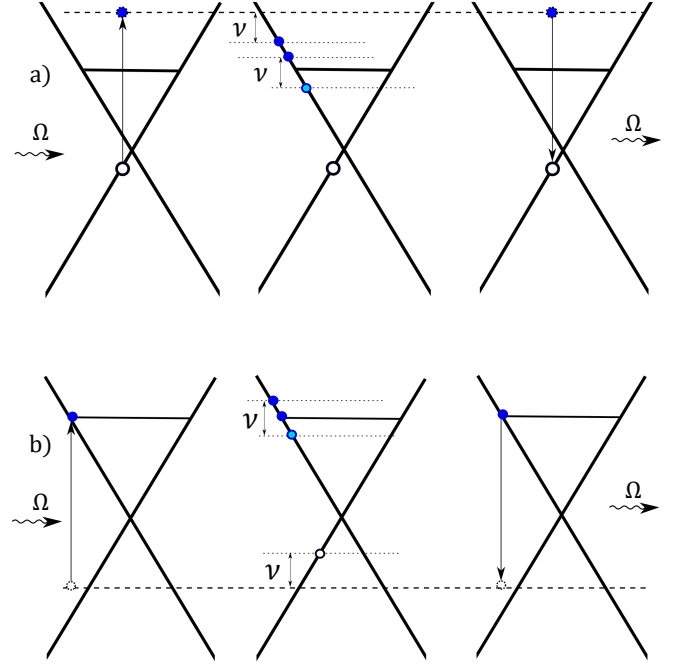
$\mathbf{p} + \mathbf{q}$, and final momenta $\mathbf{k} + \mathbf{q}$ and $\mathbf{p}$, respectively. In a Galilean-invariant system, momentum-conserving electron-electron scattering does not lead to current relaxation and thus does not affect the conductivity. Indeed, we see that $\Delta\mathbf{v} = 0$ if $\mathbf{v}_{\mathbf{k}}^{+,+} = \mathbf{k}/m$ with m being the electron mass. A Dirac metal has finite conductivity only inasmuch as it violates Galilean invariance. Furthermore, even if the system is not Galilean-invariant but isotropic, $\Delta\mathbf{v}$ vanishes if all the momenta in Eq. (68) are projected onto the Fermi surface and, to get a finite conductivity, one needs to expand $\Delta\mathbf{v}$ near the Fermi surface. For $\Omega \ll E_{\mathrm{F}}$, a typical deviation of the quasiparticle energy from the Fermi energy is on the order of Ω. Then $(\Delta\mathbf{v})^2$ can be estimated as

$$(\Delta\mathbf{v})^2 \sim w^2 \left(\frac{\Omega}{k_{\mathrm{F}}} \right)^2, \qquad (69)$$

where the "non-parabolicity coefficient"

$$w = 1 - \frac{1}{2} \frac{\mathrm{d}^2 \epsilon_{\mathbf{k}}}{\mathrm{d}k^2} \frac{\mathrm{d}(k^2)}{\mathrm{d}\epsilon_{\mathbf{k}}} \bigg|_{k=k_{\mathrm{F}}} \qquad (70)$$

quantifies a deviation from Galilean invariance [29]. Introducing a gapped Dirac spectrum, $\epsilon_{\mathbf{k}} = \sqrt{v_{\mathrm{D}}^2 k^2 + \Delta^2}$, for a moment, we get

$$w = 1 - \frac{\Delta^2}{(\Delta + E_{\mathrm{F}})^2}. \qquad (71)$$

For $E_{\mathrm{F}} \gg \Delta$, the Dirac spectrum is almost linear, and thus the deviation from the Galilean-invariant case is the strongest. In this case, $w = 1 - \Delta^2/E_{\mathrm{F}}^2 \approx 1$. For $E_{\mathrm{F}} \ll \Delta$, the gapped Dirac spectrum is almost parabolic and, correspondingly, w is small: $w \approx 2E_{\mathrm{F}}/\Delta \ll 1$.

To obtain an order-of-magnitude estimate for the conductivity due to ee interaction, one can replace the trace part of Eq. (64) by $(\Delta\mathbf{v})^2$, and use Eq. (69) with $w = 1$ for $(\Delta\mathbf{v})^2$ (gapless Dirac spectrum). This yields the following estimate for the conductivity

$$\Re\sigma_{\mathrm{ee}}(\Omega) \sim \frac{e^2}{\Omega^3} \int_{\mathbf{k}} \theta(-\xi_{\mathbf{k}}^+)\theta(\Omega + \xi_{\mathbf{k}}^+)|\Im\Sigma_{\mathrm{ee}}(\mathbf{k}, \Omega + \xi_{\mathbf{k}}^+)|(\Delta\mathbf{v})^2. \qquad (72)$$

As discussed just below Eq. (65), the theta-function constraints in the equation above come from the current-current bubble with the choice of $\Omega > 0$. Furthermore,

$$\Im\Sigma_{\mathrm{ee}}(\mathbf{k}, \omega) \sim -\int_{\nu}\int_{\mathbf{p},\mathbf{q}} V_{\mathrm{st}}^2(\mathbf{q})\theta(\xi_{\mathbf{k}+\mathbf{q}}^+)\theta(-\xi_{\mathbf{p}}^+)\theta(\xi_{\mathbf{p}+\mathbf{q}}^+)\delta(\omega + \nu - \xi_{\mathbf{k}+\mathbf{q}}^+)\delta(\nu + \xi_{\mathbf{p}+\mathbf{q}}^+ - \xi_{\mathbf{p}}^+) \qquad (73)$$

is the imaginary part of the self-energy due to ee interaction. As long as $\Omega \ll E_{\mathrm{F}}$, typical electronic momenta are close to k_{F}, therefore, $\xi_{\mathbf{k}}^+ \sim \Omega$, and the integral over $\mathbf{k}$ gives a factor of $\mathcal{N}_{\mathrm{F},3}\Omega$. Therefore,

$$\Re\sigma_{\mathrm{ee}}(\Omega) \sim e^2 \mathcal{N}_{F,3} \frac{|\Im\Sigma_{\mathrm{ee}}(\Omega)|}{\Omega^2} \left(\frac{\Omega}{k_{\mathrm{F}}} \right)^2, \qquad (74)$$

where $\Sigma_{\mathrm{ee}}(\Omega) \equiv \Sigma_{\mathrm{ee}}(k_{\mathrm{F}}, \Omega)$.

For the Hubbard case, the self-energy is of the usual FL form,

$$\Im\Sigma_{\mathrm{ee}}(\Omega) \sim -(N\alpha_{\mathrm{H}})^2 \frac{\Omega^2}{E_{\mathrm{F}}}, \qquad (75)$$

and thus

$$\Re\sigma_{\mathrm{ee}}(\Omega) \sim e^2 k_{\mathrm{F}}(N\alpha_{\mathrm{H}})^2 \left(\frac{\Omega}{E_{\mathrm{F}}} \right)^2. \qquad (76)$$

A detailed calculation presented in Appendix B gives

$$\Re\sigma_{\mathrm{ee}}(\Omega) = \frac{38}{4725\pi} \frac{e^2 k_{\mathrm{F}}}{\hbar}(N\alpha_{\mathrm{H}})^2 \left(\frac{\Omega}{E_{\mathrm{F}}} \right)^2, \qquad (77)$$

which agrees with the estimate (76).

The Coulomb case for $\Omega \ll \omega_{\mathrm{p3}} \ll E_{\mathrm{F}}$ is similar to the Hubbard one, in a sense that the self-energy is also of the canonical FL form, except for a different coupling constant:

$$\Im\Sigma_{\mathrm{ee}}(\Omega) \sim -\frac{\kappa_3}{k_{\mathrm{F}}} \frac{\Omega^2}{E_{\mathrm{F}}}. \qquad (78)$$

Consequently, the conductivity is obtained by replacing $(N\alpha_{\mathrm{H}})^2$ with κ_3/k_{F} in Eq. (76),

$$\Re\sigma_{\mathrm{ee1}}^{\mathrm{C}}(\Omega) \sim e^2 \kappa_3 \left(\frac{\Omega}{E_{\mathrm{F}}} \right)^2. \qquad (79)$$

The actual calculation gives

$$\Re\sigma_{\mathrm{ee1}}^{\mathrm{C}}(\Omega) = \frac{1}{480} \frac{e^2 k_{\mathrm{F}}}{\hbar} \alpha_{\mathrm{C}} \left(\frac{\Omega}{E_{\mathrm{F}}} \right)^2, \qquad (80)$$

which agrees with the estimate in Eq. (79).[45]

In the range of frequencies $\omega_{\mathrm{p3}} \ll \Omega \ll E_{\mathrm{F}}$, electrons interact with their own plasmon modes. In this regime, we can replace the screened Coulomb potential with the bare one, as specified in Eq. (36). Recalling also that the imaginary part of the retarded polarization bubble behaves as $\Im\pi_{0,\mathrm{R}}(\mathbf{q}, \omega) \sim \mathcal{N}_{\mathrm{F},3}\omega/v_{\mathrm{F}}q$ for $|\omega|/v_{\mathrm{F}} \leq q \ll$
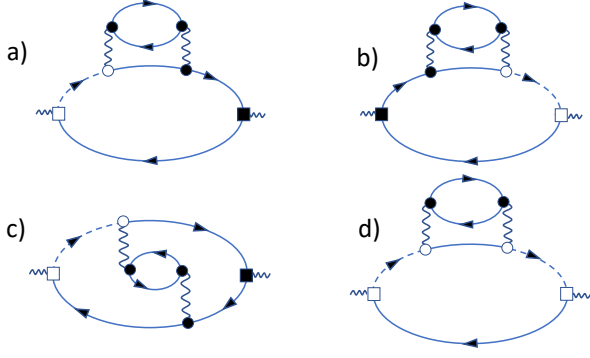
Figure 5. Examples of single-hole (a-c) and two-hole (d) diagrams. Solid (dashed) lines depict the Green's functions in the diagonal basis [Eq. (10c)] for positive (negative) helicities. The filled and blank circles denote matrix elements of ee and eh interactions, respectively. The filled and blank squares denote the intra- and inter-band current vertices, respectively.

k_F, we obtain the following estimate for the imaginary part of the self-energy

$$\Im\Sigma_{ee}(\Omega) \sim -\frac{\kappa_3^4}{\mathcal{N}_{F,3}v_F^2}\int_0^\Omega d\nu\,\nu \int_{\max\{\Omega,\Omega-\nu\}/v_F}^\infty \frac{dq}{q^4}$$
$$\sim -\frac{\kappa_3^2}{k_F^2}\frac{\omega_{p3}^2}{\Omega}. \tag{81}$$

A crossover between Eqs. (78) and (81) occurs at $\Omega \sim \omega_{p3}$, as it should. Substituting Eq. (81) into (74), we obtain

$$\Re\sigma_{ee2}^C(\Omega) \sim e^2\frac{\kappa_3^4}{k_F^3}\frac{E_F}{\Omega} \sim \frac{e^6 k_F^2}{\hbar v_D \Omega}, \tag{82}$$

and the actual calculation gives

$$\Re\sigma_{ee2}^C(\Omega) = \frac{(3-4\ln 2)}{24\pi}\frac{e^2 k_F}{\hbar}\alpha_C^4\left(\frac{E_F}{\Omega}\right), \tag{83}$$

which matches the estimate (82). Equations (80) and (83) imply that the conductivity exhibits a maximum at $\Omega \sim \omega_{p3}$.

2. Absorption processes involving up to two holes

We now turn to absorption processes that involve holes. There are two types of such processes: with one hole (eh1) and with two holes (eh2). Recalling that $s_3 = s_4 = +1$ in the all-frequencies regime (cf. Sec. IV A 1), we have two choices: $s_1 = -s_2 = \pm 1$, which corresponds to eh1, and $s_1 = s_2 = -1$, which corresponds to eh2. Examples of eh1 and eh2 diagrams are shown in Fig. 5, where the solid and dashed lines depict the electron and hole Green's functions, respectively, given by Eq. (10c) with $s = \pm 1$.

We first look at the eh1 case, when the sum over helicities in the second line of Eq. (66) contains two

terms: one with $s_1 = +1, s_2 = -1$ and another one with $s_1 = -1, s_2 = +1$. In eh1 diagrams (Fig. 5a-c), one of the current vertices is of the intra-band type while another one is of the inter-band type. In self-energy diagrams a and b, the current vertices enter at the same momenta and are thus orthogonal to each other, see Eqs. (13) and (14). Therefore, the eh1 self-energy diagrams vanish. On the other hand, vertex-type diagrams, e.g., diagram c in Fig. 5, contain current vertices at different momenta, which are not orthogonal to each other, and thus the vertex contribution is finite. In what follows, we will analyze the eh1 vertex diagrams, whose general algebraic structure is given by Eq. (66).

As soon as a scattering process involves at least one hole, constraints due to momentum conservation are lifted, and the factor of $(\Delta\mathbf{v})^2$ does not bring an additional smallness to the result. However, in contrast to the ee case, typical energies involved are now on the order of E_F rather than Ω, and the eh1 contribution to the conductivity still scales as Ω^2. Indeed, the sum over $s_1 = -s_2 = \pm 1$ in Eq. (66) gives a factor of $1/(\Omega - 2\epsilon_{\mathbf{k+q}})(\Omega + 2\epsilon_\mathbf{k})$ which, for $\Omega \ll E_F$ and $\epsilon_\mathbf{k}, \epsilon_{\mathbf{k+q}} \approx E_F$, is of order $1/E_F^2$, as opposed to $1/\Omega^2$ for the ee case, cf. Eq. (74). Next, the intra- and inter-band matrix elements of the velocity can be estimated as v_D. Finally, a joint between the dashed and solid lines brings in an inter-band matrix element, $\langle\bar{\mathbf{k}}, +|\bar{\mathbf{k}}', -\rangle$, where $\bar{\mathbf{k}}$ and $\bar{\mathbf{k}}'$ are the typical electron momenta. With all of the above taken into account, the eh1 contribution to the conductivity can be estimated as

$$\Re\sigma_{eh1} \sim e^2\mathcal{N}_{F,3}v_D^2\left|\langle\bar{\mathbf{k}}, +|\bar{\mathbf{k}}', -\rangle\right|\frac{|\Im\Sigma_{ee}(\Omega)|}{E_F^2}. \tag{84}$$

For Hubbard interaction, $\Im\Sigma_{ee}(\Omega)$ is given by Eq. (75), while $|\bar{\mathbf{k}} - \bar{\mathbf{k}}'| \sim k_F$ and this $\left|\langle\bar{\mathbf{k}}, +|\bar{\mathbf{k}}', -\rangle\right| \sim 1$. Then

$$\Re\sigma_{eh1}(\Omega) \sim e^2 k_F(N\alpha_H)^2\left(\frac{\Omega}{E_F}\right)^2, \tag{85}$$

which is of the same order as the ee contribution, Eq. (76). The actual calculation of the eh1 contribution gives

$$\Re\sigma_{eh1}(\Omega) = \frac{4}{945\pi}\frac{e^2 k_F}{\hbar}(N\alpha_H)^2\left(\frac{\Omega}{E_F}\right)^2, \tag{86}$$

which matches the estimate Eq. (85).

The two-hole case is similar to the single-hole one, except for now there are two matrix elements between electron and hole states, see Fig. 5c. Therefore, the eh2 contribution to the conductivity can be estimated as

$$\Re\sigma_{eh2}(\Omega) \sim e^2\mathcal{N}_{F,3}v_D^2\left|\langle\bar{\mathbf{k}}, +|\bar{\mathbf{k}}', -\rangle\right|^2\frac{\Im\Sigma_{ee}(\Omega)}{E_F^2}. \tag{87}$$

For Hubbard interaction, the matrix element is on the order of unity, and

$$\Re\sigma_{eh2}(\Omega) \sim \Re\sigma_{eh1}(\Omega) \sim \Re\sigma_{ee}(\Omega), \tag{88}$$

whereas the actual calculation gives

$$\Re\sigma_{\mathrm{eh2}}(\Omega) = \frac{2}{189\pi} \frac{e^2 k_{\mathrm{F}}}{\hbar} (N\alpha_{\mathrm{H}})^2 \left(\frac{\Omega}{E_{\mathrm{F}}}\right)^2. \quad (89)$$

The final result for the conductivity at the lowest frequencies ($\Omega \ll E_{\mathrm{F}}$) due to Hubbard interaction is the sum of the *ee*, *eh1*, and *eh2* contributions, given by Eqs. (77), (86), and (89):

$$\Re\sigma_{\mathrm{LF}}(\Omega) = \frac{4}{175\pi} \frac{e^2 k_{\mathrm{F}}}{\hbar} (N\alpha_{\mathrm{H}})^2 \left(\frac{\Omega}{E_{\mathrm{F}}}\right)^2. \quad (90)$$

Note that Eq. (90) is valid for a gapless Dirac spectrum. For an almost parabolic spectrum, e.g., a gapped Dirac spectrum in the limit of $E_{\mathrm{F}} \ll \Delta$, the *ee* contribution is suppressed due to a small value of the non-parabolicity coefficient w [cf. Eq. (70)]. The *eh1* and *eh2* contributions are also suppressed because the eigenstates of the Hamiltonians (7b) and (17b) are either electron-like or hole-like and, therefore, the matrix elements $\langle\mathbf{k},+|\mathbf{k}',-\rangle$ are small. In addition, there is also a partial cancellation between the diagrams in this case [46]. As a result, the total conductivity for an almost parabolic Dirac spectrum acquires a small factor of $(E_{\mathrm{F}}/\Delta)^2 \ll 1$. This is why these contributions were neglected in Refs. [31, 35–38].

For Coulomb interaction, $|\bar{\mathbf{k}} - \bar{\mathbf{k}}'| \sim \kappa_3 \ll k_{\mathrm{F}}$ and, therefore, the matrix element between almost orthogonal electron and hole states is small: $\left|\langle\bar{\mathbf{k}},+|\bar{\mathbf{k}}',-\rangle\right| \sim \kappa_3/k_{\mathrm{F}} \ll 1$. Therefore, the *eh1* and *eh2* contributions to the conductivity are smaller than the *ee* one in Eq. (79) by a factor of κ_3/k_{F} and $(\kappa_3/k_{\mathrm{F}})^2$, respectively. Thus, these contributions can be neglected, and the leading contribution to the conductivity for the Coulomb case is still given by Eqs. (80) and (83).

B. Intermediate frequencies: $\omega_{\mathrm{I}} \leq \Omega < \omega_{\mathrm{D}}$

In the intermediate frequency regime, there are eight possible terms contributing for each type of diagrams. These terms are specified by the helicities $s_3 = -s_4$ and four possibilities of $s_1, s_2 = \pm 1$ therein. As shown in Sec. IV A 2), these terms start to contribute only for Ω above the indirect threshold, $\omega_{\mathrm{I}} = E_{\mathrm{F}}$, which is below the direct (Pauli) threshold $\omega_{\mathrm{D}} = 2E_{\mathrm{F}}$. Previous work by Gavoret et al. [31] and others after them [35, 38] has studied only the diagrams allowed by the Hamiltonian (16). For the Dirac spectrum, all diagrams are allowed and we analyze the leading-order ones, either within the large-N or RPA approximations.

1. Threshold behavior for $\Omega \gtrsim \omega_{\mathrm{I}}$

Analytic results in the intermediate frequency regime can be obtained only for frequencies just above ω_{I}, where absorption due to AM processes just becomes allowed
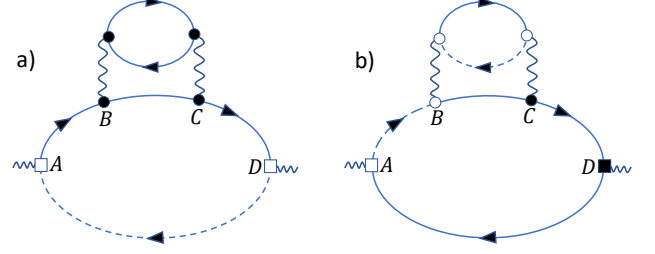

Figure 6. Examples of diagrams describing Auger-Meitner scattering processes. Diagram *a* corresponds to the case of $s_3 = -1, s_4 = +1$, when absorption occurs as depicted in Fig. 4*a*. Diagram *b* corresponds to the case of $s_3 = +1, s_4 = -1$, when absorption occurs as depicted in Fig. 4*b*. The filled and blank circles denote matrix elements of *ee* and *eh* interactions, respectively, while the filled and blank squares denote the intra- and inter-band current vertices, respectively. The lines connecting vertices A and B, and C and D can, in general, be of either helicity; the diagrams shown in the figure correspond to specific choices of those helicities.

(see Sec. IV A 2). For the rest of this regime, we will have to defer to numerical computation, discussed in Sec. V D.

To simplify analysis, we note that the contributions for the $s_3 = +1, s_4 = -1$ case can be mapped onto the $s_3 = -1, s_4 = +1$ one just by relabelling the helicities. Thus, we need to consider only the $s_4 = +1, s_3 = -1$ case. The sum over $\mathcal{S}_B = \{s_1, s_2\} = \{\pm 1, \pm 1\}$ in Eq. (64) contains terms of three types: $t_1 \sim 1/\Omega^2$, $t_2 \sim 1/\Omega\min\{\Omega, \varepsilon_{\mathbf{k}}\}$, and $t_3 \sim 1/\min\{\Omega^2, \varepsilon_{\mathbf{k}}^2\}$. Near the threshold, $\Omega \gtrsim \omega_{\mathrm{I}} = E_{\mathrm{F}}$ while $\varepsilon_{\mathbf{k}} \approx E_{\mathrm{F}}$. Therefore, $t_1 \sim t_2 \sim t_3 \sim 1/E_{\mathrm{F}}^2$. Next, the current vertex is $\sim v_{\mathrm{D}}$, and the conductivity due AM processes can be estimated as

$$\Re\sigma_{\mathrm{AM}}(\Omega) \sim \frac{e^2}{\omega_{\mathrm{I}}} \frac{v_{\mathrm{D}}^2}{E_{\mathrm{F}}^2} \int_{\mathbf{k}} \theta(\omega_{\mathrm{I}} + \delta\Omega + \xi_{\mathbf{k}}^-)$$
$$\times |\Im\Sigma_{\mathrm{ee}}(\mathbf{k}, \omega_{\mathrm{I}} + \delta\Omega + \xi_{\mathbf{k}}^-)|, \quad (91)$$

where $\delta\Omega \equiv \Omega - \omega_{\mathrm{I}} \ll E_{\mathrm{F}}$ and $\Im\Sigma_{\mathrm{ee}}(\mathbf{k}, \omega)$ is given by Eq. (73). The theta function imposes a constraint $\omega_{\mathrm{I}} + \delta\Omega + \xi_{\mathbf{k}}^- > 0$ or $\epsilon_{\mathbf{k}} < \delta\Omega$. Therefore, the integral over k in Eq. (91) is confined to a narrow region near the Dirac point

$$k \lesssim k_0 \equiv \frac{\delta\Omega}{v_{\mathrm{D}}} \ll k_{\mathrm{F}}. \quad (92)$$

Under this condition, $\Im\Sigma_{\mathrm{ee}}$ for Hubbard interaction is still of the FL form, but with Ω replaced by $\delta\Omega$, i.e., $\Im\Sigma_{\mathrm{ee}} \sim (\delta\Omega)^2$. For Hubbard interaction, the self-energy is given by Eq. (76) with Ω replaced by $\delta\Omega$. Collecting all the estimates together, we obtain

$$\Re\sigma_{\mathrm{AM}}(\Omega) \sim e^2 k_{\mathrm{F}} (N\alpha_{\mathrm{H}})^2 \left(\frac{\delta\Omega}{E_{\mathrm{F}}}\right)^5,$$
$$(93)$$

while the actual calculation gives

$$\Re\sigma_{\mathrm{AM}}(\Omega) = \frac{71}{3240\pi}\frac{e^2 k_{\mathrm{F}}}{\hbar}(N\alpha_{\mathrm{H}})^2\theta(\delta\Omega)\left(\frac{\delta\Omega}{E_{\mathrm{F}}}\right)^5. \quad (94)$$

For Coulomb interaction, we have

$$\Re\sigma_{\mathrm{AM,C}}(\Omega) = \frac{71}{3240\pi}\frac{e^2 k_{\mathrm{F}}}{\hbar}\alpha_{\mathrm{C}}^4\theta(\delta\Omega)\left(\frac{\delta\Omega}{E_{\mathrm{F}}}\right)^5 \quad (95)$$

for $\delta\Omega \ll \omega_{\mathrm{p3}} \ll E_{\mathrm{F}}$. The results for the Hubbard and Coulomb cases are identical, up to a different coupling constant, because, close to the indirect threshold, the Coulomb interaction is effectively a constant, equal to $4\pi e^2/k_{\mathrm{F}}^2$.

In fact, the results in Eqs. (94) and (95) can be readily generalized for an arbitrary dimensionality and spectrum. Indeed, the dependence on $\delta\Omega$ comes from the $(\delta\Omega)^2$-scaling of the self-energy, which does not depend on dimensionality (as long as $d \geq 2$), and the factor of k_0^d, whose dependence on $\delta\Omega$ is determined both by the dimensionality and the energy spectrum. In particular, for $\epsilon_{\mathbf{k}} \propto k^a$, we obtain

$$\beta_{\mathrm{A}} = d/a + 2. \quad (96)$$

For $d = 3$ and $a = 1$ this gives $\beta_{\mathrm{A}} = 5$, in agreement with Eq. (94), while for $d = 3$ and $a = 2$ we obtain $\beta_{\mathrm{A}} = 7/2$, in agreement with Ref. [31].

Note that the threshold singularities due to AM processes occur in the presence of slowly varying contributions from the *ee*, *eh1*, and *eh2* processes, which were discussed in Sec. V A. Certainly, the asymptotic forms of these contributions, Eqs. (90) and (83), are no longer valid for $\Omega \sim \omega_{\mathrm{I}} = E_{\mathrm{F}}$. However, if we naively extrapolate these expressions to the region of $\Omega \gtrsim \omega_{\mathrm{I}}$, we would find that the threshold singularities are completely masked by slowly varying contributions, unless, of course, one differentiates the total conductivity with respect to Ω an appropriate number of times.[47] This result is confirmed by numerical calculations presented in Secs. V D and VI D. Only if the spectrum is gapped and almost parabolic, i.e., $E_{\mathrm{F}} \ll \Delta$, can the threshold singularities be detected against the background of other contributions [see the discussion after Eq. (90)].

2. Generic frequencies in the interval $\omega_{\mathrm{I}} \lesssim \Omega \lesssim \omega_{\mathrm{D}}$

For a generic frequency above $\omega_{\mathrm{I}} = E_{\mathrm{F}}$ but below $\omega_{\mathrm{D}} = 2E_{\mathrm{F}}$ and away from both thresholds, we can obtain only an estimate for AM contribution to the conductivity, by replacing $\delta\Omega$ in Eqs. (94) and (95) with E_{F}. This yields

$$\Re\sigma_{\mathrm{AM}}(\Omega) \sim \frac{e^2 k_{\mathrm{F}}}{\hbar}\begin{cases} (N\alpha_{\mathrm{H}})^2, \\ \alpha_{\mathrm{C}}^4, \end{cases} \quad (97)$$

for the Hubbard and Coulomb cases, respectively. Extrapolating the asymptotic results for the electron-electron and electron-hole contributions by putting $\Omega \sim$

E_{F} in Eqs. (90) and (83), we see that all the contributions are comparable to each other in this range. The numerical results in this range are discussed in Sec. V D.

C. High frequencies: $\Omega > \omega_{\mathrm{D}}$

At the level of non-interacting electrons, the optical conductivity of undoped and gapless 3D Dirac metal scales linearly with frequency [see Eq. (2)]. In the doped case, the onset of the linear scaling is shifted to ω_{D}:

$$\Re\sigma_{\mathrm{NI3}}(\Omega) = \frac{Ne^2\Omega}{24\pi\hbar v_{\mathrm{D}}}\theta(\Omega - \omega_{\mathrm{D}}). \quad (98)$$

To the best of our knowledge, effects of electron-electron interaction in 3D Dirac systems were studied only for the undoped case. In this case, the Coulomb interaction is marginally irrelevant and, consequently, the Dirac velocity acquires an upward logarithmic renormalization while the coupling constant is renormalized downward [14, 16]. The optical conductivity also experiences a logarithmic renormalization and, at $\Omega \to 0$, the slope of the linear scaling approaches a universal limit of $1 + 1/(N + 1)$ [15]. By analogy with the 2D case, however (see Sec. VI C), we expect the optical conductivity to exhibit a logarithmic singularity at $\Omega = \omega_{\mathrm{I}}$ both for Coulomb and Hubbard interactions. Renormalization of the optical conductivity is the first-order interaction effect, while the absorption processes studied in this paper are second-order ones. Therefore, the latter should be subleading to the former for $\Omega > \omega_{\mathrm{D}}$. Due to the lack of known first-order results for the doped case in this range, we will model the optical conductivity by its non-interacting value in Eq. (98).

D. Numerical results in 3D

We evaluate Eq. (45) numerically for each diagram, for frequencies up to $\omega_{\mathrm{D}} = 2E_{\mathrm{F}}$ assuming Hubbard interaction. [To treat the Coulomb case for Ω comparable to E_{F}, we would need to use the exact dynamic interaction in Eq. (30), which is very expensive computationally.] Then we sum the results according to Eqs. (43) and (40) to obtain the total Eq. (23). The conductivity in units $e^2 k_{\mathrm{F}}\alpha_{\mathrm{H}}^2 N^2/\hbar$ for $\Omega < \omega_{\mathrm{D}}$ is plotted in the main panel of Fig. 7, left axis. For the region $\Omega > \omega_{\mathrm{D}}$, where, at least in the weak-coupling limit, absorption by non-interacting Dirac electrons dominates over interaction-induced absorption, we plot the non-interacting result, Eq. (98), normalized by $e^2 k_{\mathrm{F}} N/\hbar$ (right vertical axis). It is worth pointing out that the rescaled conductivity is numerically small for almost the entire range of $\Omega < \omega_{\mathrm{D}}$, except for a narrow window near ω_{D}, where the weak-coupling approximation breaks down (see a more detailed discussion at the end of this section). This implies that the interaction effects are numerically weaker than they can be expected to be. For example, for $\Omega \sim E_{\mathrm{F}}$ an order
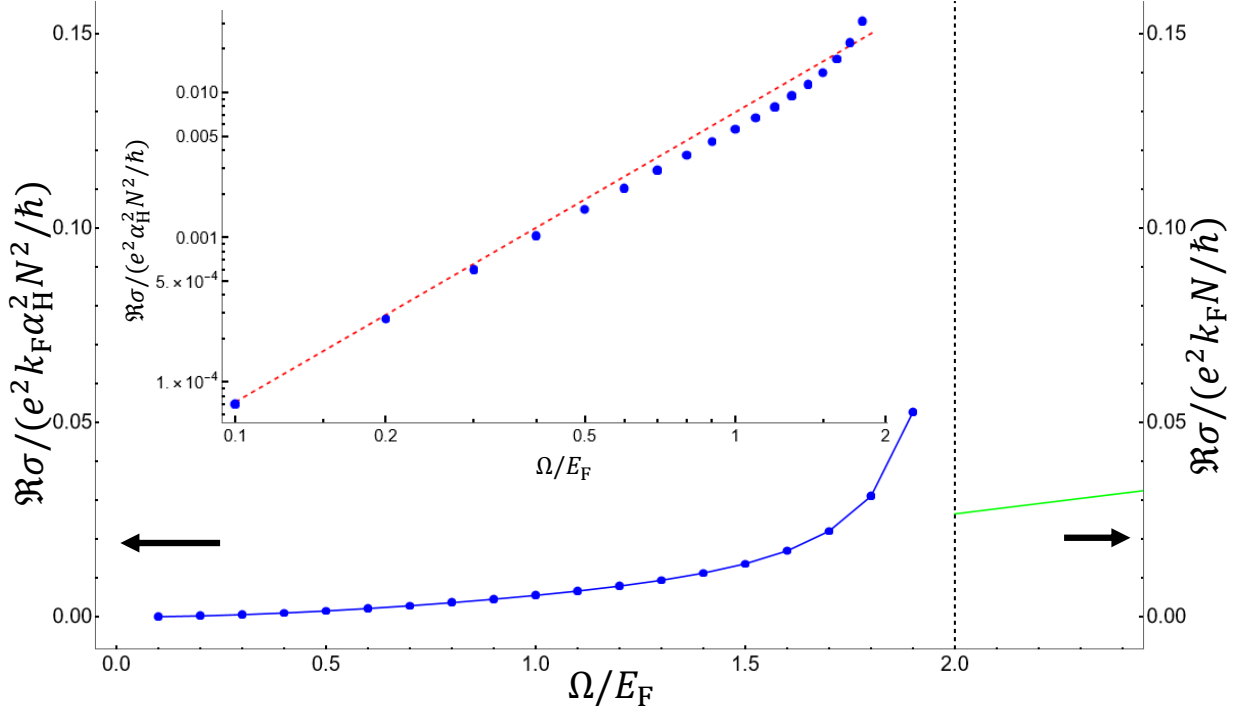
Figure 7. Numerical results for the optical conductivity, $\Re\sigma(\Omega)$, as a function of Ω (in units of E_F) for a gapless 3D Dirac metal with a Hubbard-like interaction. The left vertical axis is in units of $(e^2 k_F/\hbar)N^2\alpha_H^2$, where N is the total degeneracy, e.g., the number of distinct Dirac points, and α_H is the dimensionless coupling constant of Hubbard interaction. The blue dots are the numerically evaluated values of $\Re\sigma(\Omega)$, while the continuous blue curve is a guide to the eye. The green line is the non-interacting result, Eq. (98), plotted along the right vertical axis in units of $(e^2 k_F/\hbar)N$. The dashed vertical line demarcates the direct (Pauli) threshold at $\omega_D = 2E_F$. Inset: The conductivity in the range of $0 \leq \Omega < 2E_F$ on a log-log scale (blue dots). The red dashed line is the analytic result for $\Omega \ll E_F$, Eq. (90), which is extrapolated beyond the nominal range of its validity.

of magnitude estimate for the rescaled conductivity is a number of order one. Instead, the actual result at, for example, $\Omega/E_F = 1.1$, is equal to 0.00667. This feature is in agreement with the asymptotic results for $\Omega \ll E_F$ in Table II, all of which have small numerical coefficients.

Also, as expected (see Sec. V B 1), the threshold singularity due to AM processes at $\Omega = \omega_I = E_F$ is completely masked by the ee and eh contributions due to the non-parabolicity of the Dirac spectrum: there is no trace of the AM singularity in the main panel of Fig. 7. We illustrate this point further in Fig. 8, in which the contributions to the conductivity from all but AM processes and from AM processes are plotted separately. As can be seen from the figure, the AM contribution is smaller by orders of magnitude than the sum of other contributions near the indirect threshold, and becomes comparable to the latter only near the direct threshold of $2E_F$. While these plots are for a model Hubbard interaction, we expect a similar behavior for a more realistic Coulomb case, because the threshold singularity is not sensitive to the type of interaction. The inset in Fig. 7 shows the numer-

ical results (blue dots) plotted versus the low-frequency analytic result, Eq. (90), on a log-log scale. As we see, the analytic result still works well up to $\Omega \approx E_F$.

Lastly, we see an upturn in $\Re\sigma(\Omega)$ as Ω approaches $2E_F$ from below. This indicates that our perturbative approach, in which the Green's functions in all diagrams of Fig. 2 are replaced by the free ones, breaks down near the direct threshold, more precisely, when $0 < \omega_D - \Omega \lesssim \alpha_H^2 E_F$ for the Hubbard case and for $0 < \omega_D - \Omega \lesssim \alpha_C^4 E_F$ for the Coulomb case. This breakdown can be seen from, e.g., Eq. (64). Indeed, substituting $s_1 = s_2 = +1, s_3 = -1$ into the denominators in Eq. (64), we see that the product of two fractions becomes equal to $1/(\Omega - 2\epsilon_k)^2$. Now, from the paragraph above Eq. (92), we know that $\epsilon_k < \delta\Omega = \Omega - E_F$ in the intermediate-frequency regime, i.e., for $E_F \leq \Omega < 2E_F$. As Ω approaches $2E_F$, the maximum value of $2\epsilon_k$ also approaches $2E_F$, and the integral over $\mathbf{k}$ diverges. In principle, this singularity should be mitigated by re-summation of the perturbation theory, which is beyond the scope of this work.
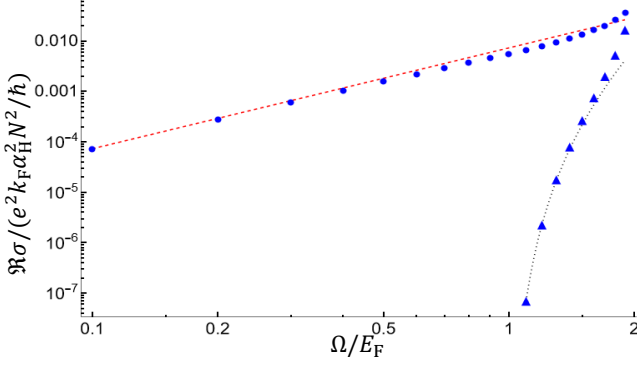
Figure 8. Numerically evaluated all-frequencies contribution, as defined in Sec. IV A 1, (blue dots) and the intermediate frequency contribution, as defined in Sec. IV A 2, (blue triangles) to the optical conductivity as a function of Ω (in units of E_F) for a gapless 3D Dirac metal with Hubbard interaction. The left vertical axis is in the units of $(e^2 k_F/\hbar) N^2 \alpha_H^2$, where N is the total degeneracy, e.g., the number of distinct Dirac points, and α_H is the dimensionless coupling constant of Hubbard interaction [Eq. (27)]. Also plotted is the low-frequency asymptotic result for the all-frequency contribution, Eq. (90), (red dashed curve) and the asymptotic result for the AM contribution near E_F, Eq. (94), (black dotted curve).

VI. OPTICAL CONDUCTIVITY OF A 2D DIRAC METAL

Just as in 3D, we first discuss the lowest frequency regime for 2D, and then the intermediate and high-frequency regimes.

A. Lowest frequencies: $\Omega \ll E_F$

As in the 3D case, this regime corresponds to $s_3 = s_4 = +1$. The conductivity can be split into two contributions: a purely electron one and a contribution from processes that involve up to two holes.

1. Intra-band absorption due to electron-electron interaction

The reasoning about partial cancellation of diagrams for an isotropic spectrum follows the same lines as for the 3D case, see Sec. V A 1. We thus have exactly the same expressions for the conductivity as in Eqs. (72) and (73), but now with the momentum integrals being 2D rather than 3D. The self-energy in 2D has an extra logarithmic factor; however, this factor cancels between different diagrams. Nevertheless, the q integrand in Eq. (73) has an extra factor of q in the denominator, which does lead to a logarithmic enhancement of the conductivity compared to the 3D case, cf. Ref. [29].

For Hubbard interaction, we estimate the conductivity as

$$\Re\sigma_{ee}(\Omega) \sim e^2 (N\alpha_H)^2 \left(\frac{\Omega}{E_F}\right)^2 \ln\left(\frac{E_F}{\Omega}\right),$$
(99)

whereas the actual calculation gives

$$\Re\sigma_{ee}(\Omega) = \frac{e^2}{\hbar}(N\alpha_H)^2 \left(\frac{1}{80\pi^2}\ln\frac{E_F}{\Omega} + \frac{30\ln 2 - 1}{1200\pi^2}\right)\left(\frac{\Omega}{E_F}\right)^2.$$
(100)

Note that Eq. (100) contains not only the leading logarithmic term but also a subleading one. Keeping the subleading term is necessary for comparison with the *eh1* and *eh2* contributions, which do not have a logarithmic enhancement.

As in 3D, the case of Coulomb interaction in the region $\Omega \ll \omega_{p2} \ll E_F$ is similar to the Hubbard one. Explicit calculation shows that

$$\Re\sigma_{ee1}^C(\Omega) = \frac{e^2}{\hbar}\left(\frac{1}{80\pi^2}\ln\frac{\omega_{p2}}{\Omega} + \frac{5\ln 2 - 2}{16\pi^2}\right)\left(\frac{\Omega}{E_F}\right)^2,$$
(101)

where ω_{p2} is defined in Eq. (32). The leading logarithmic term in the last equation coincides with the result of Ref. [29]. Note that, in contrast to the 3D case, the conductivity depends on the coupling constant of the Coulomb interaction only via the cutoff of the logarithmic term.

In the range of frequencies $\omega_{p2} \ll \Omega \ll E_F$, the estimate for the self-energy in Eq. (81) is modified as

$$\Im\Sigma_{ee}(\Omega) \sim -\frac{\kappa_2^2}{\mathcal{N}_{F,2} v_F^2} \int_0^\Omega \mathrm{d}\nu\,\nu \int_{\max\{\Omega,\Omega-\nu\}/v_F}^\infty \frac{\mathrm{d}q}{q^3}$$
$$\sim -\omega_{p2}.$$
(102)

In contrast to the 3D case, the self-energy remains constant in this frequency interval and, according to Eq. (76), the same is true for the conductivity. The actual calculation gives

$$\Re\sigma_{ee2}^C(\Omega) = \frac{5}{576\pi^2}\frac{e^2}{\hbar}\frac{e^2}{v_D}.$$
(103)

2. Absorption processes involving up to two holes

Now we analyze the scattering processes which involve up two holes. Again, the general reasoning here is exactly the same as the 3D eh case. Namely, there are two types of such processes: with one hole (*eh1*, $s_1 = -s_2 = \pm 1$) and with two holes (*eh2*, $s_1 = s_2 = -1$), with the same corresponding conditions on the helicities as in the 3D case.

The estimates for the *eh1* and *eh2* contributions to the conductivity are the same as in the 3D case, i.e., they

are given by Eqs. (85) and (88), modulo a replacement $e^2 k_\mathrm{F} \to e^2$.

Therefore, the estimates for the *eh1* and *eh2* contributions in 2D read

$$\Re\sigma_{\mathrm{eh1}}(\Omega) \sim \Re\sigma_{\mathrm{eh2}}(\Omega) \sim e^2 \alpha_\mathrm{H}^2 \left(\frac{\Omega}{E_\mathrm{F}}\right)^2, \quad (104)$$

whereas the actual calculation shows that

$$\Re\sigma_{\mathrm{eh1}} = \Re\sigma_{\mathrm{eh2}} = \frac{1}{96\pi^2} \frac{e^2}{\hbar} (N\alpha_\mathrm{H})^2 \left(\frac{\Omega}{E_\mathrm{F}}\right)^2. \quad (105)$$

Adding up the *eh1* and *eh2* contributions, we have

$$\begin{aligned}
\Re\sigma_{\mathrm{eh}}(\Omega) &= \Re\sigma_{\mathrm{eh1}}(\Omega) + \Re\sigma_{\mathrm{eh2}}(\Omega) \\
&= \frac{1}{48\pi^2} \frac{e^2}{\hbar} (N\alpha_\mathrm{H})^2 \left(\frac{\Omega}{E_\mathrm{F}}\right)^2.
\end{aligned} \quad (106)$$

While the combined *eh* contribution is smaller than the leading logarithmic term in *ee* contribution [cf. Eq. (100)], it is of the same order as the next-to-leading *ee* term. The total conductivity at the lowest frequencies ($\Omega \ll E_\mathrm{F}$) is then a sum of Eq. (100) and Eq. (106):

$$\Re\sigma_{\mathrm{LF}}(\Omega) = \frac{e^2}{\hbar}(N\alpha_\mathrm{H})^2 \left(\frac{1}{80\pi^2}\ln\frac{E_\mathrm{F}}{\Omega} + \frac{5\ln 2 + 4}{200\pi^2}\right)\left(\frac{\Omega}{E_\mathrm{F}}\right)^2. \quad (107)$$

In terms of numbers, the logarithmic term becomes the leading one for $\Omega/E_\mathrm{F} < 0.05$.

As in the 3D case, the *eh* contribution for Coulomb interaction is smaller than the *ee* one by a factor of α_C, and thus Eqs. (101) and (103) are the leading contributions to the conductivity in the corresponding frequency intervals. Note that the logarithmic term in Eq. (101) becomes the leading one only at very low frequencies: $\Omega/\omega_{\mathrm{p2}} < 6.6 \times 10^{-4}$.

B. Intermediate frequencies: $\omega_\mathrm{I} \le \Omega < \omega_\mathrm{D}$

The analysis of the optical conductivity of a 2D Dirac metal in the intermediate frequency regime is completely analogous to the 3D case, discussed in Sec. V B. As in 3D, the analytic results are attainable only for $\Omega \gtrsim \omega_\mathrm{I}$, where AM processes just start to contribute. In fact, in Sec. V B 1 we have already derived a general expression for the scaling exponent β_A, see Eq. (96). For the case of $d = 2$ and $a = 2$, we obtain $\beta_\mathrm{A} = 3$, in agreement with Ref. [38]. For our case of $d = 2$ and $a = 1$, this equation gives $\beta_\mathrm{A} = 4$. Without repeating the same steps as in 3D, we just present the results for the Hubbard case

$$\Re\sigma_{\mathrm{AM}} = \frac{5}{108\sqrt{3}\pi} \frac{e^2}{\hbar} (N\alpha_\mathrm{H})^2 \theta(\delta\Omega) \left(\frac{\delta\Omega}{E_\mathrm{F}}\right)^4 \quad (108)$$

and for the Coulomb case

$$\Re\sigma_{\mathrm{AM,C}} = \frac{5}{108\sqrt{3}\pi} \frac{e^2}{\hbar} \alpha_\mathrm{C}^2 \theta(\delta\Omega) \left(\frac{\delta\Omega}{E_\mathrm{F}}\right)^4. \quad (109)$$

As in the 3D case, the results for the Hubbard and Coulomb cases are identical for the reason explained in Sec. V B 1. Also, as in 3D, the estimates for the conductivity for a generic frequency within the interval $\{\omega_\mathrm{I}, \omega_\mathrm{D}\}$ and away from either of the thresholds, can be obtained by replacing Ω with E_F in Eq. (100) and assuming that Eq. (103) continues to be valid within an order of magnitude for $\Omega \sim E_F$. This gives

$$\Re\sigma_{\mathrm{AM}}(\Omega) \sim \frac{e^2}{\hbar} \left\{ \begin{array}{l} (N\alpha_\mathrm{H})^2, \\ \alpha_\mathrm{C}^2, \end{array} \right. \quad (110)$$

for the Hubbard and Coulomb cases, respectively.

C. High frequencies: $\Omega > \omega_\mathrm{D}$

The optical response of 2D Dirac metals, e.g., graphene, has been studied extensively; see, e.g., reviews [10–12] and references therein. At the non-interacting level, the optical conductivity has a universal form, given by Eq. (1). At finite doping, this result is modified to

$$\Re\sigma_{\mathrm{NI2}}(\Omega) = \frac{e^2 N}{16\hbar} \theta(\Omega - \omega_\mathrm{D}). \quad (111)$$

As in 3D, the Coulomb interaction is also marginally irrelevant in 2D, which leads to an upward logarithmic renormalization of the Dirac velocity and, consequently, to the downward renormalization of the coupling constant. On the other hand, Hubbard interaction is irrelevant and can be neglected for frequencies below the ultraviolet cutoff of the model.

The optical conductivity of doped graphene was studied by Abedinpour et al. [39] to first order in both Coulomb and Hubbard interaction. As expected, the results reduce to those for the undoped case in the limit of $E_\mathrm{F} \ll \Omega$. Near the direct threshold $\omega_\mathrm{D} = 2E_\mathrm{F}$, the conductivity is logarithmically enhanced compared to the non-interacting value for both Coulomb and Hubbard cases. Because the absorption processes studied in this paper occur to second order in the interaction, they are subleading to those studied in Ref. [39] and, therefore, we will not extend our results to the region $\Omega > \omega_\mathrm{D}$.

D. Numerical results in 2D

We evaluated the optical conductivity numerically for Hubbard interaction in a way similar to the 3D case, The results are shown in Fig. 9. The conductivity in units of $(e^2/\hbar)\alpha_\mathrm{H}^2 N^2$ in the range of $\Omega < \omega_\mathrm{D} = 2E_\mathrm{F}$ is plotted on the left axis of the main panel. The inset shows the same data on the log-log scale (blue dots) and the low-frequency analytic result from Eq. (100) (red dashed line). On the right axis of the main panel, we plot the conductivity in units of $e^2 N/16\hbar$ for the non-interacting case, given by Eq. (111), (green solid line) and the analytic result to first order in Hubbard interaction from Ref. [39] for $\alpha_\mathrm{H} = 0.045$ (red solid curve).
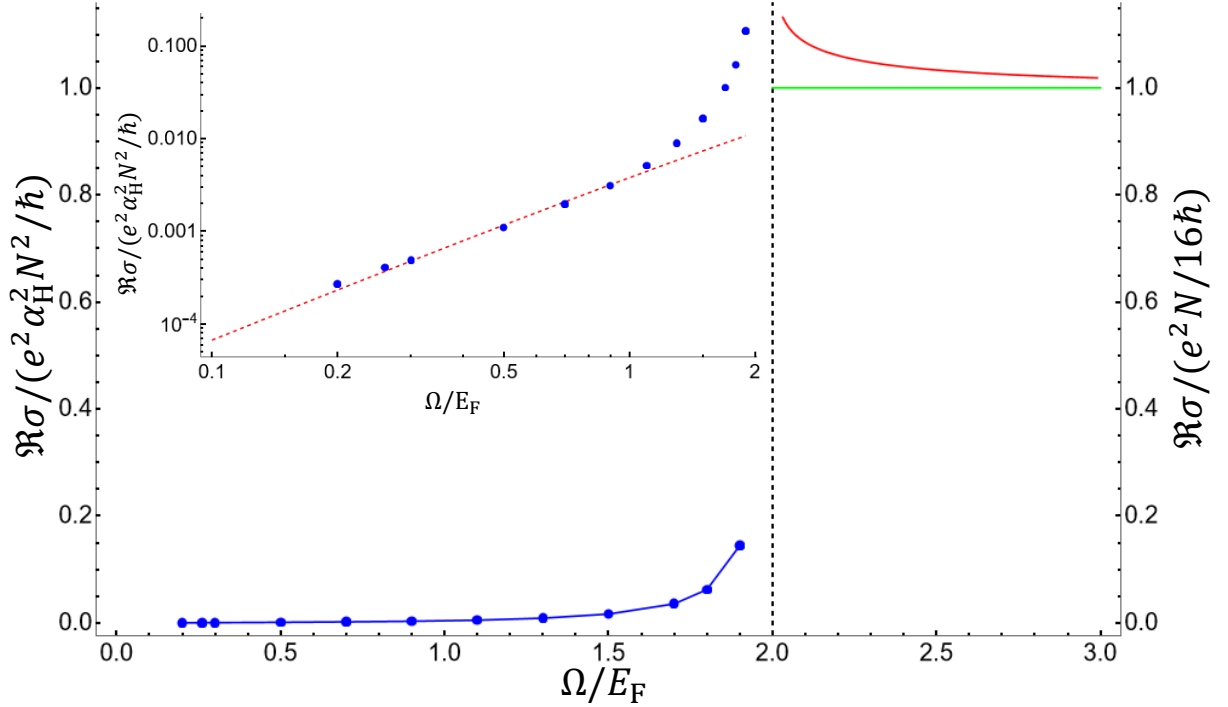
Figure 9. Numerical results for the optical conductivity, $\Re\sigma(\Omega)$, as a function of Ω (in units of E_{F}) for a gapless 2D Dirac metal with a Hubbard-like interaction. The left vertical axis is in units of $(e^2/\hbar)N^2\alpha_{\mathrm{H}}^2$, where N is the total degeneracy, e.g., the number of distinct Dirac points, and α_{H} is the dimensionless coupling constant of Hubbard interaction. The blue dots are the numerically evaluated values of $\Re\sigma(\Omega)$, while the continuous blue curve is a guide to the eye. The dashed vertical line demarcates the direct (Pauli) threshold at $\omega_{\mathrm{D}} = 2E_{\mathrm{F}}$. The green solid line is the non-interacting result, Eq. (111), plotted along the right vertical axis in units of $e^2 N/16\hbar$. The red solid line is the analytic result from Ref. [39] to first order in Hubbard interaction for $\alpha_{\mathrm{H}} = 0.045$. Inset: The conductivity in the range of $0 < \Omega < 2E_{\mathrm{F}}$ on a log-log scale (blue dots). The red dashed line is the analytic result for $\Omega \ll E_{\mathrm{F}}$, Eq. (100), which is extrapolated beyond the nominal range of its validity.

As in the 3D case, the rescaled conductivity is small compared to unity even for $\Omega \sim E_{\mathrm{F}}$. Also, as in 3D, the threshold AM singularity from the on-set of AM processes at $\Omega = \omega_{\mathrm{I}}$ is washed out, see Fig. 10.

VII. CONCLUSIONS

We studied optical absorption is 2D and 3D Dirac metals due to electron-electron (ee) and electron-hole (eh) interactions. The latter were described by two models: a Hubbard-like interaction, with a radius shorter than the Fermi wavelength but longer than the lattice spacing, and a dynamically screened Coulomb potential. To keep the perturbation theory under control, both types of interactions were assumed to be weak. The optical conductivity, $\Re\sigma(\Omega)$, was obtained by computing the leading diagrams for the current-current correlation functions, in the large-N approximation for the Hubbard case and in the random-phase approximation for the Coulomb case. The main focus of this paper is the behavior of $\Re\sigma(\Omega)$ in the range of frequencies $0 < \Omega < \omega_{\mathrm{D}} = 2E_{\mathrm{F}}$, where absorption is blocked by the Pauli principle in the single-

particle picture. This range is further split into two ranges: $0 < \Omega < \omega_{\mathrm{I}} = E_{\mathrm{F}}$ (I) and $\omega_{\mathrm{I}} < \Omega < \omega_{\mathrm{D}}$ (II).

In range I, absorption starts at the lowest frequencies. The conductivity in this range comes from purely ee scattering, which is allowed to contribute due to broken Galilean invariance, and from certain eh scattering processes, which involve up to two holes. For $\Omega \ll E_{\mathrm{F}}$, we derived the analytic results for the conductivity, which are presented in Tables II and III, for the Hubbard and Coulomb cases respectively. In both cases, $\Re\sigma(\Omega)$ scales as $\Omega^2 \ln\Omega$ in 2D and as Ω^2 in 3D. In other words, the effective current relaxation rate, $1/\tau_j \equiv (k_{\mathrm{F}}/v_{\mathrm{D}} n e^2)\Omega^2\Re\sigma(\Omega)$ scales as $\Omega^4 \ln\Omega$ in 2D and as Ω^4 in 3D. (Here, n is the carrier number density, k_{F} is the Fermi momentum, and v_{D} is the Dirac velocity.) The ee contribution to $\Re\sigma(\Omega)$ has been derived in Ref. [29] for the Coulomb case by a different method,
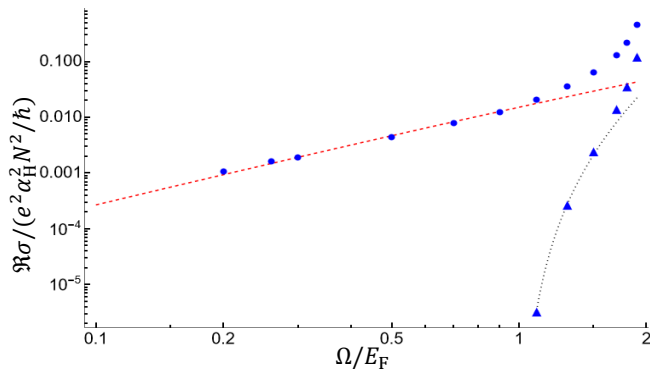
Figure 10. Numerically evaluated all-frequencies contribution, as defined in Sec. IV A 1, (blue dots) and the intermediate frequency contribution, as defined in Sec. IV A 2, (blue triangles) to the optical conductivity as a function of Ω (in units of $E_{\rm F}$) for a gapless 2D Dirac metal with Hubbard interaction. The left vertical axis is in the units of $(e^2/\hbar)\alpha_{\rm H}^2 N^2$, where N is the total degeneracy and $\alpha_{\rm H}$ is the dimensionless coupling constant of Hubbard interaction [Eq. (27)]. Also plotted are the low frequency analytical result for the all-frequency contribution, Eq. (107) (red dashed curve) and the analytical result for the AM contribution near $E_{\rm F}$, Eq. (108) (black dotted curve).

via the Heisenberg equations of motion for the current operator, and our results for this contribution agree with those of Ref. [29] (modulo a discrepancy in the numerical coefficient in 3D). Remarkably, the *eh* contribution, studied in this paper, is comparable to the *ee* one in 3D and subleading to the *ee* in 2D only in the leading logarithmic sense. For the rest of range I, $\Re\sigma(\Omega)$ was calculated numerically.

In range II, another type *eh* scattering processes, similar the Auger-Meitner (AM) processes in atomic physics [32–34], start to contribute to the conductivity. These processes have been studied extensively in the context of doped semiconductors (see, e.g., Refs. [31, 35–38]), but only in the model of parabolic bands, within which absorption in range I is absent, and the onset of absorption due to AM processes at $\Omega = \omega_{\rm I}$ is manifested by a threshold singularity in $\Re\sigma(\Omega)$. We showed that a similar singularity also exists for Dirac metals. However, in contrast

to the parabolic-bands case, the AM singularity occurs at the background of absorption due to *ee* and other *eh* processes, which start to contribute in region I, but continue to contribute in region II as well. Our numerical calculations show that the AM threshold singularity is completely masked by these other processes.

In the range of $\Omega \sim E_{\rm F}$ (but not in the immediate vicinity of either $E_{\rm F}$ and $2E_{\rm F}$), all *ee* and *eh* scattering processes give comparable contributions to $\Re\sigma(\Omega)$. As $E_{\rm F}$ is the only energy scale in this regime, the effective current relaxation rate is of order $gE_{\rm F}$, where g is the dimensionless coupling constant for either type of interaction. However, our analytic and numerical results show that the numerical coefficient C in the relation $1/\tau_j = CgE_{\rm F}$ is anomalously small, on the order of 10^{-3}, i.e., in reality $1/\tau_j \ll E_{\rm F}$ even at $g = 1$. This may explain the observation of well-resolved collective modes below $2E_{\rm F}$ in the helical surface state of a doped 3D topological insulator [48] (see Ref. [49] for more details).

As mentioned in Sec. I, experiments on monolayer graphene find significant optical absorption at frequencies above the Drude tail but below $2E_{\rm F}$ [17–21] and also significant Raman response in the same frequency range [22]. In real materials, absorption in this frequency range is not only due to *ee* and *eh* interactions, but also due to electron-impurity and electron-phonon scattering. Moreover, it was argued in Ref. [25] that the data of Ref. [17] can be well explained by taking into account only electron-impurity and electron-phonon scattering (with an addition of excitonic effects [26]). We hope that future experiments on samples with higher mobilities will be able to resolve intrinsic, *ee* and *eh* contributions to absorption.

[1] A. H. Castro Neto, F. Guinea, N. M. R. Peres, K. S. Novoselov, and A. K. Geim, Rev. Mod. Phys. **81**, 109 (2009).

[2] M. Z. Hasan and C. L. Kane, Rev. Mod. Phys. **82**, 3045 (2010).

[3] O. Vafek and A. Vishwanath, Annu. Rev. Conden. Matt. Phys. **5**, 83 (2014).

[4] A. Burkov, Annu. Rev. Conden. Matt. Phys. **9**, 359 (2018).

[5] N. P. Armitage, E. J. Mele, and A. Vishwanath, Rev. Mod. Phys. **90**, 015001 (2018).

[6] For the purposes of present discussion, the topological distinction between Weyl and Dirac materials is irrelevant, and we will be referring to both of the them as to "Dirac materials".

[7] P. Hosur, S. A. Parameswaran, and A. Vishwanath, Phys. Rev. Lett. **108**, 046602 (2012).

[8] P. E. C. Ashby and J. P. Carbotte, Phys. Rev. B **89**, 245121 (2014).

[9] Throughout the paper, we set $\hbar = 1$ in the intermediate results but display it in the final results for the conductivity. Also, without loss of generality, we take $\Omega > 0$ and assume that the Fermi energy lies in the upper Dirac cone, i.e., in the conduction band.

[10] N. M. R. Peres, Rev. Mod. Phys. **82**, 2673 (2010).

[11] S. Das Sarma, S. Adam, E. H. Hwang, and E. Rossi, Rev. Mod. Phys. **83**, 407 (2011).

[12] V. N. Kotov, B. Uchoa, V. M. Pereira, F. Guinea, and A. H. Castro Neto, Rev. Mod. Phys. **84**, 1067 (2012).

[13] P. Hosur and X. Qi, C. R. Physique **14**, 857 (2013).

[14] B. Rosenstein and M. Lewkowicz, Phys. Rev. B **88**, 045108 (2013).

[15] B. Roy and V. Juričić, Phys. Rev. B **96**, 155117 (2017).

[16] A. A. Abrikosov and S. Beneslavskii, Sov. Phys.–JETP **32**, 699 (1971).

[17] Z. Q. Li, E. A. Henriksen, Z. Jiang, Z. Hao, M. C. Martin, P. Kim, H. L. Stormer, and D. N. Basov, Nature Physics **4**, 532 (2008).

[18] K. F. Mak, M. Y. Sfeir, Y. Wu, C. H. Lui, J. A. Misewich, and T. F. Heinz, Phys. Rev. Lett. **101**, 196405 (2008).

[19] J. Horng, C.-F. Chen, B. Geng, C. Girit, Y. Zhang, Z. Hao, H. A. Bechtel, M. Martin, A. Zettl, M. F. Crommie, Y. R. Shen, and F. Wang, Phys. Rev. B **83**, 165113 (2011).

[20] K. F. Mak, L. Ju, F. Wang, and T. F. Heinz, Solid State Comm. **152**, 1341 (2012).

[21] G. S. Jenkins, C. Lane, B. Barbiellini, A. B. Sushkov, R. L. Carey, F. Liu, J. W. Krizan, S. K. Kushwaha, Q. Gibson, T.-R. Chang, H.-T. Jeng, H. Lin, R. J. Cava, A. Bansil, and H. D. Drew, Phys. Rev. B **94**, 085121 (2016).

[22] E. Riccardi, M.-A. Méasson, M. Cazayous, A. Sacuto, and Y. Gallais, Phys. Rev. Lett. **116**, 066805 (2016).

[23] N. M. R. Peres, J. M. B. Lopes dos Santos, and T. Stauber, Phys. Rev. B **76**, 073412 (2007).

[24] T. Stauber, N. M. R. Peres, and A. H. Castro Neto, Phys. Rev. B **78**, 085418 (2008).

[25] N. M. R. Peres, T. Stauber, and A. H. C. Neto, Europhys. Lett. **84**, 38002 (2008).

[26] N. M. R. Peres, R. M. Ribeiro, and A. H. Castro Neto, Phys. Rev. Lett. **105**, 055501 (2010).

[27] We will be referring to fermions in the conduction band as "electrons" and to fermions in the valence band (lower Dirac cone) as "holes".

[28] A. Principi, G. Vignale, M. Carrega, and M. Polini, Phys. Rev. B **88**, 195405 (2013).

[29] P. Sharma, A. Principi, and D. L. Maslov, Phys. Rev. B **104**, 045142 (2021).

[30] An earlier result of Ref. [28] was missing a logarithmic factor in the 2D case.

[31] J. Gavoret, P. Nozières, B. Roulet, and M. Combescot, J. de Physique **30**, 987 (1969).

[32] L. Meitner, Zeitschrift für Physik **9**, 131 (1922).

[33] P. Auger, C. R. Acad. Sci. **177**, 169 (1923).

[34] D. Matsakis, A. Coster, B. Laster, and R. Sime, Physics Today **72**, 10 (2019).

[35] A. E. Ruckenstein and S. Schmitt-Rink, Phys. Rev. B **35**, 7551 (1987).

[36] T. Uenoyama and L. J. Sham, Phys. Rev. Lett. **65**, 1048 (1990).

[37] P. Hawrylak, Phys. Rev. B **44**, 3821 (1991).

[38] D. Pimenov, J. von Delft, L. Glazman, and M. Goldstein, Phys. Rev. B **96**, 155310 (2017).

[39] S. H. Abedinpour, G. Vignale, A. Principi, M. Polini, W.-K. Tse, and A. H. MacDonald, Phys. Rev. B **84**, 045429 (2011).

[40] The rationale behind transitioning from $\Im\Pi_{\mathcal{S}',\mathrm{R}}^{J}(\Omega)$ to $\mathcal{R}_{\mathcal{S}}^{J}(\Omega)$, which differ only in labeling of the helicities, is mere convenience. Namely, it allows one to systematically collect contributions with similar behaviors into $\mathcal{R}_{\mathcal{S}}^{J}(\Omega)$.

[41] A. Rosch and P. C. Howell, Phys. Rev. B **72**, 104510 (2005).

[42] A. Rosch, Ann. der Physik **15**, 526 (2006).

[43] D. L. Maslov and A. V. Chubukov, Rep. Prog. Phys. **80**, 026503 (2016).

[44] For $\mathbf{k} \to \mathbf{k}'$, $\Phi_{\mathbf{k},\mathbf{k}'}^{+;+} \to 1$, and Eq. (67) is reduced to the result of Ref. [29], which considered a Dirac metal with long-range Coulomb interaction.

[45] We are using this opportunity to point out that the numerical coefficient in the result for the same quantity in Ref. [29] by a subset of current authors (PS and DLM) is incorrect.

[46] A. Goyal and D. L. Maslov, in preparation.

[47] We need to use Eq. (83) for the Coulomb case because we are in the interval $\omega_{\mathrm{p3}} \ll E_{\mathrm{F}} \lesssim \Omega$.

[48] H.-H. Kung, S. Maiti, X. Wang, S.-W. Cheong, D. L. Maslov, and G. Blumberg, Phys. Rev. Lett. **119**, 136802 (2017).

[49] D. L. Maslov, A. Kumar, and S. Maiti, JETP **135**, 549 (2022).

[50] The two terms for the self-energy diagram corresponds to two distinct diagrams, labeled as SE_1 and SE_2 in Fig. 2. For the rest of the diagrams, the two terms appear only in the algebraic expressions rather as distinct diagrams.

Appendix A: General structure of the diagrams for the optical conductivity

In this Appendix, we derive the general forms of the contributions from particular diagrams for the current-current correlation function in Fig. 2. These forms are valid for Hubbard interaction for all frequencies of interest, $\Omega < 2E_{\mathrm{F}}$, and for Coulomb interaction for $\Omega \ll E_F$. We discuss only the self-energy and vertex diagrams; the analysis of the Aslamazov-Larkin diagrams follows the same lines.

1. Some common properties

As explained in Sec. III B, the imaginary parts of the contributions from the self-energy (SE) and vertex (V) diagrams to the current-current correlation function contain a dynamic polarization bubble $\pi_{\mathrm{dyn}}(\mathbf{q}, i\nu) = \pi_0(\mathbf{q}, i\nu) - \pi_0(\mathbf{q}, 0)$. For practical purposes, however, it is more convenient to replace $\pi_{\mathrm{dyn}}(\mathbf{q}, i\nu)$ by the full bubble, $\pi_0(\mathbf{q}, i\nu)$, with the understanding that its static part will drop out on taking the imaginary part. Then the self-energy and vertex diagrams can be written as

$$\Pi^{\mathrm{SE,V}}(i\Omega) = \frac{1}{d} \int_{\mathbf{q}} T \sum_{\nu} \pi_1^{\mathrm{SE,V}}(\mathbf{q}, i\nu; i\Omega) V_{\mathrm{st}}^2(\mathbf{q}) \pi_0(\mathbf{q}, i\nu), \tag{A1}$$

where SE stands for both SE_1 and SE_2 parts of the SE diagram, $V_{\mathrm{st}}(\mathbf{q})$ is either a (momentum-independent) Hubbard interaction or statically screened Coulomb potential,

$$\pi_0(\mathbf{q}, i\nu) = -\frac{1}{4} \sum_{s_4', s_6' = \pm 1} \int_{\mathbf{P}} \mathrm{Tr}\left(\hat{M}_{\mathbf{P}}^{s_6'} \hat{M}_{\mathbf{P+q}}^{s_4'} \right) \frac{\left[n_{\mathrm{F}}(\xi_{\mathbf{P}}^{s_6'}) - n_{\mathrm{F}}(\xi_{\mathbf{P+q}}^{s_4'}) \right]}{i\nu - \xi_{\mathbf{P+q}}^{s_4'} + \xi_{\mathbf{P}}^{s_6'}} \tag{A2}$$

is the polarization bubble, and $\pi_1^{\mathrm{SE,V}}(\mathbf{q}, i\nu; i\Omega)$ are given by

$$\begin{aligned}
\pi_1^{\mathrm{SE}_1}(\mathbf{q}, i\nu; i\Omega) &= -\int_{\mathcal{K}} \mathrm{Tr}\left(\hat{\mathbf{v}} \hat{G}(\mathcal{K}+\mathcal{W}) \hat{G}(\mathcal{K}+\mathcal{Q}+\mathcal{W}) \hat{G}(\mathcal{K}+\mathcal{W}) \cdot \hat{\mathbf{v}} \hat{G}(\mathcal{K}) \right) \\
\pi_1^{\mathrm{SE}_2}(\mathbf{q}, i\nu; i\Omega) &= -\int_{\mathcal{K}} \mathrm{Tr}\left(\hat{\mathbf{v}} \hat{G}(\mathcal{K}+\mathcal{W}) \cdot \hat{\mathbf{v}} \hat{G}(\mathcal{K}) \hat{G}(\mathcal{K}+\mathcal{Q}) \hat{G}(\mathcal{K}) \right) \\
\pi_1^{\mathrm{V}}(\mathbf{q}, i\nu; i\Omega) &= -\int_{\mathcal{K}} \mathrm{Tr}\left(\hat{\mathbf{v}} \hat{G}(\mathcal{K}+\mathcal{W}) \hat{G}(\mathcal{K}+\mathcal{Q}+\mathcal{W}) \cdot \hat{\mathbf{v}} \hat{G}(\mathcal{K}+\mathcal{Q}) \hat{G}(\mathcal{K}) \right).
\end{aligned} \tag{A3}$$

It will be convenient to introduce a quantity

$$\tilde{\Sigma}_s(\mathbf{k}, \mathbf{q}, i\omega) = T \sum_{\nu} g_s(\mathbf{k}, i\omega + i\nu) \pi_0(\mathbf{q}, i\nu), \tag{A4}$$

whose meaning is that $\tilde{\Sigma}_s(\mathbf{k}+\mathbf{q}, \mathbf{q}, i\omega)$ is the self-energy with fixed momentum transfer $\mathbf{q}$ (but without the interaction potential). Evaluating the Matsubara sum over ν and performing analytic continuation as in $i\omega \to \omega + i0^+$, we obtain

$$\tilde{\Sigma}_{s,\mathrm{R}}(\mathbf{k}, \mathbf{q}, \omega) = \frac{1}{4} \sum_{s_4', s_6' = \pm 1} \int_{\mathbf{P}} \left[\mathrm{Tr}(\hat{M}_{\mathbf{P}}^{s_6'} \hat{M}_{\mathbf{P+q}}^{s_4'}) \right] \left[n_{\mathrm{F}}(\xi_{\mathbf{P}}^{s_6'}) - n_{\mathrm{F}}(\xi_{\mathbf{P+q}}^{s_4'}) \right] \frac{\left[n_{\mathrm{F}}(\xi_{\mathbf{k}}^{s}) + n_{\mathrm{B}}(\xi_{\mathbf{P+q}}^{s_4'} - \xi_{\mathbf{P}}^{s_6'}) \right]}{\omega + \xi_{\mathbf{P+q}}^{s_4'} - \xi_{\mathbf{P}}^{s_6'} - \xi_{\mathbf{k}}^{s} + i0^+}. \tag{A5}$$

At $T = 0$ the last equation is reduced to

$$\tilde{\Sigma}_{s,\mathrm{R}}(\mathbf{k}, \mathbf{q}, \omega) = \frac{1}{4} \sum_{s_4', s_6' = \pm 1} \int_{\mathbf{P}} \frac{\mathrm{Tr}(\hat{M}_{\mathbf{P}}^{s_6'} \hat{M}_{\mathbf{P+q}}^{s_4'})}{\omega + \xi_{\mathbf{P+q}}^{s_4'} - \xi_{\mathbf{P}}^{s_6'} - \xi_{\mathbf{k}}^{s} + i0^+} \left[\theta(\xi_{\mathbf{P}}^{s_6'}) \theta(-\xi_{\mathbf{P+q}}^{s_4'}) \theta(\xi_{\mathbf{k}}^{s}) + \theta(-\xi_{\mathbf{P}}^{s_6'}) \theta(\xi_{\mathbf{P+q}}^{s_4'}) \theta(-\xi_{\mathbf{k}}^{s}) \right]. \tag{A6}$$

We also note a useful identity, namely, that for any real functions $h_{1,2}(\omega)$, and functions $f_{1,2}(\omega)$ of the form

$$f_{1,2}(\omega) = \frac{1}{\omega - x_{1,2}} + i y_{1,2} \delta(\omega - x_{1,2}), \tag{A7}$$

we have

$$\begin{aligned}
&\int \mathrm{d}\omega \left[h_1(\omega) \Re f_1(\Omega + \omega) \Im f_2(\omega) + h_2(\omega) \Im f_1(\omega) \Re f_2(\Omega + \omega) \right] \\
&= \frac{y_2 h_1(x_2) - y_1 h_2(-\Omega + x_1)}{\Omega + x_2 - x_1}.
\end{aligned} \tag{A8}$$

This identity will appear often in our discussion.

2. Self-energy diagrams

a. SE$_1$ diagram

Explicitly, the first self-energy diagram (SE$_1$) in Fig. 2 reads

$$\Pi^{\mathrm{SE}_1}(i\Omega) = \frac{1}{16d} \sum_{\mathcal{S}_{\mathrm{SE}_1}} \int_{\mathbf{k},\mathbf{q}} \mathrm{Tr}\left(\hat{\mathbf{v}} \hat{M}_{\mathbf{k}}^{s'_1} \hat{M}_{\mathbf{k}+\mathbf{q}}^{s'_5} \hat{M}_{\mathbf{k}}^{s'_2} \cdot \hat{\mathbf{v}} \hat{M}_{\mathbf{k}}^{s'_3}\right) V_{\mathrm{st}}^2(\mathbf{q}) W_{\mathrm{SE}_1}(i\Omega), \tag{A9}$$

where $\mathcal{S}_{\mathrm{SE}_1} = \{s'_1, s'_2, s'_3, s'_5\}$,

$$W_{\mathrm{SE}_1}(\mathbf{k}, \mathbf{q}, i\Omega) = T \sum_{\omega} g_{s'_1}(\mathbf{k}, i\omega + i\Omega) g_{s'_2}(\mathbf{k}, i\omega + i\Omega) g_{s'_3}(\mathbf{k}, i\omega) \tilde{\Sigma}_{s'_5}(\mathbf{k} + \mathbf{q}, \mathbf{q}, i\omega + i\Omega) \tag{A10}$$

$$\equiv T \sum_{\omega} A_{\mathrm{SE}_1}(\mathbf{k}, \mathbf{q}, i\omega + i\Omega) g_{s'_3}(\mathbf{k}, i\omega),$$

$$A_{\mathrm{SE}_1}(\mathbf{k}, \mathbf{q}, i\omega + i\Omega) = g_{s'_1}(\mathbf{k}, i\omega + i\Omega) g_{s'_2}(\mathbf{k}, i\omega + i\Omega) \tilde{\Sigma}_{s'_5}(\mathbf{k} + \mathbf{q}, \mathbf{q}, i\omega + i\Omega), \tag{A11}$$

and $\tilde{\Sigma}_{s'_5}(\mathbf{k} + \mathbf{q}, \mathbf{q}, i\omega + i\Omega)$ is defined in Eq. (A4). We focus on evaluating $W_{\mathrm{SE}_1}(i\Omega)$ first and switch the primed helicity labels to unprimed ones at this point (cf. footnote VII in the main text). Upon summation over ω and analytic continuation as in $i\Omega \to \Omega + i0^+$, for obtain for the imaginary part:

$$\Im W_{\mathrm{SE}_1,\mathrm{R}}(\mathbf{k}, \mathbf{q}, \Omega) = -\frac{1}{\pi} \int_{-\infty}^{\infty} d\omega \left[n_{\mathrm{F}}(\omega) - n_{\mathrm{F}}(\omega + \Omega)\right] \Im g_{s_3,\mathrm{R}}(\mathbf{k}, \omega) \Im A_{\mathrm{SE}_1,\mathrm{R}}(\mathbf{k}, \mathbf{q}, \omega + \Omega),$$

$$= -\frac{1}{\pi} \int_{-\Omega}^{0} d\omega \Im g_{s_3,\mathrm{R}}(\mathbf{k}, \omega) \Im A_{\mathrm{SE}_1,\mathrm{R}}(\mathbf{k}, \mathbf{q}, \omega + \Omega), \tag{A12}$$

where at the last step we implemented the conditions $T = 0$ and $\Omega > 0$, and

$$\Im A_{\mathrm{SE}_1}(\mathbf{k}, \mathbf{q}, \omega + \Omega) = \Im\left[g_{s_1,\mathrm{R}}(\mathbf{k}, \omega + \Omega) g_{s_2}(\mathbf{k}, \omega + \Omega) \tilde{\Sigma}_{s_5,\mathrm{R}}(\mathbf{k} + \mathbf{q}, \mathbf{q}, \omega + \Omega)\right] \tag{A13a}$$

$$= \Re\left[g_{s_1,\mathrm{R}}(\mathbf{k}, \omega + \Omega) g_{s_2,\mathrm{R}}(\mathbf{k}, \omega + \Omega)\right] \Im\tilde{\Sigma}_{s_5,\mathrm{R}}(\mathbf{k}, \mathbf{q}, \omega + \Omega) + \Im\left[g_{s_1,\mathrm{R}}(\mathbf{k}, \omega + \Omega) g_{s_2,\mathrm{R}}(\mathbf{k}, \omega + \Omega)\right] \Re\tilde{\Sigma}_{s_5,\mathrm{R}}(\mathbf{k} + \mathbf{q}, \mathbf{q}, \omega + \Omega). \tag{A13b}$$

We will now show that the second term in Eq. (A13b), proportional to $\Re\tilde{\Sigma}_{s_5}(\mathbf{k}, \mathbf{q}, \omega + \Omega)$, does not contribute to the real part of the conductivity for $\Omega < \omega_{\mathrm{D}}$. Indeed, the prefactor of $\Re\tilde{\Sigma}_{s_5}(\mathbf{k}, \mathbf{q}, \omega + \Omega)$ reads

$$\Im\left[g_{s_1,\mathrm{R}}(\mathbf{k}, \omega + \Omega) g_{s_2,\mathrm{R}}(\mathbf{k}, \omega + \Omega)\right] = -\frac{\pi\delta(\Omega + \omega - \xi_{\mathbf{k}}^{s_2})}{\Omega + \omega - \xi_{\mathbf{k}}^{s_1}} + (s_1 \leftrightarrow s_2). \tag{A14}$$

Because $\Im A_{\mathrm{SE}_1,\mathrm{R}}(\mathbf{k}, \mathbf{q}, \omega + \Omega)$ in Eq. (A12) is multiplied by

$$\Im g_{s_3}(\mathbf{k}, \omega) = -\pi\delta(\omega - \xi_{\mathbf{k}}^{s_3}), \tag{A15}$$

we can put $\omega = \xi_{\mathbf{k}}^{s_3}$ in Eq. (A14). Then the delta function in the first term of Eq. (A14) implies that $\Omega = (s_2 - s_3)\epsilon_{\mathbf{k}}$. Since we chose $\Omega > 0$, the delta function is non-zero only if $s_2 = +1$ and $s_3 = -1$. Therefore, $\Omega = 2\epsilon_{\mathbf{k}}$ or $\epsilon_{\mathbf{k}} = \Omega/2$. However, the limits of integration over ω in Eq. (A12) along with the condition $\omega = \xi_{\mathbf{k}}^{s_3}$ imply that $-\Omega < \xi_k^{s_3} = -\epsilon_{\mathbf{k}} - E_{\mathrm{F}}$. Thus, we have $-\Omega < -\Omega/2 - E_{\mathrm{F}}$ or $\Omega > 2E_{\mathrm{F}} = \omega_{\mathrm{D}}$. The second term in Eq. (A14) is analyzed in a similar way and with the same result.

Now we show that the first term in Eq. (A13b), proportional to $\Im\tilde{\Sigma}_{s_5}(\mathbf{k} + \mathbf{q}, \mathbf{q}, \omega + \Omega)$, does contribute to the real part of the conductivity for $\Omega < \omega_{\mathrm{D}}$. The contribution of this term to $\Im W_{\mathrm{SE}_1,\mathrm{R}}$ (denoted by superscript 1) is given by

$$\Im W_{\mathrm{SE}_1,\mathrm{R}}^{(1)}(\mathbf{k}, \mathbf{q}, \Omega) = -\frac{1}{\pi} \Re\left[g_{s_1,\mathrm{R}}(\mathbf{k}, \Omega + \xi_{\mathbf{k}}^{s_3}) g_{s_2,\mathrm{R}}(\mathbf{k}, \Omega + \xi_{\mathbf{k}}^{s_3})\right] \int_{-\Omega}^{0} d\omega \Im\tilde{\Sigma}_{s_5,\mathrm{R}}(\mathbf{k} + \mathbf{q}, \mathbf{q}, \omega + \Omega) \Im g_{s_3,\mathrm{R}}(\mathbf{k}, \omega). \tag{A16}$$

Note that, formally speaking, the real part of the product of two Green's function in the equation above contains a highly singular term: $\left[\delta\left(\Omega + \xi_{\mathbf{k}}^{s_3} - \xi_{\mathbf{k}}^{s_1}\right)\right]^2$. In fact, it can be shown that such a term only renormalizes the Drude

weight but does not contribute to the regular part of the conductivity. Postponing the proof till Sec. A 2 c, we now proceed discarding this term. From Eq. (A6),

$$\Im\tilde{\Sigma}_{s_5,\mathrm{R}}(\mathbf{k}+\mathbf{q},\mathbf{q},\omega+\Omega) = -\frac{\pi}{4}\sum_{s_4,s_6=\pm 1}\int_{\mathbf{p}}\mathrm{Tr}(\hat{M}_{\mathbf{p}}^{s_6}\hat{M}_{\mathbf{p}+\mathbf{q}}^{s_4})\times\delta(\omega+\Omega+\xi_{\mathbf{p}+\mathbf{q}}^{s_4}-\xi_{\mathbf{p}}^{s_6}-\xi_{\mathbf{k}+\mathbf{q}}^{s_5})$$
$$\times\left[\theta(\xi_{\mathbf{p}}^{s_6})\theta(-\xi_{\mathbf{p}+\mathbf{q}}^{s_4})\theta(\xi_{\mathbf{k}+\mathbf{q}}^{s_5})+\theta(-\xi_{\mathbf{p}}^{s_6})\theta(\xi_{\mathbf{p}+\mathbf{q}}^{s_4})\theta(-\xi_{\mathbf{k}+\mathbf{q}}^{s_5})\right]. \quad (A17)$$

Because $\Omega+\omega>0$, the delta function in the equation above implies that $\xi_{\mathbf{p}+\mathbf{q}}^{s_4}-\xi_{\mathbf{p}}^{s_6}-\xi_{\mathbf{k}+\mathbf{q}}^{s_5}<0$. Comparing this condition with the ones imposed by the theta functions, we see that only the first set of theta functions is non-zero Integrating over ω with the help of Eq. (A15), we obtain

$$\Im W_{\mathrm{SE}_1,\mathrm{R}}^{(1)}(\mathbf{k},\mathbf{q},\Omega) = -\frac{\pi}{4}\sum_{s_4,s_6=\pm 1}\int_{\mathbf{p}}\mathrm{Tr}(\hat{M}_{\mathbf{p}}^{s_6}\hat{M}_{\mathbf{p}+\mathbf{q}}^{s_4})\theta(\Omega+\xi_{\mathbf{k}}^{s_3})\theta(-\xi_{\mathbf{k}}^{s_3})\theta(\xi_{\mathbf{p}}^{s_6})\theta(-\xi_{\mathbf{p}+\mathbf{q}}^{s_4})\theta(\xi_{\mathbf{k}+\mathbf{q}}^{s_5})$$
$$\times\delta(\Omega+\xi_{\mathbf{k}}^{s_3}+\xi_{\mathbf{p}+\mathbf{q}}^{s_4}-\xi_{\mathbf{p}}^{s_6}-\xi_{\mathbf{k}+\mathbf{q}}^{s_5}). \quad (A18)$$

Substituting the last result into $\Im\Pi_{\mathrm{R}}^{\mathrm{SE}_1}$, obtained by analytic continuation of Eq. (A9), yields

$$\Im\Pi_{\mathrm{R}}^{\mathrm{SE}_1}(\Omega) = -\frac{\pi}{64}\sum_{\mathcal{S}_{\mathrm{SE}_1}}\int_{\mathbf{k},\mathbf{q}}\mathrm{Tr}\left(\hat{\mathbf{v}}\hat{M}_{\mathbf{k}}^{s_1}\hat{M}_{\mathbf{k}+\mathbf{q}}^{s_5}\hat{M}_{\mathbf{k}}^{s_2}\cdot\hat{\mathbf{v}}\hat{M}_{\mathbf{k}}^{s_3}\right)V_{\mathrm{st}}^2(\mathbf{q})\times\frac{1}{\Omega-\xi_{\mathbf{k}}^{s_1}+\xi_{\mathbf{k}}^{s_3}}\frac{1}{\Omega-\xi_{\mathbf{k}}^{s_2}+\xi_{\mathbf{k}}^{s_3}}\times$$
$$\times\sum_{s_4,s_6=\pm 1}\int_{\mathbf{p}}\mathrm{Tr}(\hat{M}_{\mathbf{p}}^{s_6}\hat{M}_{\mathbf{p}+\mathbf{q}}^{s_4})\theta(\Omega+\xi_{\mathbf{k}}^{s_3})\theta(-\xi_{\mathbf{k}}^{s_3})\theta(\xi_{\mathbf{p}}^{s_6})\theta(-\xi_{\mathbf{p}+\mathbf{q}}^{s_4})\theta(\xi_{\mathbf{k}+\mathbf{q}}^{s_5})\delta(\Omega+\xi_{\mathbf{k}}^{s_3}+\xi_{\mathbf{p}+\mathbf{q}}^{s_4}-\xi_{\mathbf{p}}^{s_6}-\xi_{\mathbf{k}+\mathbf{q}}^{s_5}). \quad (A19)$$

Relabeling $\mathbf{p}\to\mathbf{p}-\mathbf{q}$ and then $\mathbf{p}\to-\mathbf{p}$, and using that $\epsilon_{\mathbf{k}}=\epsilon_{-\mathbf{k}}$, we find

$$\Im\Pi_{\mathrm{R}}^{\mathrm{SE}_1}(\Omega) = -\frac{\pi^2}{32}\sum_{\mathcal{S}}\int_{\mathbf{k},\mathbf{p},\mathbf{q},\nu}\mathrm{Tr}\left(\hat{\mathbf{v}}\hat{M}_{\mathbf{k}}^{s_1}\hat{M}_{\mathbf{k}+\mathbf{q}}^{s_5}\hat{M}_{\mathbf{k}}^{s_2}\cdot\hat{\mathbf{v}}\hat{M}_{\mathbf{k}}^{s_3}\right)\mathrm{Tr}(\hat{M}_{-\mathbf{p}-\mathbf{q}}^{s_6}\hat{M}_{-\mathbf{p}}^{s_4})V_{\mathrm{st}}^2(\mathbf{q})\times\frac{1}{\Omega-\xi_{\mathbf{k}}^{s_1}+\xi_{\mathbf{k}}^{s_3}}\frac{1}{\Omega-\xi_{\mathbf{k}}^{s_2}+\xi_{\mathbf{k}}^{s_3}}$$
$$\times\theta(\Omega+\xi_{\mathbf{k}}^{s_3})\theta(-\xi_{\mathbf{k}}^{s_3})\theta(\xi_{\mathbf{p}+\mathbf{q}}^{s_6})\theta(-\xi_{\mathbf{p}}^{s_4})\theta(\xi_{\mathbf{k}+\mathbf{q}}^{s_5})\delta(\Omega+\nu+\xi_{\mathbf{k}}^{s_3}-\xi_{\mathbf{k}+\mathbf{q}}^{s_5})\delta(\nu-\xi_{\mathbf{p}}^{s_4}+\xi_{\mathbf{p}+\mathbf{q}}^{s_6}), \quad (A20)$$

where we have re-introduced $\int_{\nu}=\int d\nu/2\pi$. Thus,

$$\Im\Pi^{\mathrm{SE}_1}(\Omega) = -\frac{\pi^2}{32}\sum_{\mathcal{S}}\int_{\mathbf{k},\mathbf{p},\mathbf{q},\nu}V_{\mathrm{st}}^2(\mathbf{q})\times\mathcal{T}_{\mathcal{S}}^{\mathrm{SE}_1}\mathcal{G}_{\mathcal{S}}^{\mathrm{SE}_1}$$
$$\times\theta(\Omega+\xi_{\mathbf{k}}^{s_3})\theta(-\xi_{\mathbf{k}}^{s_3})\theta(\xi_{\mathbf{p}+\mathbf{q}}^{s_6})\theta(-\xi_{\mathbf{p}}^{s_4})\theta(\xi_{\mathbf{k}+\mathbf{q}}^{s_5})\delta(\Omega+\nu+\xi_{\mathbf{k}}^{s_3}-\xi_{\mathbf{k}+\mathbf{q}}^{s_5})\delta(\nu-\xi_{\mathbf{p}}^{s_4}+\xi_{\mathbf{p}+\mathbf{q}}^{s_6}), \quad (A21)$$

where

$$\mathcal{T}_{\mathcal{S}}^{\mathrm{SE}_1} = \frac{1}{d}\mathrm{Tr}\left(\hat{\mathbf{v}}\hat{M}_{\mathbf{k}}^{s_1}\hat{M}_{\mathbf{k}+\mathbf{q}}^{s_5}\hat{M}_{\mathbf{k}}^{s_2}\cdot\hat{\mathbf{v}}\hat{M}_{\mathbf{k}}^{s_3}\right)\mathrm{Tr}\left(\hat{M}_{-\mathbf{p}-\mathbf{q}}^{s_6}\hat{M}_{-\mathbf{p}}^{s_4}\right) \quad (A22a)$$

$$\mathcal{G}_{\mathcal{S}}^{\mathrm{SE}_1} = \frac{1}{\Omega-\xi_{\mathbf{k}}^{s_1}+\xi_{\mathbf{k}}^{s_3}}\frac{1}{\Omega-\xi_{\mathbf{k}}^{s_2}+\xi_{\mathbf{k}}^{s_3}}. \quad (A22b)$$

The last equation gives the SE$_1$ part of Eq. (47) in the main text.

b. SE$_2$ diagram

On the Matsubara axis, the second self-energy diagram (SE$_2$) in Fig. 2 is related to the SE$_1$ one via

$$\Pi^{\mathrm{SE}_2}(i\Omega) = \Pi^{\mathrm{SE}_1}(-i\Omega), \quad (A23)$$

which, upon analytic continuation, implies that

$$\Im\Pi_{\mathrm{R}}^{\mathrm{SE}_2}(\Omega) = \Im\Pi_{\mathrm{A}}^{\mathrm{SE}_1}(-\Omega) = -\Im\Pi_{\mathrm{R}}^{\mathrm{SE}_1}(-\Omega), \quad (A24)$$

where $\Pi_{\mathrm{A}}^{\mathrm{SE}_1}(\varepsilon)$ is the advanced correlation function. Note that although the total correlation function is a real function of time and, therefore, the imaginary part of its Fourier transform is an odd function of frequency, the partial contributions to the total correlation function from different diagrams do not have definite parity. Therefore, Eq. (A24) cannot be simplified further. In the previous section, we considered $\Im\Pi_{\mathrm{R}}^{\mathrm{SE}_1}(\Omega)$ for $\Omega>0$; all we have to

do now is the extend this analysis for $\Omega < 0$. Omitting the steps, which are almost identical to those in the previous section, we present only the final result:

$$\Im\Pi^{\mathrm{SE}_2}(\Omega) = -\frac{\pi^2}{32}\sum_{\mathcal{S}}\int_{\mathbf{k},\mathbf{p},\mathbf{q},\nu} V_{\mathrm{st}}^2(\mathbf{q}) \times \mathcal{T}_{\mathcal{S}}^{\mathrm{SE}_2}\mathcal{G}_{\mathcal{S}}^{\mathrm{SE}_2}$$
$$\times \theta(\Omega + \xi_{\mathbf{k}}^{s_3})\theta(-\xi_{\mathbf{k}}^{s_3})\theta(\xi_{\mathbf{p}+\mathbf{q}}^{s_6})\theta(-\xi_{\mathbf{p}}^{s_4})\theta(\xi_{\mathbf{k}+\mathbf{q}}^{s_5})\delta(\Omega + \nu + \xi_{\mathbf{k}}^{s_3} - \xi_{\mathbf{k}+\mathbf{q}}^{s_5})\delta(\nu - \xi_{\mathbf{p}}^{s_4} + \xi_{\mathbf{p}+\mathbf{q}}^{s_6}), \quad (A25)$$

where

$$\mathcal{T}_{\mathcal{S}}^{\mathrm{SE}_2} = \mathrm{Tr}\left(\hat{\mathbf{v}}\hat{M}_{-\mathbf{k}-\mathbf{q}}^{s_1}\hat{M}_{-\mathbf{k}}^{s_3}\hat{M}_{-\mathbf{k}-\mathbf{q}}^{s_2}\cdot\hat{\mathbf{v}}\hat{M}_{-\mathbf{k}-\mathbf{q}}^{s_5}\right)\mathrm{Tr}\left(\hat{M}_{\mathbf{p}}^{s_4}\hat{M}_{\mathbf{p}+\mathbf{q}}^{s_6}\right) \quad (A26a)$$

$$\mathcal{G}_{\mathcal{S}}^{\mathrm{SE}_2} = \frac{1}{\Omega - \xi_{\mathbf{k}+\mathbf{q}}^{s_5} + \xi_{\mathbf{k}+\mathbf{q}}^{s_1}}\frac{1}{\Omega - \xi_{\mathbf{k}+\mathbf{q}}^{s_5} + \xi_{\mathbf{k}+\mathbf{q}}^{s_2}}. \quad (A26b)$$

Thus we have derived the SE$_2$ part of Eq. (47) in the main text.

c. Elimination of singular terms

In Sec. A 2 a, we argued that the singularities of the $\delta^2(x)$ type, occurring in e.g., Eq. (A16), can be ignored. Here, we prove this statement. Because the singularity occurs already for the case when all helicities are the same, we put $s_1 = s_2 = s_3 = s_5 \equiv s$ and suppress the helicity index. Also, since the momentum-dependence of the self-energy is irrelevant for the present argument, we denote temporarily $\tilde{S}(i\omega) \equiv \hat{\Sigma}_s(\mathbf{k}+\mathbf{q},\mathbf{k},i\omega)$. Adding Eq. (A16) to the corresponding contribution from diagram SE$_2$, we obtain

$$W_{\mathrm{SE}}(i\Omega) = W_{\mathrm{SE1}}(i\Omega) + W_{\mathrm{SE2}}(i\Omega) = T\sum_{\omega}g^2(\mathbf{k},i\omega)\tilde{S}(i\omega)\left[g(\mathbf{k},i\omega - i\Omega) + g(\mathbf{k},i\omega + i\Omega)\right], \quad (A27)$$

where we also made a change of variables $i\omega \rightarrow i\omega + i\Omega$ in W_{SE1}. Applying the identity

$$g_s(\mathbf{k},i\varepsilon)g_{s'}(\mathbf{k},i\varepsilon') = \frac{1}{i(\varepsilon' - \varepsilon) - \xi_{\mathbf{k}}^{s'} + \xi_{\mathbf{k}}^{s}}\left[g_s(\mathbf{k},i\varepsilon) - g_{s'}(\mathbf{k},i\varepsilon')\right] \quad (A28)$$

with $s = s'$ to Eq. (A27) twice, we obtain

$$W_{\mathrm{SE}}(i\Omega) = \frac{1}{(i\Omega)^2}T\sum_{\omega}\left[g(\mathbf{k},i\omega + i\Omega) + g(\mathbf{k},i\omega - i\Omega) - 2g(\mathbf{k},i\omega)\right]\tilde{S}(i\omega). \quad (A29)$$

Summing over ω and performing analytic continuation, we get

$$W_{\mathrm{SE,R}}(\Omega) = \frac{\mathcal{Z}(\Omega)}{(\Omega + i0^+)^2}, \quad (A30)$$

where

$$\mathcal{Z}(\Omega) = \int\frac{d\omega}{\pi}n_{\mathrm{F}}(\omega)\left\{g_{\mathrm{R}}(\mathbf{k},\omega + \Omega)\Im\tilde{S}_{\mathrm{R}}(\omega) + \Im g_{\mathrm{R}}(\mathbf{k},\omega)\tilde{S}_{\mathrm{A}}(\omega - \Omega) + g_{\mathrm{A}}(\mathbf{k},\omega - \Omega)\Im\tilde{S}_{\mathrm{R}}(\omega) + \Im g_{\mathrm{R}}(\mathbf{k},\omega)\tilde{S}_{\mathrm{R}}(\omega + \Omega)\right.$$
$$\left. - 2\Im\left[g_{\mathrm{R}}(\mathbf{k},\omega)\tilde{S}_{\mathrm{R}}(\omega)\right]\right\}. \quad (A31)$$

Taking the imaginary part of Eq. (A30), we find

$$\Im W_{\mathrm{SE,R}}(\Omega) = \frac{\Im\mathcal{Z}(\Omega)}{\Omega^2} + \Im\frac{1}{(\Omega + i0^+)^2}\Re\mathcal{Z}(\Omega). \quad (A32)$$

It is the second term that contains an essential singularity. We re-write the singular part as

$$\Im\frac{1}{(\Omega + i0^+)^2}\Re\mathcal{Z}(\Omega) = -\Im\left(\frac{\partial}{\partial\Omega}\frac{1}{\Omega + i0^+}\right)\Re\mathcal{Z}(\Omega) = \pi\delta'(\Omega)\Re\mathcal{Z}(\Omega) = -\pi\delta(\Omega)\frac{\partial}{\partial\Omega}\Re\mathcal{Z}(\Omega)\bigg|_{\Omega=0}. \quad (A33)$$

The imaginary part of the retarded current-current correlator must be an odd function of Ω, and the same is true for $\Im W_{\mathrm{SE,R}}(\Omega)$ and $\Im\mathcal{Z}(\Omega)$. But then $\Re\mathcal{Z}(\Omega)$ is odd in Ω, and its derivative must vanish at $\Omega \rightarrow 0$ at least as Ω, which means that left-hand side of Eq. (A33) is proportional to $\Omega\delta(\Omega)$. Recalling also that $\Re\sigma(\Omega) = -\Im\Pi_{\mathrm{R}}(\Omega)/\Omega$, we see that the singular part of Eq. (A33) only renormalizes the weight of the delta function term in the conductivity. Such a term is rendered finite by taking momentum-relaxing scattering, e.g., scattering by impurities, into account, but is of no interest to our study and can be safely discarded.

3. Vertex diagram

Explicitly, the vertex diagram (V) in Fig. 2 reads

$$\Pi^{\mathrm{V}}(i\Omega) = \frac{1}{16d} \sum_{\mathcal{S}_{\mathrm{V}}} \int_{\mathbf{k},\mathbf{q}} \mathrm{Tr}\left(\hat{\mathbf{v}}\hat{M}^{s_1'}_{\mathbf{k}}\hat{M}^{s_2'}_{\mathbf{k}+\mathbf{q}} \cdot \hat{\mathbf{v}}\hat{M}^{s_3'}_{\mathbf{k}+\mathbf{q}}\hat{M}^{s_5'}_{\mathbf{k}}\right) V^2_{\mathrm{st}}(\mathbf{q})$$

$$\times T\sum_{\omega}T\sum_{\nu} g_{s_1'}(\mathbf{k}, i\omega + i\Omega)g_{s_2'}(\mathbf{k}+\mathbf{q}, i\omega + i\nu + i\Omega)g_{s_3'}(\mathbf{k}+\mathbf{q}, i\omega + i\nu)g_{s_5'}(\mathbf{k}, i\omega)\pi_0(\mathbf{q}, i\nu), \qquad (A34)$$

where $\mathcal{S}_{\mathrm{V}} = \{s_1', s_2', s_3', s_5'\}$. Applying the identity (A28) to the pairs of the Green's functions with the same momenta, using Eq. (A2) for $\pi_0(\mathbf{q}, i\nu)$, and summing over ν, we obtain

$$\Pi^{\mathrm{V}}(i\Omega) = \frac{1}{16d} \sum_{\mathcal{S}_{\mathrm{V}}} \int_{\mathbf{k},\mathbf{q}} \mathrm{Tr}\left(\hat{\mathbf{v}}\hat{M}^{s_1'}_{\mathbf{k}}\hat{M}^{s_2'}_{\mathbf{k}+\mathbf{q}} \cdot \hat{\mathbf{v}}\hat{M}^{s_3'}_{\mathbf{k}+\mathbf{q}}\hat{M}^{s_5'}_{\mathbf{k}}\right) V^2_{\mathrm{st}}(\mathbf{q}) \frac{1}{i\Omega - \xi^{s_1'}_{\mathbf{k}} + \xi^{s_5'}_{\mathbf{k}}} \frac{1}{i\Omega - \xi^{s_2'}_{\mathbf{k}+\mathbf{q}} + \xi^{s_3'}_{\mathbf{k}+\mathbf{q}}}$$

$$\times W_{\mathrm{V}}(\mathbf{k}, \mathbf{q}, i\Omega), \qquad (A35)$$

where

$$W_{\mathrm{V}}(\mathbf{k}, \mathbf{q}, i\Omega) = T\sum_{\omega}\left[g_{s_5'}(\mathbf{k}, i\omega) - g_{s_1'}(\mathbf{k}, i\omega + i\Omega)\right]\left[\tilde{\Sigma}_{s_3'}(\mathbf{k}+\mathbf{q}, \mathbf{q}, i\omega) - \tilde{\Sigma}_{s_2'}(\mathbf{k}+\mathbf{q}, \mathbf{q}, i\omega + i\Omega)\right], \qquad (A36)$$

and $\tilde{\Sigma}_s(\mathbf{k}, \mathbf{q}, i\omega)$ is defined in Eq. (A6).

Upon summation over ω and analytic continuation, we obtain for the real and imaginary parts of the retarded counterpart of W_{V} (as for the self-energy diagram, we also switch to unprimed helicities at this point, cf. footnote VII in the main text):

$$\Re W_{\mathrm{V,R}}(\mathbf{k}, \mathbf{q}, \Omega) = -\frac{1}{\pi}\int d\omega\, n_{\mathrm{F}}(\omega)\left[\Im\left(g_{s_5,\mathrm{R}}(\mathbf{k}, \omega)\tilde{\Sigma}_{s_3,\mathrm{R}}(\mathbf{k}+\mathbf{q}, \mathbf{q}, \omega)\right) + \Im\left(g_{s_1,\mathrm{R}}(\mathbf{k}, \omega)\tilde{\Sigma}_{s_2,\mathrm{R}}(\mathbf{k}+\mathbf{q}, \mathbf{q}, \omega)\right)\right.$$

$$- \left(\Re\tilde{\Sigma}_{s_2,\mathrm{R}}(\mathbf{k}+\mathbf{q}, \mathbf{q}, \omega + \Omega)\Im g_{s_5,\mathrm{R}}(\mathbf{k}, \omega) + \Re g_{s_5,\mathrm{A}}(\mathbf{k}, \omega - \Omega)\Im\tilde{\Sigma}_{s_2,\mathrm{R}}(\mathbf{k}+\mathbf{q}, \mathbf{q}, \omega)\right.$$

$$\left.\left. + \Re g_{s_1,\mathrm{R}}(\mathbf{k}, \omega + \Omega)\Im\tilde{\Sigma}_{s_3,\mathrm{R}}(\mathbf{k}+\mathbf{q}, \mathbf{q}, \omega) + \Re\tilde{\Sigma}_{s_3,\mathrm{A}}(\mathbf{k}+\mathbf{q}, \mathbf{q}, \omega - \Omega)\Im g_{s_1,\mathrm{R}}(\mathbf{k}, \omega)\right)\right], \quad (A37)$$

$$\Im W_{\mathrm{V,R}}(\mathbf{k}, \mathbf{q}, \Omega) = -\frac{1}{\pi}\int d\omega\left[n_{\mathrm{F}}(\omega + \Omega) - n_{\mathrm{F}}(\omega)\right]\left[\Im\tilde{\Sigma}_{s_2,\mathrm{R}}(\mathbf{k}+\mathbf{q}, \mathbf{q}, \omega + \Omega)\Im g_{s_5,\mathrm{R}}(\mathbf{k}, \omega)\right.$$

$$\left. + \Im g_{s_1,\mathrm{R}}(\mathbf{k}, \omega + \Omega)\Im\tilde{\Sigma}_{s_3,\mathrm{R}}(\mathbf{k}+\mathbf{q}, \mathbf{q}, \omega)\right]. \qquad (A38)$$

The imaginary part of the current-current correlator is then given by

$$\Im\Pi^{\mathrm{V}}_{\mathrm{R}}(\Omega) = \frac{1}{16d}\sum_{\mathcal{S}_{\mathrm{V}}} \int_{\mathbf{k},\mathbf{q}} \mathrm{Tr}\left(\hat{\mathbf{v}}\hat{M}^{s_1}_{\mathbf{k}}\hat{M}^{s_2}_{\mathbf{k}+\mathbf{q}} \cdot \hat{\mathbf{v}}\hat{M}^{s_3}_{\mathbf{k}+\mathbf{q}}\hat{M}^{s_5}_{\mathbf{k}}\right) V^2_{\mathrm{st}}(\mathbf{q})\mathcal{B}(\mathbf{k}, \mathbf{q}, \Omega), \qquad (A39)$$

where

$$\mathcal{B}(\mathbf{k}, \mathbf{q}, \Omega) = \frac{\Im W_{\mathrm{V,R}}(\mathbf{k}, \mathbf{q}, \Omega)}{(\Omega - \xi^{s_1}_{\mathbf{k}} + \xi^{s_5}_{\mathbf{k}})(\Omega - \xi^{s_2}_{\mathbf{k}+\mathbf{q}} + \xi^{s_3}_{\mathbf{k}+\mathbf{q}})} - \pi\left(\frac{\delta(\Omega - \xi^{s_2}_{\mathbf{k}+\mathbf{q}} + \xi^{s_3}_{\mathbf{k}+\mathbf{q}})}{\Omega - \xi^{s_1}_{\mathbf{k}} + \xi^{s_5}_{\mathbf{k}}} + \frac{\delta(\Omega - \xi^{s_1}_{\mathbf{k}} + \xi^{s_5}_{\mathbf{k}})}{\Omega - \xi^{s_2}_{\mathbf{k}+\mathbf{q}} + \xi^{s_3}_{\mathbf{k}+\mathbf{q}}}\right)\Re W_{\mathrm{V,R}}(\mathbf{k}, \mathbf{q}, \Omega),$$

$$(A40)$$

and where we omitted the term with an essential singularity, which is similar to the singular term in the self-energy diagram discussed in Sec. A 2 c. We will now show that only the first term in Eq. (A40) contributes to the real part of the conductivity for $0 < \Omega < 2E_{\mathrm{F}}$. The reasoning is similar to but more involved than the reasoning in Sec. A 2.

Using the constraints imposed by the delta functions in front of $\Re W_{\mathrm{V}}(\mathbf{k}, \mathbf{q}, \Omega)$, we obtain that, for $\Omega > 0$, only the sets

$$s_2 = +1, s_3 = -1 \text{ and } s_1 = +1, s_5 = -1 \qquad (A41)$$

are allowed for the first and second terms in the round brackets, respectively. This implies that $\epsilon_{\mathbf{k}+\mathbf{q}} = \Omega/2$ and $\epsilon_{\mathbf{k}} = \Omega/2$ in the first and second terms, respectively. Next, we will show that $\epsilon_{\mathbf{k}+\mathbf{q}} > E_{\mathrm{F}}$ and $\epsilon_{\mathbf{k}} > E_{\mathrm{F}}$ in the first and second terms, respectively, which will imply that the corresponding contribution to $\Im\Pi^{\mathrm{V}}_{\mathrm{R}}(\Omega)$ is non-zero only if

$\Omega > 2E_\mathrm{F}$. To see the constraints imposed on $\epsilon_{\mathbf{k+q}}$ and $\epsilon_{\mathbf{k}}$, we write down an explicit form of $\Re W_{\mathrm{V,R}}(\mathbf{k},\mathbf{q},\Omega)$, using Eqs. (A37), (A8), and (A5). After some re-arrangement, we get

$$
\Re W_{\mathrm{V,R}}(\mathbf{k},\mathbf{q},\Omega) = \frac{1}{4}\sum_{s_4,s_6=\pm1}\int_{\mathbf{p}}\left[\mathrm{Tr}(\hat{M}_{\mathbf{p}}^{s_6}\hat{M}_{\mathbf{p+q}}^{s_4})\right]\left[n_\mathrm{F}(\xi_{\mathbf{p}}^{s_6}) - n_\mathrm{F}(\xi_{\mathbf{p+q}}^{s_4})\right]
$$
$$
\times\left[f_{s_3}\frac{n_\mathrm{F}(\xi_{\mathbf{k}}^{s_5}) - n_\mathrm{F}(-\xi_{\mathbf{p+q}}^{s_4} + \xi_{\mathbf{p}}^{s_6} + \xi_{\mathbf{k+q}}^{s_3})}{\xi_{\mathbf{k}}^{s_5} + \xi_{\mathbf{p+q}}^{s_4} - \xi_{\mathbf{p}}^{s_6} - \xi_{\mathbf{k+q}}^{s_3}} - f_{s_2}\frac{n_\mathrm{F}(\xi_{\mathbf{k}}^{s_5}) - n_\mathrm{F}(-\xi_{\mathbf{p+q}}^{s_4} + \xi_{\mathbf{p}}^{s_6} + \xi_{\mathbf{k+q}}^{s_2})}{\Omega + \xi_{\mathbf{k}}^{s_5} + \xi_{\mathbf{p+q}}^{s_4} - \xi_{\mathbf{p}}^{s_6} - \xi_{\mathbf{k+q}}^{s_2}}\right.
$$
$$
\left.+ f_{s_2}\frac{n_\mathrm{F}(\xi_{\mathbf{k}}^{s_1}) - n_\mathrm{F}(-\xi_{\mathbf{p+q}}^{s_4} + \xi_{\mathbf{p}}^{s_6} + \xi_{\mathbf{k+q}}^{s_2})}{\xi_{\mathbf{k}}^{s_1} + \xi_{\mathbf{p+q}}^{s_4} - \xi_{\mathbf{p}}^{s_6} - \xi_{\mathbf{k+q}}^{s_2}} - f_{s_3}\frac{n_\mathrm{F}(-\xi_{\mathbf{p+q}}^{s_4} + \xi_{\mathbf{p}}^{s_6} + \xi_{\mathbf{k+q}}^{s_3}) - n_\mathrm{F}(\xi_{\mathbf{k}}^{s_1})}{\Omega - \xi_{\mathbf{k}}^{s_1} - \xi_{\mathbf{p+q}}^{s_4} + \xi_{\mathbf{p}}^{s_6} + \xi_{\mathbf{k+q}}^{s_3}}\right], \tag{A42}
$$

where $f_s = n_\mathrm{F}(\xi_{\mathbf{k+q}}^s) + n_\mathrm{B}(\xi_{\mathbf{p+q}}^{s_4} - \xi_{\mathbf{p}}^{s_6})$. The difference of the Fermi functions in the first line of Eq. (A42) is non-zero only if either $\xi_{\mathbf{p}}^{s_6} > 0$ and $\xi_{\mathbf{p+q}}^{s_4} < 0$, or vice versa. Now we analyze these two options one by one.

For $\xi_{\mathbf{p}}^{s_6} > 0$ and $\xi_{\mathbf{p+q}}^{s_4} < 0$, we have $f_s = -\theta(\xi_{\mathbf{k+q}}^s)$ and thus $\xi_{\mathbf{k+q}}^{s_{2,3}} > 0$. The combination of these conditions implies that the arguments of the Fermi functions containing three terms are positive, and thus the arguments of the Fermi functions containing a single term must be negative. With that, Eq. (A42) is simplified to

$$
\Re W_{\mathrm{V,R}}(\Omega) = -\frac{1}{4}\sum_{s_4,s_6=\pm1}\int_{\mathbf{p}}\mathrm{Tr}(\hat{M}_{\mathbf{p}}^{s_6}\hat{M}_{\mathbf{p+q}}^{s_4})\theta(\xi_{\mathbf{p}}^{s_6})\theta(-\xi_{\mathbf{p+q}}^{s_4})
$$
$$
\times\left[\theta(-\xi_{\mathbf{k}}^{s_5})\left(\frac{\theta(\xi_{\mathbf{k+q}}^{s_2})}{\Omega + \xi_{\mathbf{k}}^{s_5} + \xi_{\mathbf{p+q}}^{s_4} - \xi_{\mathbf{p}}^{s_6} - \xi_{\mathbf{k+q}}^{s_2}} - \frac{\theta(\xi_{\mathbf{k+q}}^{s_3})}{\xi_{\mathbf{k}}^{s_5} + \xi_{\mathbf{p+q}}^{s_4} - \xi_{\mathbf{p}}^{s_6} - \xi_{\mathbf{k+q}}^{s_3}}\right)\right.
$$
$$
\left.-\theta(-\xi_{\mathbf{k}}^{s_1})\left(\frac{\theta(\xi_{\mathbf{k+q}}^{s_2})}{\xi_{\mathbf{k}}^{s_1} + \xi_{\mathbf{p+q}}^{s_4} - \xi_{\mathbf{p}}^{s_6} - \xi_{\mathbf{k+q}}^{s_2}} + \frac{\theta(\xi_{\mathbf{k+q}}^{s_3})}{\Omega - \xi_{\mathbf{k}}^{s_1} - \xi_{\mathbf{p+q}}^{s_4} + \xi_{\mathbf{p}}^{s_6} + \xi_{\mathbf{k+q}}^{s_3}}\right)\right]. \tag{A43}
$$

Now, we focus on the first term in the round brackets in Eq. (A40). Using the constraint following from $\delta(\Omega - \xi_{\mathbf{k+q}}^{s_2} + \xi_{\mathbf{k+q}}^{s_3})$, we arrive at

$$
\Re W_{\mathrm{V,R}}(\xi_{\mathbf{k+q}}^{s_2} - \xi_{\mathbf{k+q}}^{s_3}) = \frac{1}{4}\sum_{s_4,s_6=\pm1}\int_{\mathbf{p}}\mathrm{Tr}(\hat{M}_{\mathbf{p}}^{s_6}\hat{M}_{\mathbf{p+q}}^{s_4})\theta(\xi_{\mathbf{p}}^{s_6})\theta(-\xi_{\mathbf{p+q}}^{s_4})\left[\theta(\xi_{\mathbf{k+q}}^{s_3}) - \theta(\xi_{\mathbf{k+q}}^{s_2})\right]
$$
$$
\times\left[\frac{\theta(-\xi_{\mathbf{k}}^{s_5})}{\xi_{\mathbf{k}}^{s_5} + \xi_{\mathbf{p+q}}^{s_4} - \xi_{\mathbf{p}}^{s_6} - \xi_{\mathbf{k+q}}^{s_3}} + \frac{\theta(-\xi_{\mathbf{k}}^{s_1})}{\xi_{\mathbf{k+q}}^{s_2} - \xi_{\mathbf{k}}^{s_1} - \xi_{\mathbf{p+q}}^{s_4} + \xi_{\mathbf{p}}^{s_6}}\right]. \tag{A44}
$$

The RHS of the last equation is non-zero only if the arguments of the theta functions in the first pair square brackets are of opposite signs. According to Eq. (A41), $s_3 = -1$ while $s_2 = 1$. Therefore, $\xi_{\mathbf{k+q}}^{s_3} < 0$ and $\xi_{\mathbf{k+q}}^{s_2} = \epsilon_{\mathbf{k+q}} - E_\mathrm{F} > 0$. $\epsilon_{\mathbf{k+q}} > E_\mathrm{F}$. But because $\epsilon_{\mathbf{k+q}} = \Omega/2$ for the first term in the round brackets of Eq. (A40), we have the condition that $\Omega > 2E_\mathrm{F}$. Thus, this term only contributes for frequencies above ω_D and is not relevant for our analysis.

The second term in the round brackets of Eq. (A40) is simplified using the condition following from $\delta(\Omega - \xi_{\mathbf{k}}^{s_1} + \xi_{\mathbf{k}}^{s_5})$:

$$
\Re W_{\mathrm{V,R}}(\xi_{\mathbf{k}}^{s_1} - \xi_{\mathbf{k}}^{s_5}) = \frac{1}{4}\sum_{s_4,s_6=\pm1}\int_{\mathbf{p}}\mathrm{Tr}(\hat{M}_{\mathbf{p}}^{s_6}\hat{M}_{\mathbf{p+q}}^{s_4})\theta(\xi_{\mathbf{p}}^{s_6})\theta(-\xi_{\mathbf{p+q}}^{s_4})\left[\theta(-\xi_{\mathbf{k}}^{s_5}) - \theta(-\xi_{\mathbf{k}}^{s_1})\right]
$$
$$
\times\left[\frac{\theta(\xi_{\mathbf{k+q}}^{s_3})}{\xi_{\mathbf{k}}^{s_5} + \xi_{\mathbf{p+q}}^{s_4} - \xi_{\mathbf{p}}^{s_6} - \xi_{\mathbf{k+q}}^{s_3}} + \frac{\theta(\xi_{\mathbf{k+q}}^{s_2})}{\xi_{\mathbf{k+q}}^{s_2} - \xi_{\mathbf{k}}^{s_1} - \xi_{\mathbf{p+q}}^{s_4} + \xi_{\mathbf{p}}^{s_6}}\right]. \tag{A45}
$$

Using the constraints on s_1 and s_5 from Eq. (A41) again, we conclude that $\epsilon_{\mathbf{k}} > E_\mathrm{F}$. But because $\epsilon_{\mathbf{k}} = \Omega/2$ for the second term in the round brackets of Eq. (A40), we again have the condition that $\Omega > 2E_\mathrm{F}$.

The case of $\xi_{\mathbf{p}}^{s_6} < 0$ and $\xi_{\mathbf{p+q}}^{s_4} > 0$ is analyzed in the same way and with the same result. Therefore, the term proportional to $\Re W_{\mathrm{V,R}}(\Omega)$ in Eq. (A40) is absent for $\Omega < 2E_\mathrm{F}$.

Focusing now on the first term of Eq. (A40), we obtain, after some re-arrangements and re-labelling of momenta and helicities, the following final expression for the vertex diagram for $\Omega < 2E_\mathrm{F}$:

$$
\Im\Pi_\mathrm{R}^\mathrm{V}(\Omega) = \frac{\pi^2}{32}\sum_\mathcal{S}\int_{\mathbf{k,p,q},\nu}V_{\mathrm{st}}^2(\mathbf{q})\left[\mathcal{T}_\mathcal{S}^{\mathrm{V}_1}\mathcal{G}_\mathcal{S}^{\mathrm{V}_1} + \mathcal{T}_\mathcal{S}^{\mathrm{V}_2}\mathcal{G}_\mathcal{S}^{\mathrm{V}_2}\right]
$$
$$
\times\theta(-\xi_{\mathbf{k}}^{s_3})\theta(\xi_{\mathbf{k+q}}^{s_5})\theta(-\xi_{\mathbf{p}}^{s_4})\theta(\xi_{\mathbf{p+q}}^{s_6})\delta(\Omega + \nu + \xi_{\mathbf{k}}^{s_3} - \xi_{\mathbf{k+q}}^{s_5})\delta(\nu + \xi_{\mathbf{p+q}}^{s_6} - \xi_{\mathbf{p}}^{s_4}), \tag{A46}
$$

where, for the sake of convenience, we re-introduced $\int_\nu = \int d\nu/2\pi$ and

$$\mathcal{T}_{\mathcal{S}}^{V_1} = \frac{1}{d} \text{Tr} \left(\hat{\mathbf{v}} \hat{M}_{\mathbf{k}}^{s_1} \hat{M}_{\mathbf{k+q}}^{s_5} \cdot \hat{\mathbf{v}} \hat{M}_{\mathbf{k+q}}^{s_2} \hat{M}_{\mathbf{k}}^{s_3} \right) \text{Tr} \left(\hat{M}_{-\mathbf{p-q}}^{s_6} \hat{M}_{-\mathbf{p}}^{s_4} \right) \tag{A47a}$$

$$\mathcal{T}_{\mathcal{S}}^{V_2} = \frac{1}{d} \text{Tr} \left(\hat{\mathbf{v}} \hat{M}_{-\mathbf{k-q}}^{s_5} \hat{M}_{-\mathbf{k}}^{s_1} \cdot \hat{\mathbf{v}} \hat{M}_{-\mathbf{k}}^{s_3} \hat{M}_{-\mathbf{k-q}}^{s_2} \right) \text{Tr} \left(\hat{M}_{\mathbf{p}}^{s_4} \hat{M}_{\mathbf{p+q}}^{s_6} \right) \tag{A47b}$$

$$\mathcal{G}_{\mathcal{S}}^{V_1} = \mathcal{G}_{\mathcal{S}}^{V_2} = \frac{1}{\Omega - \xi_{\mathbf{k}}^{s_1} + \xi_{\mathbf{k}}^{s_3}} \frac{1}{\Omega - \xi_{\mathbf{k+q}}^{s_5} + \xi_{\mathbf{k+q}}^{s_2}}. \tag{A47c}$$

Thus we have derived Eq. (48) of the main text.

4. Sum of the self-energy and vertex diagrams

Adding up Eqs. (A21), (A25), and (A46), we obtain the combined contribution of the self-energy and vertex diagram for $0 < \Omega < \omega_D = 2E_F$:

$$\Im\Pi_R^{\text{SE+V}}(\Omega) = \Im\Pi_R^{\text{SE}_1}(\Omega) + \Im\Pi_R^{\text{SE}_2}(\Omega) + \Im\Pi_R^{\text{V}}(\Omega) = -\frac{\pi^2}{32} \sum_{\mathcal{S}} \int_{\mathbf{k,p,q}} \int_\nu V_{\text{st}}^2(\mathbf{q}) \times \theta(-\xi_{\mathbf{k}}^{s_3})\theta(\xi_{\mathbf{k+q}}^{s_5})\theta(-\xi_{\mathbf{p}}^{s_4})\theta(\xi_{\mathbf{p+q}}^{s_6})$$

$$\times \delta(\Omega + \nu + \xi_{\mathbf{k}}^{s_3} - \xi_{\mathbf{k+q}}^{s_5})\delta(\nu + \xi_{\mathbf{p+q}}^{s_6} - \xi_{\mathbf{p}}^{s_2}) \left[\mathcal{T}_{\mathcal{S}}^{\text{SE}_1}\mathcal{G}_{\mathcal{S}}^{\text{SE}_1} + \mathcal{T}_{\mathcal{S}}^{\text{SE}_2}\mathcal{G}_{\mathcal{S}}^{\text{SE}_2} - \mathcal{T}_{\mathcal{S}}^{V_1}\mathcal{G}_{\mathcal{S}}^{V_1} - \mathcal{T}_{\mathcal{S}}^{V_2}\mathcal{G}_{\mathcal{S}}^{V_2} \right]. \tag{A48}$$

Similar computations for PAL and CAL diagrams give Eqs. (49) and (50), respectively.

Appendix B: Asymptotic expressions for the conductivity

As an example, we derive an asymptotic expression for the purely electron-electron contribution to the conductivity of a 3D Dirac metal with Hubbard interaction in the limit $\Omega \ll E_F$. We start with the general result (45), which we reproduce below for the reader's convenience:

$$\mathcal{R}_{\mathcal{S}}^{J_u}(\Omega) = K^{J_u} \int_{\mathbf{k,p,q}} \int_\nu V_{\text{st}}^2(\mathbf{q}) \mathcal{T}_{\mathcal{S}}^{J_u}(\mathbf{k,p,q}) \, \mathcal{G}_{\mathcal{S}}^{J_u}(\mathbf{k,p,q},\Omega)$$

$$\times \theta(-\xi_{\mathbf{k}}^{s_3})\theta(-\xi_{\mathbf{p}}^{s_4})\theta(\xi_{\mathbf{k+q}}^{s_5})\theta(\xi_{\mathbf{p+q}}^{s_6})\delta(\Omega + \nu + \xi_{\mathbf{k}}^{s_3} - \xi_{\mathbf{k+q}}^{s_5})\delta(\nu + \xi_{\mathbf{p+q}}^{s_6} - \xi_{\mathbf{p}}^{s_4}), \tag{B1}$$

where $\mathcal{T}_{\mathcal{S}}^{J_u}(\mathbf{k,p,q})$ and $\mathcal{G}_{\mathcal{S}}^{J_u}(\mathbf{k,p,q})$ are defined in Eqs. (47)-(50), respectively. We remind the reader that the purely electron-electron contribution corresponds to all helicities being positive, i.e.,

$$\mathcal{S} = \mathcal{S}_+ \equiv \{s_1 = 1, s_2 = 1, s_3 = 1, s_4 = 1, s_5 = 1, s_6 = 1\}. \tag{B2}$$

In a more explicit form,

$$\mathcal{R}_{\mathcal{S}_+}^{J_u}(\Omega) = \lambda_3^2 K^{J_u} \int_0^\infty \frac{dk\,k^2}{(2\pi)^3} \int_0^\infty \frac{dp\,p^2}{(2\pi)^3} \int_0^\infty \frac{dq\,q^2}{(2\pi)^3} \int_{-\infty}^\infty \frac{d\nu}{2\pi}$$

$$\times \int_0^\pi d\theta_{\mathbf{q\hat{z}}} \sin\theta_{\mathbf{q\hat{z}}} \int_0^{2\pi} d\phi_{\mathbf{q,\hat{z}}} \int_0^\pi d\theta_{\mathbf{kq}} \sin\theta_{\mathbf{kq}} \int_0^{2\pi} d\phi_{\mathbf{k,q}} \int_0^\pi d\theta_{\mathbf{pq}} \sin\theta_{\mathbf{pq}} \int_0^{2\pi} d\phi_{\mathbf{p,q}} \mathcal{T}_{\mathcal{S}_+}^{J_u}(\mathbf{k,p,q})\mathcal{G}_{\mathcal{S}_+}^{J_u}(\mathbf{k,p,q})$$

$$\times \theta(-\xi_{\mathbf{k}}^+)\theta(-\xi_{\mathbf{p}}^+)\theta(\xi_{\mathbf{k+q}}^+)\theta(\xi_{\mathbf{p+q}}^+)\delta(\Omega + \nu + \xi_{\mathbf{k}}^+ - \xi_{\mathbf{k+q}}^+)\delta(\nu + \xi_{\mathbf{p+q}}^+ - \xi_{\mathbf{p}}^+), \tag{B3}$$

where $\theta_{\mathbf{nn'}}$ is the angle between vectors $\mathbf{n}$ and $\mathbf{n'}$, and $\phi_{\mathbf{n,n'}}$ is the azimuthal angle of vector $\mathbf{n}$ in a spherical system with vector $\mathbf{n'}$ taken as the polar axis. Now we solve the integrals over $\theta_{\mathbf{kq}}$ and $\theta_{\mathbf{pq}}$, using the delta functions in in the expression above, which yields

$$\int_0^\pi d\theta_{\mathbf{kq}} \sin\theta_{\mathbf{kq}} \int_0^\pi d\theta_{\mathbf{pq}} \sin\theta_{\mathbf{pq}} \mathcal{T}_{\mathcal{S}_+}^{J_u}(\mathbf{k,p,q})\mathcal{G}_{\mathcal{S}_+}^{J_u}(\mathbf{k,p,q})\delta(\Omega + \nu + \epsilon_{\mathbf{k}} - \epsilon_{\mathbf{k+q}})\delta(\nu + \epsilon_{\mathbf{p+q}} - \epsilon_{\mathbf{p}})$$

$$= \frac{(\epsilon_{\mathbf{k}} + \nu + \Omega)(\epsilon_{\mathbf{p}} - \nu)}{\epsilon_{\mathbf{k}}\epsilon_{\mathbf{p}}v_D^2 q^2} \left[\mathcal{T}_{\mathcal{S}_+}^{J_u}(\mathbf{k,p,q})\mathcal{G}_{\mathcal{S}_+}^{J_u}(\mathbf{k,p,q}) \right]\Big|_{\cos\theta_{\mathbf{kq}}=\mu_{\mathbf{k}},\cos\theta_{\mathbf{pq}}=\mu_{\mathbf{p}}} \Theta(\mu_{\mathbf{k}}, \mu_{\mathbf{p}}), \tag{B4}$$

where $\Theta(\mu_{\mathbf{k}}, \mu_{\mathbf{p}})$ encapsulates the constraints imposed by the delta functions in Eq. (B3), i.e.,

$$\epsilon_{\mathbf{k+q}} = \Omega + \nu + \epsilon_{\mathbf{k}}, \epsilon_{\mathbf{p+q}} = \epsilon_{\mathbf{p}} - \nu, \tag{B5}$$

such that

$$-1 \leq \mu_{\mathbf{k}} = \frac{(\Omega + \nu + \epsilon_{\mathbf{k}})^2 - \epsilon_{\mathbf{k}}^2 - v_{\mathrm{D}}^2 q^2}{2\epsilon_{\mathbf{k}} v_{\mathrm{D}} q} \leq 1,$$
$$-1 \leq \mu_{\mathbf{p}} = \frac{(-\nu + \epsilon_{\mathbf{p}})^2 - \epsilon_{\mathbf{p}}^2 - v_{\mathrm{D}}^2 q^2}{2\epsilon_{\mathbf{p}} v_{\mathrm{D}} q} \leq 1. \tag{B6}$$

Note that the constraints (B5) are the same ones as in Eq. (57c) of the main text for the special case of all helicities being positive. The last two equations are resolved in terms of q, which imposes constraints on the range of integration over q. In addition, the first two theta functions in Eq. (B3) imply that $\epsilon_{\mathbf{k}} \leq E_{\mathrm{F}}$ and $\epsilon_{\mathbf{p}} \geq E_{\mathrm{F}}$ for $s_3 = s_4 = 1$, whereas the second two theta functions, in conjunction with Eq. (B5), imply that $\Omega + \nu + \epsilon_{\mathbf{k}} \geq E_{\mathrm{F}}$ and $\epsilon_{\mathbf{p}} - \nu \geq E_{\mathrm{F}}$.

Next, we switch from integration over k and p to integration over dispersions $\epsilon_{\mathbf{k}} = v_{\mathrm{D}} k$ and $\epsilon_{\mathbf{p}} = v_{\mathrm{D}} p$. Imposing explicitly all the constraints described above, we arrive at

$$\mathcal{R}_{\mathcal{S}_+}^{J_u}(\Omega) = \int_{E_{\mathrm{F}}-\Omega}^{E_{\mathrm{F}}} d\epsilon_{\mathbf{k}} \int_{\max\{0, 2E_{\mathrm{F}}-\Omega-\epsilon_{\mathbf{k}}\}}^{E_{\mathrm{F}}} d\epsilon_{\mathbf{p}} \int_{E_{\mathrm{F}}-\Omega-\epsilon_{\mathbf{k}}}^{\epsilon_{\mathbf{p}}-E_{\mathrm{F}}} d\nu \int_{\max\{(\Omega+\nu),-\nu\}/v_{\mathrm{D}}}^{\min\{(\Omega+\nu+2\epsilon_{\mathbf{k}}),(2\epsilon_{\mathbf{p}}-\nu)\}/v_{\mathrm{D}}} dq \mathcal{L}_{\mathcal{S}_+}^{J_u}(\epsilon_{\mathbf{k}}, \epsilon_{\mathbf{p}}, q, \nu, \Omega), \tag{B7}$$

where

$$\mathcal{L}_{\mathcal{S}_+}^{J_u}(\epsilon_{\mathbf{k}}, \epsilon_{\mathbf{p}}, q, \nu, \Omega) = \frac{K^{J_u} \lambda_3^2}{(2\pi)^{10} v_{\mathrm{D}}^8} \bar{\mathcal{Q}}_{\mathcal{S}_+}^{J_u}(\epsilon_{\mathbf{k}}, \epsilon_{\mathbf{p}}, q, \nu, \Omega) \epsilon_{\mathbf{k}} \epsilon_{\mathbf{p}} (\epsilon_{\mathbf{k}} + \Omega + \nu)(\epsilon_{\mathbf{p}} - \nu) \tag{B8}$$

and

$$\bar{\mathcal{Q}}_{\mathcal{S}_+}^{J_u}(\epsilon_{\mathbf{k}}, \epsilon_{\mathbf{p}}, q, \nu, \Omega) = \int_0^{\pi} d\theta_{\mathbf{qz}} \sin\theta_{\mathbf{qz}} \int_0^{2\pi} d\phi_{\mathbf{qx}} \int_0^{2\pi} d\phi_{\mathbf{kq}} \int_0^{2\pi} d\phi_{\mathbf{pq}} \left[\mathcal{T}_{\mathcal{S}_+}^{J_u}(\mathbf{k}, \mathbf{p}, \mathbf{q}) \mathcal{G}_{\mathcal{S}_+}^{J_u}(\mathbf{k}, \mathbf{p}, \mathbf{q}) \right] \Big|_{\cos\theta_{\mathbf{kq}}=\mu_{\mathbf{k}}, \cos\theta_{\mathbf{pq}}=\mu_{\mathbf{p}}}. \tag{B9}$$

For the particular case of $J_u = \mathrm{SE}_1$ and all helicities positive, we have $\mathcal{G}_{\mathcal{S}_+}^{\mathrm{SE}_1}(\mathbf{k}, \mathbf{p}, \mathbf{q}) = 1/\Omega^2$, and thus the angular integrals in Eq. (B9) involve only $\mathcal{T}_{\mathcal{S}_+}^{\mathrm{SE}_1}(\mathbf{k}, \mathbf{p}, \mathbf{q})$ in Eq. (47), which is evaluated explicitly as

$$\mathcal{T}_{\mathcal{S}_+}^{\mathrm{SE}_1}(\mathbf{k}, \mathbf{p}, \mathbf{q}) = -\frac{8 v_{\mathrm{D}}^3 q \sin\theta_{\mathbf{kq}}}{\epsilon_{\mathbf{k+q}}} \frac{\epsilon_{\mathbf{p}} + \epsilon_{\mathbf{p+q}} + q\cos\theta_{\mathbf{pq}}}{\epsilon_{\mathbf{p+q}}} \Big[8\cos 2\theta_{\mathbf{kq}} \cos\phi_{\mathbf{qx}} \sin\theta_{\mathbf{qz}} (\cos\theta_{\mathbf{qz}} \cos\phi_{\mathbf{kq}} \cos\phi_{\mathbf{qx}} - \sin\phi_{\mathbf{kq}} \sin\phi_{\mathbf{qx}})$$
$$+ \frac{1}{8} \sin 2\theta_{\mathbf{kq}} (4 + 12\cos 2\theta_{\mathbf{qz}} + 4\cos 2\theta_{\mathbf{qz}} \cos 2\phi_{\mathbf{kq}} - 4\cos 2\phi_{\mathbf{kq}} + 12\cos 2\theta_{\mathbf{qz}} \cos 2\phi_{\mathbf{qx}}$$
$$+ 4\cos 2\phi_{\mathbf{qx}} \cos 2\theta_{\mathbf{qz}} \cos 2\phi_{\mathbf{kq}} + 12\cos 2\phi_{\mathbf{kq}} \cos 2\phi_{\mathbf{qx}} - 12\cos 2\phi_{\mathbf{qx}} - 16\cos\theta_{\mathbf{qz}} \sin 2\phi_{\mathbf{kq}} \sin 2\phi_{\mathbf{qx}}) \Big]. \tag{B10}$$

Integrating Eq. (B10) over the angles and imposing the constraints from Eq. (B5), we obtain

$$\mathcal{L}_{\mathcal{S}_+}^{\mathrm{SE}_1}(\epsilon_{\mathbf{k}}, \epsilon_{\mathbf{p}}, q, \nu, \Omega) = -\frac{\lambda_3^2}{384\pi^5 v_{\mathrm{D}}^6 \Omega^2} \left((2\epsilon_{\mathbf{k}} + \Omega + \nu)^2 - v_{\mathrm{D}}^2 q^2 \right) \left((2\epsilon_{\mathbf{p}} - \nu)^2 - v_{\mathrm{D}}^2 q^2 \right). \tag{B11}$$

where we used $K^{\mathrm{SE}_1} = -\pi^2/32$ as defined in Eq. (46) of the main text.

In this particular case, the integrand of Eq. (B7) is a purely polynomial function, and thus it is possible to obtain an exact result for all frequencies $\Omega < 2E_{\mathrm{F}}$. However, this is not the case for other diagrams (except for SE_2) and for the 2D case. For consistency with these other cases, we will only evaluate the integral (B7) for $\Omega \ll E_{\mathrm{F}}$. To this end, we note that for $\Omega < E_{\mathrm{F}}$ the limits of the integral for $\epsilon_{\mathbf{p}}$ in Eq. (B7) become

$$2E_{\mathrm{F}} - \epsilon_{\mathbf{k}} - \Omega < \epsilon_{\mathbf{p}} < E_{\mathrm{F}}. \tag{B12}$$

Thus, for $\Omega \ll E_{\mathrm{F}}$ it is convenient to define new dimensionless variables

$$x = (\epsilon_{\mathbf{k}} - E_{\mathrm{F}} + \Omega)/\Omega; \; y = (\epsilon_{\mathbf{p}} - E_{\mathrm{F}})/\Omega + x; \; z = \nu/\Omega + x,$$
$$x \in (0, 1), y \in (0, x), z \in (0, y). \tag{B13}$$

Note that x, y and z are all of order 1. Also, the upper and lower limits of the integral over q in Eq. (B7) can be replaced by $2k_F$ and 0, respectively. Now we substitute $\epsilon_{\mathbf{k}}, \epsilon_{\mathbf{p}}, \nu$ in terms of x, y, z into Eq. (B11), define $r = q/2k_F$, and expand the result in x, y, z and Ω for $\Omega \ll E_F$. After the expansion, Eq. (B11) is reduced to

$$
\begin{aligned}
\mathcal{L}_{\mathcal{S}_+}^{\mathrm{SE}_1}(x, y, z, r, \Omega) = -\frac{\lambda_3^2}{384\pi^5 v_D^6}(2E_F)^2 \Big[&\left(\frac{2E_F}{\Omega}\right)^2 (r^2 - 1)^2 + \frac{4E_F}{\Omega} r^2 (r^2 - 1)(1 - 2y) \\
&+ 4r^4 \left(1 - x + x^2 - 2y - xy + 3y^2 - yz + z^2\right) \\
&- r^2 \left(5 - 10x + 10x^2 - 12xy + 12y^2 - 2z + 4xz - 12yz + 10z^2\right) \\
&+ \left(2x^2 - 4xz - 2x + 2z^2 + 2z + 1\right) + \mathcal{O}(\Omega/E_F) \Big].
\end{aligned}
$$

(B14)

Performing the four-dimensional integral

$$
\mathcal{R}_{\mathcal{S}_+}^{\mathrm{SE}_1}(\Omega) = \Omega^3 (2k_F) \int_0^1 dx \int_0^x dy \int_0^y dz \int_0^1 dr \, \mathcal{L}_{\mathcal{S}_+}^{\mathrm{SE}_1}(x, y, z, r, \Omega),
$$

(B15)

we obtain

$$
\mathcal{R}_{\mathcal{S}_+}^{\mathrm{SE}_1}(\Omega) = -\frac{\lambda_3^2}{135\pi^5} \frac{k_F^6}{v_D} \left[\frac{\Omega}{E_F} + \frac{9}{80} \left(\frac{\Omega}{E_F}\right)^3 \right].
$$

(B16a)

Similar expansions are performed for other contributions. Below we just list the results:

$$
\mathcal{R}_{\mathcal{S}_+}^{\mathrm{SE}_2}(\Omega) = -\frac{\lambda_3^2}{135\pi^5} \frac{k_F^6}{v_D} \left[\frac{\Omega}{E_F} + \frac{9}{80} \left(\frac{\Omega}{E_F}\right)^3 \right],
$$

(B16b)

$$
\mathcal{R}_{\mathcal{S}_+}^{\mathrm{V}_1}(\Omega) + \mathcal{R}_{\mathcal{S}_+}^{\mathrm{V}_2}(\Omega) = -\frac{\lambda_3^2}{135\pi^5} \frac{k_F^6}{v_D} \left[-\frac{10}{7} \frac{\Omega}{E_F} - \frac{129}{280} \left(\frac{\Omega}{E_F}\right)^3 \right],
$$

(B16c)

$$
\mathcal{R}_{\mathcal{S}_+}^{\mathrm{PAL}_1}(\Omega) + \mathcal{R}_{\mathcal{S}_+}^{\mathrm{PAL}_2}(\Omega) + \mathcal{R}_{\mathcal{S}_+}^{\mathrm{CAL}_1}(\Omega) + \mathcal{R}_{\mathcal{S}_+}^{\mathrm{CAL}_2}(\Omega) = -\frac{\lambda_3^2}{135\pi^5} \frac{k_F^6}{v_D} \left[-\frac{4}{7} \frac{\Omega}{E_F} + \frac{71}{140} \left(\frac{\Omega}{E_F}\right)^3 \right].
$$

(B16d)

The conductivity is obtained by multiplying the sum of all $\mathcal{R}_{\mathcal{S}_+}^{J_u}$ by $-1/\Omega$. The leading, linear-in-Ω terms in Eqs. (B16a)-(B16d), would then produce an Ω-independent conductivity, which would be the case for a Fermi liquid with Galilean invariance broken completely by, e.g., umklapp scattering. However, in our case Galilean invariance is broken only partially, and the conductivity is suppressed compared to the case with fully-broken Galilean invariance. Indeed, adding up Eqs. (B16a)-(B16d), we see that linear-in-Ω terms cancel out, while the sum the subleading, cubic terms reproduces Eq. (77) of the main text.

Appendix C: Combining contributions from all diagrams for intra-band absorption due to electron-electron interaction

In this Appendix, we demonstrate how the contributions from all diagrams are combined together for the case of electron-electron interaction, when all the helicities are positive: $s_i = +1$ for $i = 1 \ldots 6$. We introduce the following definitions

$$
|s_{\mathbf{k}}\rangle \equiv |\mathbf{k}, s\rangle \equiv |\psi_{\mathbf{k}, s}\rangle,
$$

(C1a)

$$
\hat{M}_{\mathbf{k}}^s = |s_{\mathbf{k}}\rangle \langle s_{\mathbf{k}}|,
$$

(C1b)

$$
\Phi_{\mathbf{k}, \mathbf{k}'}^{s, s'} = \langle s_{\mathbf{k}} | s'_{\mathbf{k}'} \rangle,
$$

(C1c)

$$
\mathbf{v}_{\mathbf{k}}^{s, s'} = \langle s_{\mathbf{k}} | \hat{\mathbf{v}} | s'_{\mathbf{k}} \rangle,
$$

(C1d)

and list the properties that will be used in this section:

$$
\langle s_{\mathbf{k}} | s'_{\mathbf{k}'} \rangle = \langle s_{-\mathbf{k}} | s'_{-\mathbf{k}'} \rangle,
$$

(C2a)

$$
\langle s_{\mathbf{k}} | s_{\mathbf{k}} \rangle = 1,
$$

(C2b)

$$
\langle s_{\mathbf{k}} | - s_{\mathbf{k}} \rangle = 0,
$$

(C2c)

$$
\mathbf{v}_{-\mathbf{k}}^{+, +} = -\mathbf{v}_{\mathbf{k}}^{+, +}.
$$

(C2d)

(C2e)

We remind the reader that an algebraic expression for each diagram is the sum of two terms, labeled as J_1 and J_2, where $J =$ SE, V, etc. denotes the type of a diagram.[50] We first combine the J_1 terms together, and then do the same for the J_2 terms. Note that, according to Eqs. (47)-(50), $\mathcal{G}_{\mathcal{S}_+}^{J_1} = \mathcal{G}_{\mathcal{S}_+}^{J_2} = 1/\Omega^2$, where $\mathcal{S}_+$ is defined in Eq. (B2). Therefore, we need to combine only the trace parts. For $\mathcal{T}_{\mathcal{S}_+}^{\text{SE}_1}$ we obtain

$$
\begin{aligned}
\mathcal{T}_{\mathcal{S}_+}^{\text{SE}_1} &= \text{Tr}\left(\hat{\mathbf{v}}\hat{M}_{\mathbf{k}}^+ \hat{M}_{\mathbf{k+q}}^+ \hat{M}_{\mathbf{k}}^+ \cdot \hat{\mathbf{v}}\hat{M}_{\mathbf{k}}^+\right)\text{Tr}(\hat{M}_{-\mathbf{p-q}}^+ \hat{M}_{-\mathbf{p}}^+) \\
&= \langle +_{\mathbf{k}}|\hat{\mathbf{v}}|+_{\mathbf{k}}\rangle \cdot \langle +_{\mathbf{k}}|+_{\mathbf{k+q}}\rangle\langle +_{\mathbf{k+q}}|+_{\mathbf{k}}\rangle\langle +_{\mathbf{k}}|\hat{\mathbf{v}}|+_{\mathbf{k}}\rangle\langle +_{\mathbf{k}}|+_{\mathbf{k}}\rangle\langle +_{-\mathbf{p}}|+_{-\mathbf{p-q}}\rangle\langle +_{-\mathbf{p-q}}|+_{-\mathbf{p}}\rangle\langle +_{-\mathbf{p}}|+_{-\mathbf{p}}\rangle \\
&= \mathbf{v}_{\mathbf{k}}^{+,+}\cdot \mathbf{v}_{\mathbf{k}}^{+,+}\langle +_{\mathbf{k}}|+_{\mathbf{k+q}}\rangle\langle +_{\mathbf{k+q}}|+_{\mathbf{k}}\rangle\left|\Phi_{\mathbf{p},\mathbf{p+q}}^{+,+}\right|^2 \\
&= \mathbf{v}_{\mathbf{k}}^{+,+}\cdot \mathbf{v}_{\mathbf{k}}^{+,+}\left|\Phi_{\mathbf{k},\mathbf{k+q}}^{+,+}\right|^2 \left|\Phi_{\mathbf{p},\mathbf{p+q}}^{+,+}\right|^2.
\end{aligned}
\tag{C3}
$$

Performing the same steps for the V_1, PAL_1 and CAL_1 contributions and adding them up, we obtain

$$
\mathcal{T}_1 \equiv \sum_{J_1=\text{SE}_1,\text{V}_1,\text{PAL}_1,\text{CAL}_1} K^{J_1}\mathcal{T}_{\mathcal{S}_+}^{J_1} = -\frac{\pi^2}{32}\mathbf{v}_{\mathbf{k}}^{+,+}\cdot\Delta\mathbf{v}\left|\Phi_{\mathbf{k},\mathbf{k+q}}^{+,+}\right|^2\left|\Phi_{\mathbf{p},\mathbf{p+q}}^{+,+}\right|^2,
\tag{C4}
$$

where K_{J_u} is defined in Eq. (46) of the main text, and

$$
\Delta\mathbf{v} = \mathbf{v}_{\mathbf{k}}^{+,+} + \mathbf{v}_{\mathbf{p+q}}^{+,+} - \mathbf{v}_{\mathbf{k+q}}^{+,+} - \mathbf{v}_{\mathbf{p}}^{+,+}.
\tag{C5}
$$

In the same way, we re-write the J_2 terms and combine them together. The only difference compared to the J_1 case is that, when combining the PAL_2 and CAL_2 contributions, we need to re-label the momenta as $\mathbf{k}\leftrightarrow\mathbf{p}$ in the integrand of Eq. (45). This can be done for the present case, when all the helicities are positive, and thus the delta and theta functions in Eq. (45) can be reduced back to their original forms by replacing first $\nu\to\nu-\Omega$ and then $\nu\to-\nu$. After these manipulations, we obtain for the sum of the J_2 terms

$$
\mathcal{T}_2 \equiv \sum_{J=\text{SE}_2,\text{V}_2,\text{PAL}_2,\text{CAL}_2} K^{J_2}\mathcal{T}_{\mathcal{S}_+}^{J_2} = \frac{\pi^2}{32}\mathbf{v}_{\mathbf{k+q}}^{+,+}\cdot\Delta\mathbf{v}\left|\Phi_{\mathbf{k},\mathbf{k+q}}^{+,+}\right|^2\left|\Phi_{\mathbf{p},\mathbf{p+q}}^{+,+}\right|^2.
\tag{C6}
$$

Adding up Eqs. (C4) and (C6), we find

$$
\mathcal{T}_{\mathcal{S}_+} \equiv \mathcal{T}_1 + \mathcal{T}_2 = -\frac{\pi^2}{32}\Delta\mathbf{v}\cdot\left(\mathbf{v}_{\mathbf{k}}^{+,+} - \mathbf{v}_{\mathbf{k+q}}^{+,+}\right)\left|\Phi_{\mathbf{k},\mathbf{k+q}}^{+,+}\right|^2\left|\Phi_{\mathbf{p},\mathbf{p+q}}^{+,+}\right|^2.
\tag{C7}
$$

Using the same reasoning as for the PAL_2 case above, we relabel $\mathbf{k}\leftrightarrow\mathbf{p}$ in Eq. (C7) and rewrite it as

$$
\mathcal{T}_{\mathcal{S}_+} = -\frac{\pi^2}{32}\Delta\mathbf{v}\cdot\left(\mathbf{v}_{\mathbf{p+q}}^{+,+} - \mathbf{v}_{\mathbf{p}}^{+,+}\right)\left|\Phi_{\mathbf{p},\mathbf{p+q}}^{+,+}\right|^2\left|\Phi_{\mathbf{k},\mathbf{k+q}}^{+,+}\right|^2,
\tag{C8}
$$

where we used that $\Delta\mathbf{v}\to-\Delta\mathbf{v}$ on $\mathbf{k}\leftrightarrow\mathbf{p}$. Adding Eqs. (C7) and (C8), we obtain a symmetrized form of $\mathcal{T}_{\mathcal{S}_+}$:

$$
\mathcal{T}_{\mathcal{S}_+} = -\frac{\pi^2}{64}\left(\Delta\mathbf{v}\right)^2\left|\Phi_{\mathbf{p},\mathbf{p+q}}^{+,+}\right|^2\left|\Phi_{\mathbf{k},\mathbf{k+q}}^{+,+}\right|^2,
\tag{C9}
$$

which is reproduced in Eq. (67) of the main text.